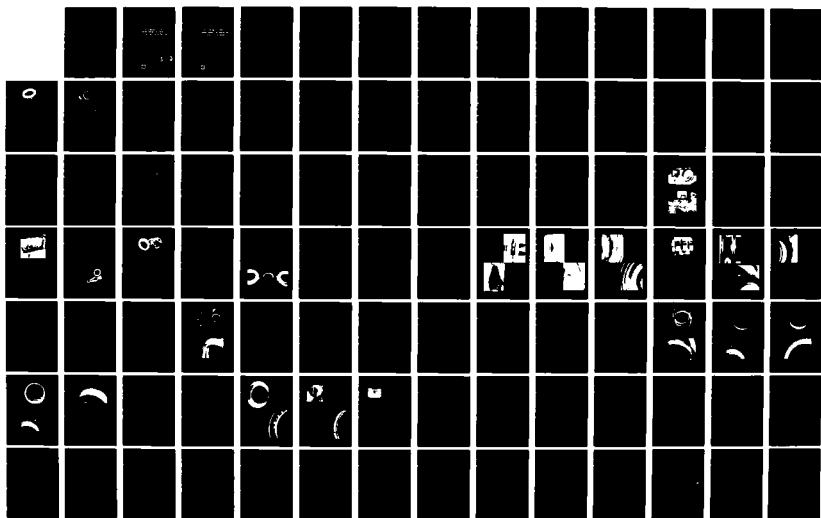


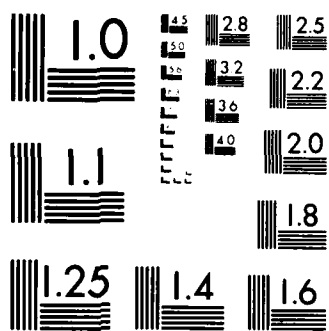
LOW LEAKAGE TURBINE SHAFT SEALS FOR ADVANCED COMBINED
CYCLE SYSTEMS(U) SOLAR TURBINES INC SAN DIEGO CA
G W HOSANG NOV 84 SR84-R-4622-36 N00024-78-C-5345

44

F/G 11/1

NL





MICROCOPY RESOLUTION TEST CHART
NATIONAL BUREAU OF STANDARDS-1963-A

Final Report

AD-A149 372

Low Leakage Turbine Shaft Seals for Advanced Combined Cycle Systems

Contract N00024-78-C-5345

FILE COPY

DTIC
ELECTE
S JAN 02 1985 D
E



074

Final Report

Low Leakage Turbine Shaft Seals for Advanced Combined Cycle Systems

Prepared by:
George W. Hosang

Prepared for:
Naval Sea Systems Command
Department of the Navy
Washington, DC 20362

SR84-R-4622-36
November 1984

Accession For	
NTIS GRA&I	<input checked="checked" type="checkbox"/>
DTIC TAB	<input type="checkbox"/>
Unannounced	<input type="checkbox"/>
Justification <i>per</i>	
By _____	
Distribution/	
Availability Codes	
Dist	Avail and/or Special
A-1	



**SOLAR
TURBINES
INCORPORATED**

SUBSIDIARY OF CATERPILLAR TRACTOR CO
P.O. Box 85376, San Diego, CA 92138-5376



TABLE OF CONTENTS

<u>Section</u>	<u>Page</u>
SYNOPSIS	xi
ACKNOWLEDGEMENT	xiii
SUMMARY	1
1 OBJECTIVE	5
2 PROGRAM APPROACH	7
3 INTRODUCTION	9
4 INVESTIGATION	13
4.1 Seal System Definition	13
4.2 Test Facility	13
4.3 Design Criteria	17
4.4 Candidate Seal Designs	18
4.5 Design Characteristics of NASA- Solar and Koppers Seals	21
4.6 Test Set-Up	23
4.6.1 Test Rig	23
4.6.2 Buffer Water Supply System	31
4.6.3 Test Plan	31
4.7 Experimental Testing	34
4.7.1 Crane-Design Seals	34
4.7.2 NASA-Solar Seals	37
4.7.3 Koppers Seals	46
4.7.4 Endurance Testing	54
4.8 Seal Bibliography	68
5 DISCUSSION OF RESULTS	69
6 DESIGN GUIDELINES	71
7 CONCLUSIONS	73
8 RECOMMENDATIONS	75

TABLE OF CONTENTS (Continued)

<u>Section</u>	<u>Page</u>
APPENDIX I - Vendor Proposed Designs	77
APPENDIX II-1 - Solar Source Control Drawing RSK 230832	91
APPENDIX II-2 - Solar Source Control Drawing RSK 230833	99
APPENDIX III - Experimental Data	105
APPENDIX IV - Design Data	121
APPENDIX V - Face Seals Bibliography	133

LIST OF FIGURES

<u>Figure</u>		<u>Page</u>
1	Crane (NASA-Solar) Spiral Groove Face Seal	2
2	Koppers Face Seal	3
3	Modified Spiral Groove Seal	4
4	Conventional Steam Systems	10
5	Automatic Water Treatment System for One Percent Make-Up	11
6	Seal Test Rig	14
7	Turbine Seal Test Rig Schematic	15
8	Seal Test Rig - Single Seal, Performance Test Configuration	16
9	Example Face Seal Arrangement for Buffer Seal System	19
10	NASA-Solar Crane Design Spiral Groove Face Seal Assembly	20
11	Koppers Face Seal Assembly	21
12	Seal Interface Pressure Profiles	22
13	Computed Performance of NASA-Solar Spiral Groove Face Seal	24
14	Computed Performance of NASA-Solar Spiral Groove Face Seal	25
15	Effects on Computed Performance of Viscosity and Spiral Groove Depth - NASA-Solar Face Seal	26
16	Test Rig Drive Assembly	30
17	Face Seal Test Rig With Solar-Furnished 37 kW DC Motor	30
18	Water System Schematic	32
19	Seal Rig Buffer Water Supply System	33
20	Endurance Cycle Test	33

LIST OF FIGURES (Continued)

<u>Figure</u>		<u>Page</u>
21	Seal Testing Rig Rotor Shaft in "Performance Test" Configuration With Crane-Design Spiral Groove Runner and One Stationary Seal	34
22	Crane-Design Stationary Seal and Housing Components	35
23	Operating Leakage - Crane Spiral Groove Seals	35
24	Operating Proximity Probe Data Versus Temperature Crane-Design Seals	36
25	NASA-Solar Design Spiral Groove Runner and Stationary Seals	37
26	Static Leakage - NASA-Solar Spiral Groove Seals	38
27	Operating Proximity Probe Data Versus Temperature - NASA-Solar Seals	39
28	Crane (NASA-Solar) Spiral Groove Seal	40
29	Outer Diameter of NASA-Solar Seal Runner, Also Shown in Figure 21, Illustrating the Location of Cavitation Erosion Damage After Initial High Speed Testing	41
30	NASA-Solar Seal Runner After Initial High Speed Testing: Closeup of the Area Between Cooling Holes Showing Cavitation Erosion	41
31	NASA-Solar Atmosphere-Side Stationary Seal Showing Cavitation Erosion After Initial High Speed Testing	42
32	NASA-Solar Seal After Initial High Speed Testing. Closeup of 12 o'clock area of atmosphere side stationary seal showing cavitation erosion.	42
33	NASA-Solar Seal After Initial High Speed Testing. Closeup of 12 o'clock area of vacuum-side stationary seal showing cavitation erosion.	43
34	NASA-Solar Seal After Initial High Speed Testing. Closeup of 6 o'clock area of vacuum-side stationary seal showing cavitation erosion.	43
35	General Arrangement of Modified Crane Housings and New Center Housing for NASA-Solar Seal Assembly	44
36	NASA-Solar Seal Runner After Testing, Close-up of the Area Between Cooling Holes Showing Caviation Erosion	45

LIST OF FIGURES (Continued)

<u>Figure</u>		<u>Page</u>
37	NASA-Solar Seal After Testing, Close-up of 12 o'clock Area of Atmosphere Side Stationary Seal Showing Cavitation Erosion	45
38	NASA-Solar Seal After Testing, Close-up of Atmosphere-Side Stationary Seal Showing Presence of Small Pieces of Epoxy	46
39	Maximum Seal Temperature Rise From Buffer Outflow	47
40	Power Characteristics - Crane NASA-Solar Seals	47
41A	Operating Leakage as a Function of Pressure, Differential and Speed-Forward (Atmosphere) NASA-Solar Seal	48
41B	Operating Leakage as a Function of Pressure, Differential and Speed - Aft (Vacuum) NASA-Solar Seal	49
42	Koppers Test Seal Assembly Components Showing Runner, Housing and One of Two Stationary Seals	50
43	Close-Up of Koppers Carbon Stationary Seal and Secondary Seal Comprising L-Shaped Split Rings and Teflon Sealing Rings	50
44	Operating Leakage Versus Speed, Pressure Differential and Temperature - Koppers Forward (Atmosphere) Seal	52
45	Operating Leakage Versus Speed, Pressure Differential and Temperature - Koppers Aft (Vacuum) Seal	53
46	Power Characteristics - Koppers Seals	54
47	Maximum Seal Temperature Rise From Buffer Outflow (Koppers Forward Seal)	55
48	Maximum Seal Temperature Rise from Buffer Outflow (Koppers Aft Seal)	56
49	Operating Proximity Probe Data Versus Temperature - Koppers Seals	57
50	Koppers Forward Stationary Seal Components After Performance Testing	58
51	Close-Up of Koppers Forward Stationary Carbon Seal Sealing Interface After Performance Testing	58
52	Forward Side of Koppers Runner After Performance Testing	59

LIST OF FIGURES (Continued)

<u>Figure</u>		<u>Page</u>
53	Close-Up of Forward Face of Koppers Runner After Performance Testing	59
54	Aft Side of Koppers Runner After Performance Testing	60
55	Close-Up of Koppers Aft Stationary Seal Sealing Interface After Performance Testing	60
56	Koppers Aft Stationary Seal Components and Center Housing After Performance Testing	61
57	Close-Up of Aft Face of Koppers Runner After Performance Testing	61
58	Corrosion on Outside Diameter of Koppers Running After Performance Testing	62
59	Koppers Face Seal Assembly, Modified	63
60	Koppers Atmosphere-Side (Forward) End Housing After Failure at 71 Hours of Endurance Test	65
61	Close-Up of Figure 60 Housing Showing Failed Anti-Rotation Dowel and Typical Secondary Damage	65
62	Close-Up of Figure 60 Housing Showing Multi-Origin Fatigue on Fatigue on Fracture Surface of One Failed Anti-Rotational Dowel	66
63	Close-Up of Figure 61 Seal Showing One of Two Areas of Pitting on Land Near Proximity Probe	66
64	Koppers Runner Showing Severe Corrosion and Erosion Pitting at Area of Material Removal (for Rotor Dynamic Balancing)	67

LIST OF TABLES

<u>Table</u>		<u>Page</u>
1	Sample Computer Program Output for NASA-Solar Spiral-Groove Face Seal	27
2	Sample Computer Program Output for NASA-Solar Spiral-Groove Face Seal	28
3	Sample Computer Program Output for NASA-Solar Spiral-Groove Face Seal	29
4	Koppers Seal Assembly Endurance Test Results	64

SYNOPSIS

Advanced combined-cycle (COGAS) steam turbine overall system complexity and reliability can profit dramatically from low-leakage seals. The most critical seal locations are the high speed mainshaft seals at the bearings. The optimum seal system was selected as utilizing the feedwater as a buffer fluid. It was further shown advantageous from at least seal performance, life and reliability standpoints to vent the turbine high pressure end also to condenser vacuum. Three candidate late state-of-the-art low/zero leakage face seal assemblies were selected for manufacture and experimental test in a specially-modified test rig. Testing demonstrated that leakage rates from zero to 11 liters/day (3 gal/day) at speeds up to 92 m/sec (310 ft/sec) could be achieved at practical values of buffer pressure. These rates therefore met both the program objective of less than 11 liters/day (3 gal/day). Higher than anticipated parasitic drag was measured. A seal design which overcomes this drag was proposed. Limited cyclic endurance testing was carried out.

ACKNOWLEDGEMENT

This work was sponsored by the U.S. Navy, Naval Sea Systems Command (NAVSEA) under contract N00024-78-C-5345. The Project Engineers were Mr. D. Marron and, latterly, Mr. M. Kandl and Mr. M. Osborne whose continued interest and support are most gratefully acknowledged. The advice, constructive criticism and help offered by Mr. C. Miller (deceased) of NAVSEA and Messrs. G. Carleton and E. Tolles of NAVSECPHILADIV, by Dr. Quandt and Messrs. B. Nield, R. Muensch, P. Bernhardt, G. Duval, and K. Sasdelli of the NSRDC Power Systems Lab at Annapolis, MD, and by Messrs. W. Anderson (retired) and L. Ludwig (deceased) of NASA-Lewis, Cleveland, OH are greatly appreciated. The assistance of Messrs. J. Sedy and A. Zobens of Lane Packing Company, Morton Grove, IL and Messrs. E. Taschenberg and J. Heck (retired) of Koppers Company, Baltimore, MD is also gratefully acknowledged. Appreciation is likewise extended to Dr. P. Stein (deceased) and Mr. E. Goldring, Stein Seal Company, Philadelphia, PA, Mr. R. Almeida, Sealol Corp., Providence, RI, and Messrs. R. Wentworth and O. Giles, Borg Warner Corp. Temecula, CA.

SUMMARY

Two face seal assemblies, one manufactured by Crane using a spiral groove configuration and the other by Koppers, met program leakage goals of less than 11 liters/day (3 gal/day) at peripheral speeds up to 90 m/sec (300 ft/sec). Both used feedwater-supplied buffer water as required by advanced combined cycle steam turbomachinery. It was shown to be advantageous, at least from seal performance, life and reliability standpoints, to vent the turbine high pressure end also to condenser vacuum.

Limited cyclic endurance testing based on a typical destroyer mission profile was carried out.

Higher-than-anticipated parasitic drag and cavitation erosion damage were encountered at the upper end of the speed range. Both of these effects were caused by using a flooded runner (in the buffer water). A further design innovation of the spiral groove seal was proposed to circumvent both problems. This involved venting the outer area of the seal chamber also to the condenser vacuum and supplying the buffer water through internal passages in the stationary seal.

The proposed spiral groove seal design that eliminates flooding of the runner was not built and tested. However, test results on the present seal configurations gave confidence in the design since all cavitation damage encountered appeared to occur as a result of the runner outer circumference being flooded. The seal interface of the vacuum side in the testing showed no indication of cavitation damage.

The results of this program are illustrated in Figures 1 through 3.

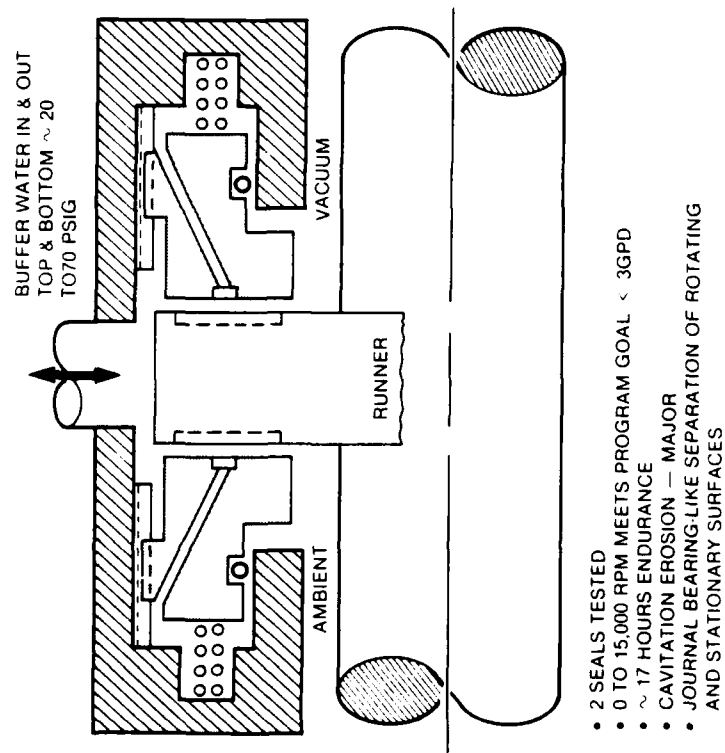
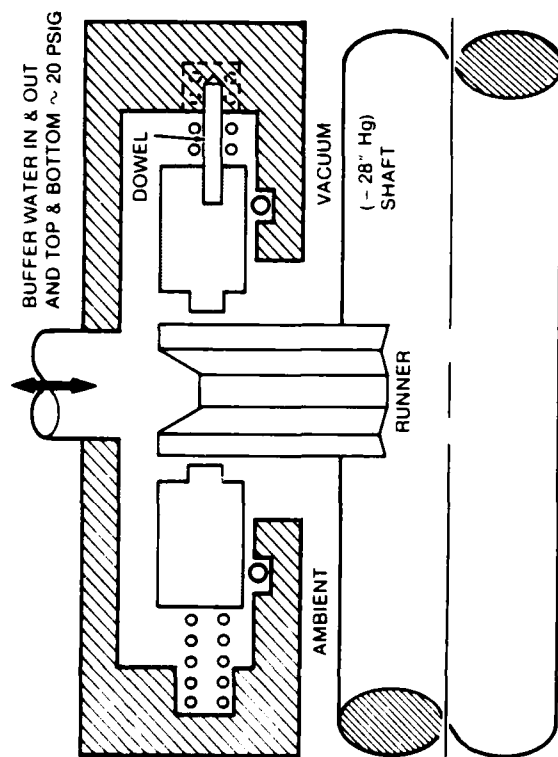


Figure 1. Crane (NASA-Solar) Spiral Groove Face Seal



STATUS

- 2 SEALS TESTED
- 0 TO 15,000 RPM LEAKAGE MEETS PROGRAM GOAL < 3GPD
- 70 HOURS OF ENDURANCE CYCLING ~ 15 HOURS @ 15,000 RPM
- PINS FAILED
- SOME CAVITATION EROSION



Figure 2. Koppers Face Seal

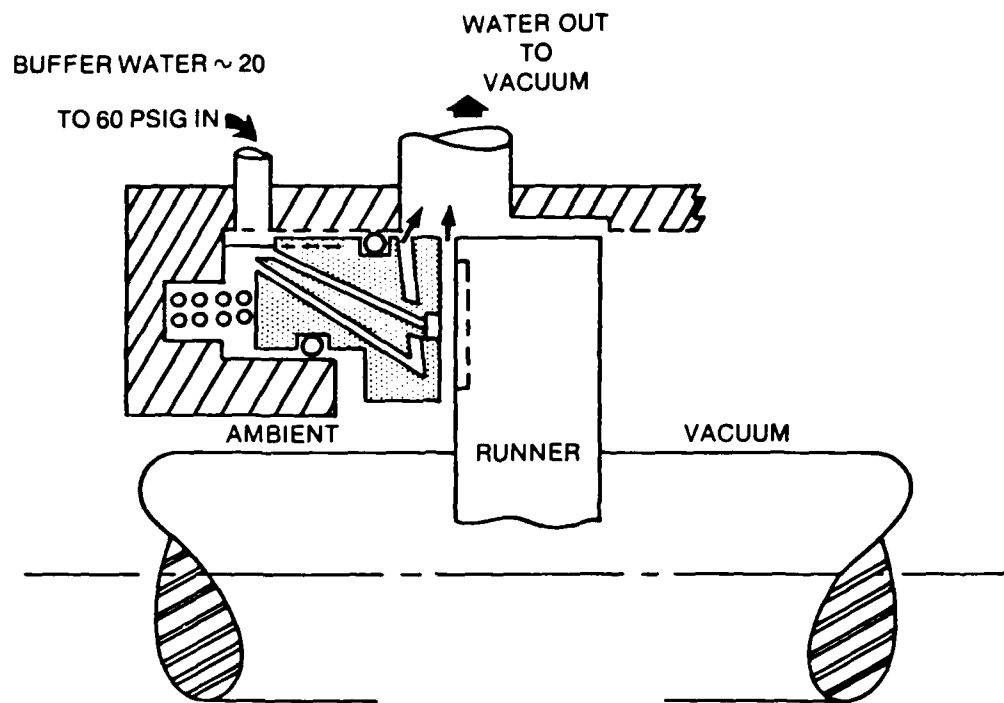


Figure 3. Modified Spiral Groove Seal

1

OBJECTIVE

The objective of this program was to adapt the latest state-of-the-art low leakage seal technology to seals of advanced combined-cycle (COGAS) steam turbines for U.S. Navy shipboard application. The purpose was to reduce system water loss to a minimum and thereby minimize make-up water requirements and water treatment system complexity. Conduct of this program in advance of the steam turbine detail design would allow the results to be factored into the overall design on a timely basis.

2

PROGRAM APPROACH

- . Establish steam turbine seal design criteria including the impact of projections of leakage rates over the anticipated turbine life on feed-water make-up system requirements.
- . Review sealing state-of-the-art.
- . Establish the most critical seal application.
- . Design and fabricate low-leakage system(s) and seals in consultation with recognized leading seal manufacturers. At least three candidate test seals would be procured.
- . Establish an experimental test facility by modifying an existing turbo-machinery test rig for realistic evaluation.
- . Conduct experimental tests, including performance and endurance running and acquisition of appropriate data, to determine the best suitable configuration for the turbine seal system.
- . Prepare design guidelines to facilitate the incorporation of that system in the actual turbine.

3

INTRODUCTION

Water treatment complexity and reliability remain primary obstacles to the introduction of combined cycles in the small (3 to 15 MW) marine, naval and industrial engines. After 40 years of development "modern steam practice" still requires complex water chemistry to control pH, O_2 and dissolved solids in the feed water and boiler steam drum. Figure 4 shows a conventional steam plant. Water chemistry must be carefully balanced to prevent corrosion in the mild steel system, scale deposits in the boiler and foaming in the steam drum. Chemicals are often added on a daily basis to maintain the system within closely monitored and controlled limits. As a consequence "blowdown" of the boiler water is necessary to keep the total dissolved solids down to acceptable limits (1500 ppm). If salt water seepage occurs in the condenser, or the makeup water has high dissolved solids, continuous blowdown may be required.

In addition to makeup water required to replace blowdown, turbine gland seal leakage, sootblower steam flow, deaerating feedheater vent losses, feedpump shaft seals, and air ejector condenser vent losses are common sources of water loss requiring makeup water. Systems with total leakage of over five percent of the steam rate have been reported.

Small steam plants incorporating conventional technology have many limitations that make them less competitive for Naval combined cycle applications. Such units should ideally have unattended operation capabilities. This would include no requirements for supplies of chemicals for water treatment and for specially trained personnel. Further, conventional systems are bulky, expensive, and have slow start-up characteristics and complex controls, particularly as compared to the gas turbine units with which they are to be integrated.

One possibility for an attractive system involves a once-through steam generator and a water treatment strategy requiring no "active" chemical additions. As a first approximation it can be assumed that most of the dissolved solids that are in the feedwater of a once-through boiler will deposit on the tubes. Therefore dissolved solids must be kept at very low levels (<0.1 ppm TDS) to prevent rapid scale build-up. Supercritical boiler practice, automotive compact boiler development work, and some nuclear power plant practice have indicated that modern mixed-bed de-ionization (DI) resins can be used to maintain dissolved solids below this limit. Since no chemicals are added to the boiler water in this process, it appears to the operator as a "passive" system particularly if the DI beds do not require frequent regeneration or replacement. Water is passed through the bed of resins and dissolved solids are removed without any action required of the operator. If the system leakage can be maintained sufficiently low, a relatively small

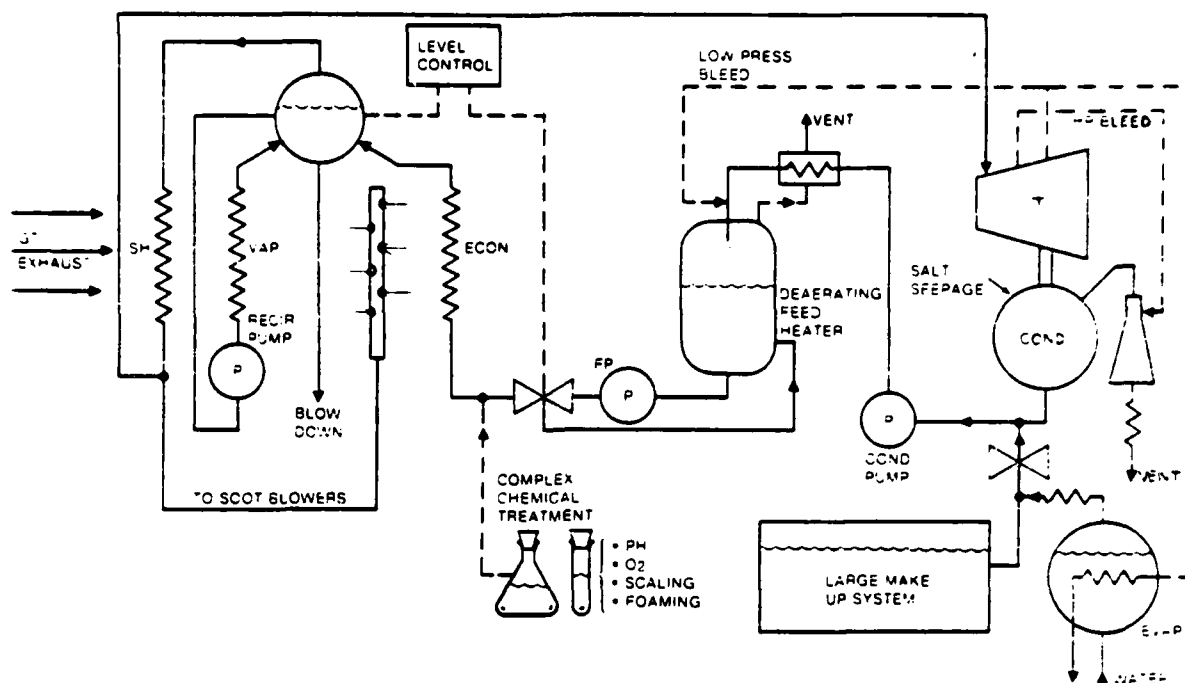


Figure 4. Conventional Steam Systems

volume of (low cost) resins can be used. As they are used up they can either be recycled back to the supplier or scrapped. Such an approach should be feasible for leakage rates as high as one percent of steam flow. Figure 5 illustrates such a system.

With state-of-the-art technology a "tight" system can be obtained in which once-through shaft leakage causes virtually all of the makeup feedwater requirements and consequent requirements for evaporators, storage tanks, DI bottle sizes, and replacement periods can be eliminated or possibly reduced to negligible factors. By elimination of large quantities of steam mixed with the air, the seal vent condenser can be eliminated and the problem of having to deaerate large quantities of water per minute would be eliminated. A much lower level of dissolved oxygen may also be obtainable with minimal air to water mixing. Modern closed-cycle refrigeration systems are examples of large scale systems where "makeup" has become a negligible problem. No fundamental physical breakthroughs are necessary to achieve these goals with the steam systems.

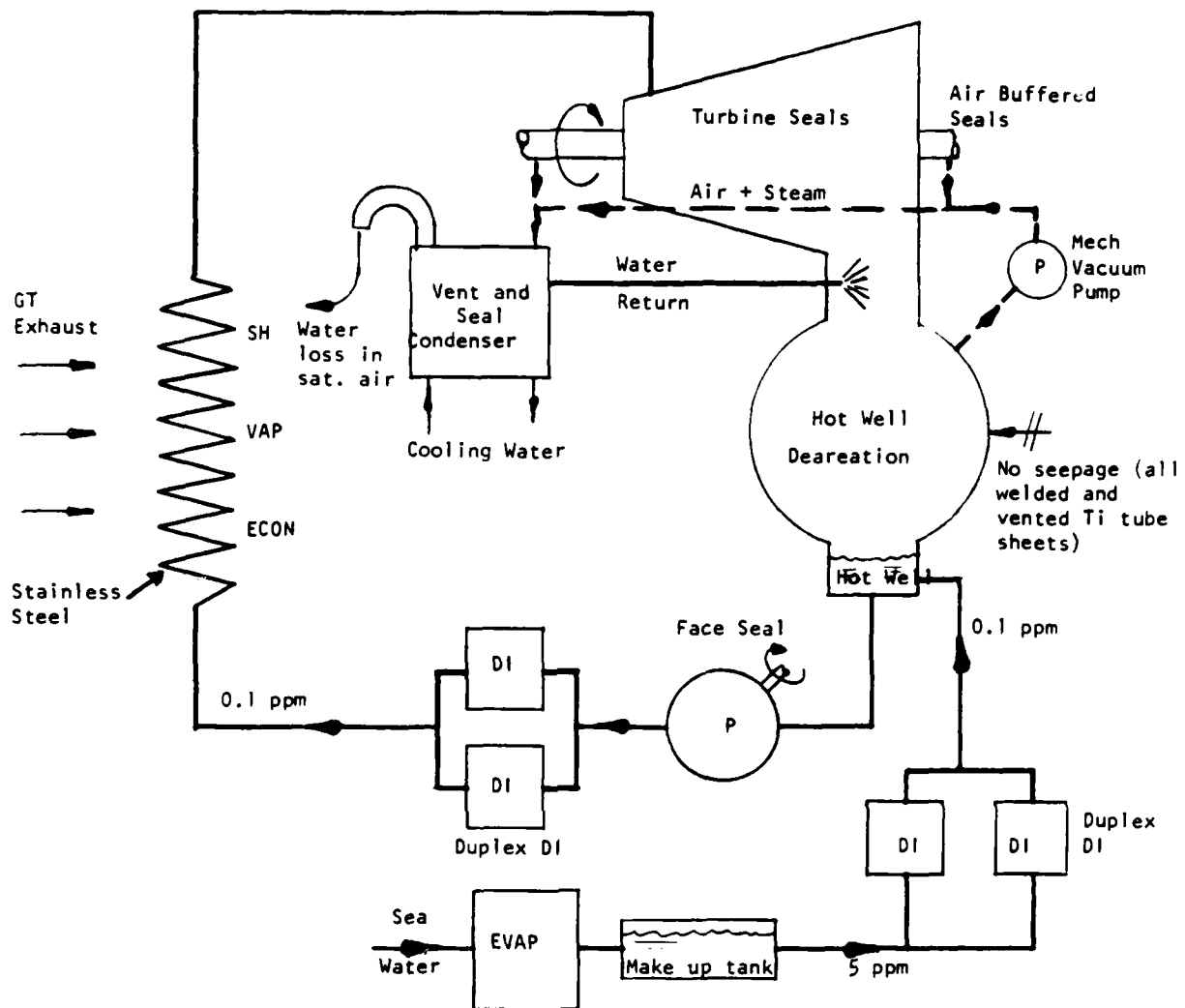


Figure 5. Automatic Water Treatment System for One Percent Make-Up

4

INVESTIGATION

4.1 SEAL SYSTEM DEFINITION

The optimum combined cycle turbine overall seal system configuration was chosen to be one having a buffer fluid. This is a proven approach in steam turbines, gas turbine engines, and (natural) gas boost compressors to minimize or eliminate loss and contamination of the process fluid. There are three logical choices of buffer fluid which, if mixed through leakage with the process water/steam, would not decompose in the superheater at 480°C (900°F). One is air which already has to be eliminated from the system and whose use, therefore, would place an added burden on the deaeration equipment. The second, process steam, would incur considerable complication, e.g. insulation requirements, to ensure that the steam did not condense in the seals and present difficult-to-handle two-phase flow conditions. Further, the presence of high-temperature steam in close proximity to the bearings could create adverse heat transfer problems for them as well as raise the possibility of large temperature gradients in the vacuum-end seals and associated components. This would render very difficult maintenance of the degrees of squareness and flatness necessary for proper operation of low leakage seals. The third, and considered most attractive, is the feedwater itself. The optimum point in the overall system to obtain the water would be from the condensate (boost) pump outlet where the pressure would, according to present system concepts, be more than adequate and the temperature would be at the system minimum, that is, as low as 33°C (92°F). At this temperature the potential for cooling is greatest, there would be no need for insulation of the buffer fluid lines and passages, the potential incorporation of water-lubricated bearings would be most facilitated, cycle efficiency loss effects would be minimized, and the technology "jump", compared to the use of steam, would also be minimal. Items which require attention would be avoidance of cavitation and boiling of the water at any interface with the condenser vacuum.

4.2 TEST FACILITY

An available test rig drive unit and speed control used previously for seal evaluations was nominated for the COGAS steam turbine seal work. A cut-away drawing of it is shown in Figure 6. Figure 7 shows a schematic of the test rig. Double face seals are shown since they were considered at least promising candidates to attain the target values of leakage and they were thought to require the most space. Figure 8 shows the detail design of the seal test chamber. It was originally intended to endurance test two seal assem-

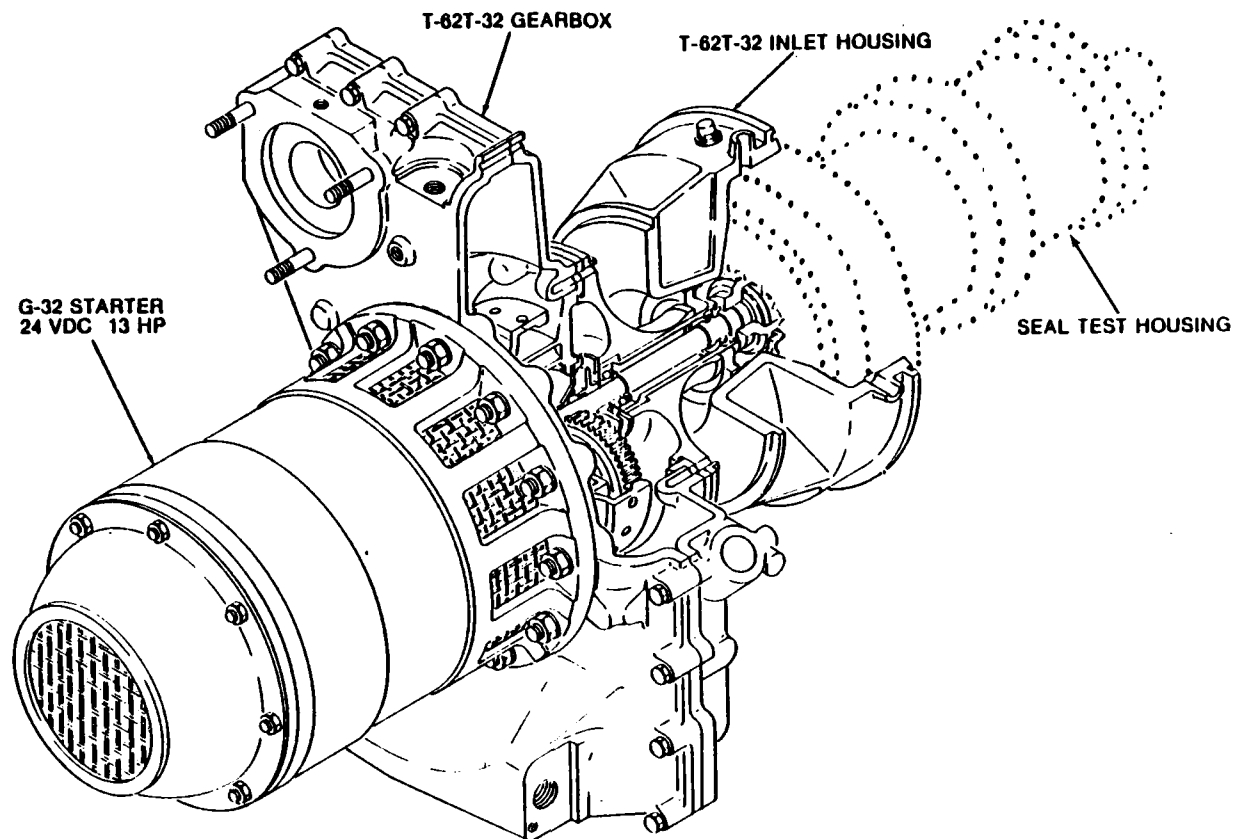


Figure 6. Seal Test Rig

blies simultaneously in a tandem rig but during the initial testing the power requirements were found excessive for the motor.

A closed-loop water circulation system was designed for integration with the test rig to provide the buffer system. The closed-loop configuration was selected for several reasons: comparative ease of water chemistry control, more accurate measurement of flows and leakage rates, and conservation of water. This system was also integrated with the vacuum pump. System flow and pressure was maintained by a two-pump assembly, one of which was powered by a variable speed drive for overall system flow control. The potential vacuum pump requirement to handle (liquid) water leaking past the test seal(s) into the vacuum chamber dictated that the pump be of the liquid-ring type and, for the purposes of leakage flow measurement and cooling, that it be wholly connected into the system. Sufficient flow measurement plumbing connections to two rotameters were provided to permit, together with collection-type measurements, accounting for all the system water (volume) and flows. Pressure and temperature regulators were included as appropriate for system control and untended operation during the endurance-test phase of the program. Additional plumbing lines were provided to permit some individual variation in buffer flow without affecting pressure, as might be required for purposes of heat rejection studies. In addition, the water tank could be sealed and

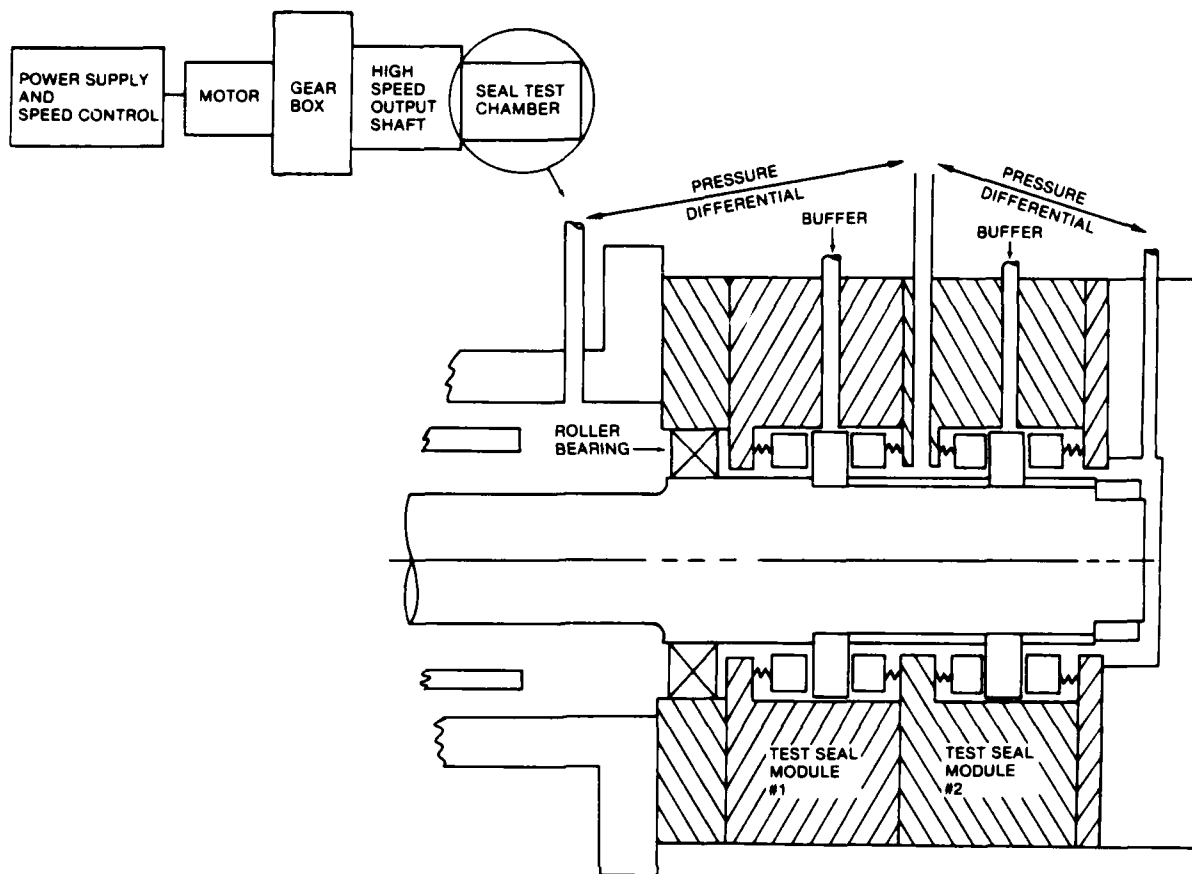


Figure 7. Turbine Seal Test Rig Schematic

bottled nitrogen bubbled through it at a slight pressure for purposes of de-oxygenation.

The instrumentation employed with the testing comprised:

- . Iron-constantan (Type J) thermocouples and a series 400A "Trendicator" acquisition system with Model 405A multi-point selectors.
- . International Technical Industries miniature magnetostrictive pressure transducers (which never functioned properly in the water "environment").
- . Bently-Nevada 190 series and special 28918-01 proximity probes and Model 3106-2800 "proximitors" (driver-detectors).
- . Tektronix Model 5103N oscilloscopes with (in varying combinations):
 - Model 5A15N amplifiers
 - Model 5A18N dual-trace amplifiers

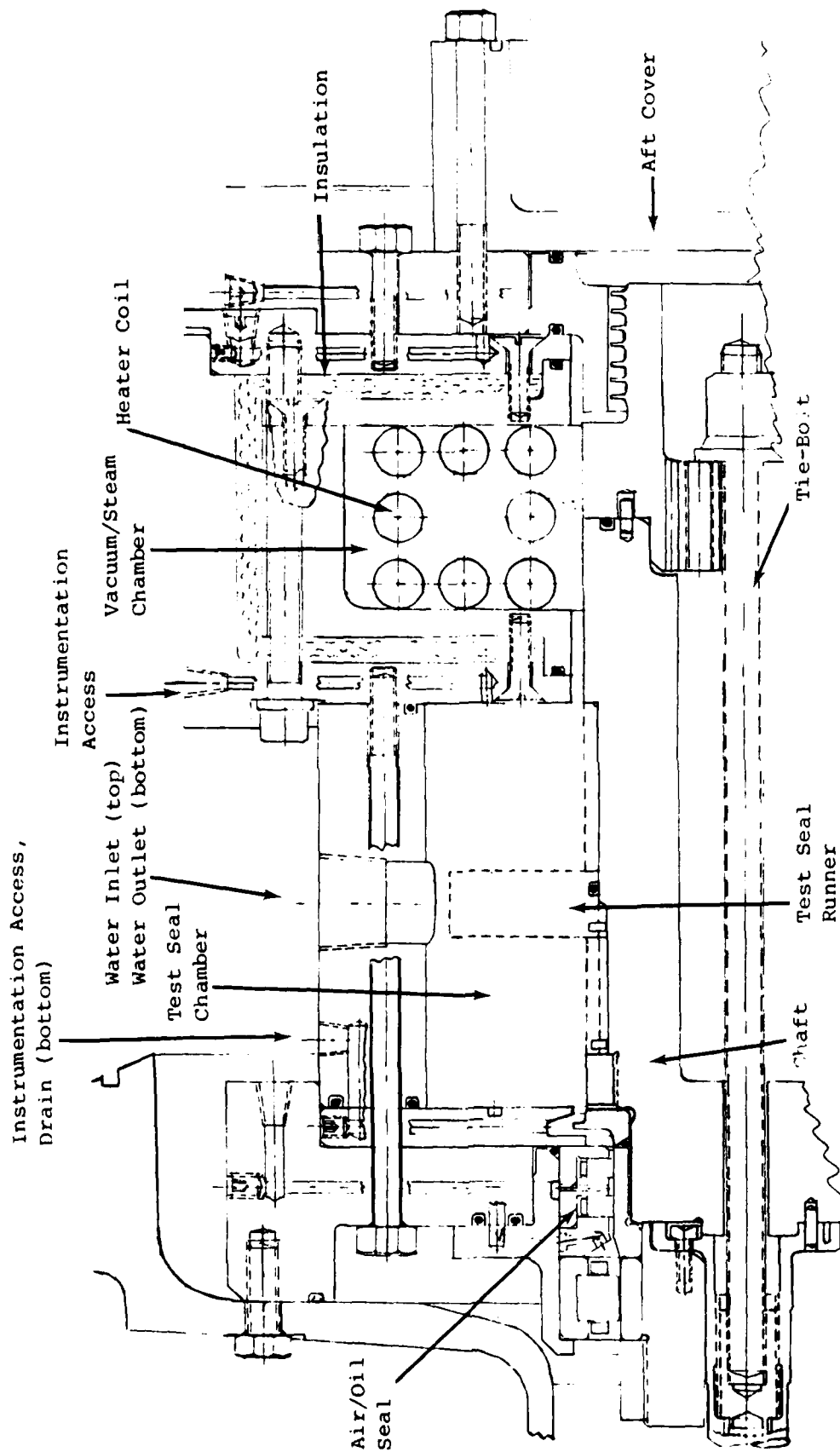


Figure 8. Seal Test Rig - Single Seal, Performance Test Configuration

- Model 5A14N 4-trace amplifier
- Model 5B10N time base
- . Ashcroft bourdon-tube, glycerine-filled pressure gages
- . Eldorado Model 225 digital frequency counter (speed indication)
- . Weksler compound pressure/vacuum gage, 0-30 in. Hg, 0-30 psi
- . Brooks Instrument, Division Emerson Industries Model 1110-09H3B1A and Model 1110-08H2B1A rotameters
- . Mid-West Instrument Company Model 111S differential pressure gage
- . Pacific Chromalox Model ARTMS-1000 thermostatically-controlled heater (in water tank).
- . Fluke Model 8000A digital multimeter

4.3 DESIGN CRITERIA

The design criteria and constraints established for and by the rig and closed-loop water system were:

- . shaft nominal diameter - 70 mm (2.75 in.)
- . nominal rotational speed - 15000 rpm
- . seal nominal mean surface speed - 90 m/sec (300 fps)
- . vacuum (sealed) - 38 mm (1.5 in.) Hg, abs.
- . bearing sumps (sealed) - atmospheric with turbine-type lubricant at bearing-generated temperatures
- . water flow, approximate maximum - 32 liters/min. (8.5 gpm)
- . simulation of actual operating conditions
 - intended seal life - 15000 hours
 - target leakage, total - less than 11.5 liters/day (3 gal/day)
 - starting - steam turbine practice
 - from windmilling idle
 - unloaded
 - emergency
 - speed range and changes comparable to prime mover (gas turbine) power turbine

- shutdown - steam turbine practice
 - potential for gas turbine-type practice
 - emergency
- static sealing capability
- . scalability for potential turbine uprating

4.4 CANDIDATE SEAL DESIGNS

Proposals were obtained from five leading seal manufacturers:

Borg-Warner, Temecula, CA
 Crane Packing Co., Morton Grove, IL
 Koppers Co., Baltimore, MD
 Sealol Corp., Providence, RI
 Stein Seal Co., Philadelphia, PA

Their submittals are shown in Appendices I-1 through I-5. After careful consideration of the relative merits of each and a parallel review by NAVSEA personnel the vendors and configurations below were selected for manufacture and testing. The candidates selected were double face seals since these offered the greatest promise for achieving target values of leakage with what was considered a conservative approach and thereby maximizing reliability potential. The face seal configuration features a (rotating) runner which is virtually identical to a hydrodynamic thrust bearing runner. A carbon stationary member is loaded against it by springs and, during operation, also by a second force arising from differential pressures and areas. For use in the buffer seal system selected for investigation here, two stationary seals were arranged on either side of the runner and the water buffer fluid confined in the area radially outward of these components, as shown in Figure 9. The flow of buffer water, obtained from the condensate boost pump, could be prescribed at any value required for adequate cooling.

Type 1. Crane Packing Co. - double spiral-groove face seals (Crane design)

- ambient side - "outward-pumping" seal with shallow spiral groove pattern on the runner to create a pumping action and pressure differential sufficient to oppose radially inward leakage of the buffer water. Any buffer water leakage at this seal interface constitutes a loss of system water.
- other side - "inward pumping" seal with shallow spiral groove pattern on the runner to create a pumping action and pressure rise to a value equal to or slightly greater than the sealed pressure.

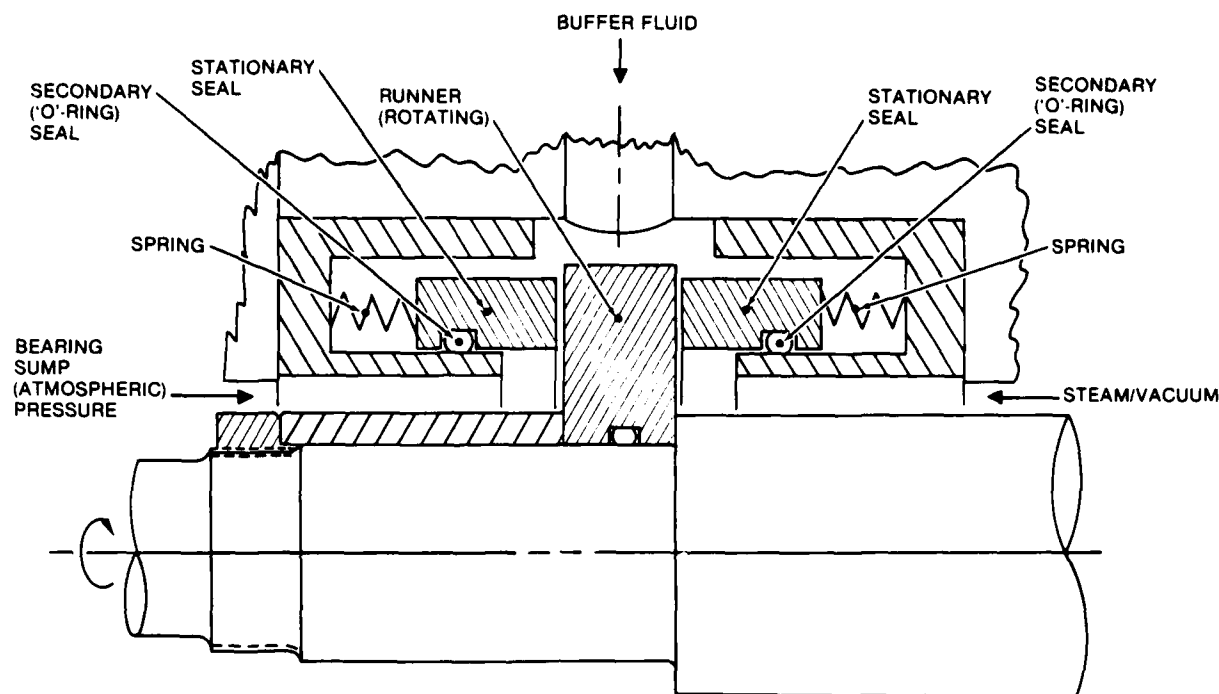


Figure 9. Example Face Seal Arrangement for Buffer Seal System

- Solar source control drawing RSK 230832, pages 1, 2 and 3 (shown in Appendix II-1) show the finalized design including interface details with the rig seal test chamber. A single runner and two pairs of stationary seals were procured, one pair of the latter with instrumentation passages. (This assembly underwent only limited testing because of a build error and a determination that system performance and reliability would be greatly enhanced by venting the seals at both ends of the steam turbine rotor to the condenser vacuum.

Type 2. Crane Packing Co. - double spiral groove face seals (NASA-Solar design).

- "outward-pumping" seals with slightly deeper spiral groove pattern than 1. above on both faces of the runner and with hydrostatic buffer water supply to create a pumping action and pressure rise to oppose buffer water leakage to atmosphere (external loss from system) and to the vacuum side; buffer pressure somewhat greater than ambient.
- Solar source control drawing RSK 230832 pages 1, 4, and 5 (in Appendix II-1) show the finalized design including interface details with the rig seal test chamber. This assembly utilized common housing components with 1. above.

A single runner and one pair of stationary seals with instrumentation passages were procured. Figure 10 shows a labelled cross-section of this assembly complete with instrumentation.

Type 3. Koppers Co. - double face seals.

- nominally rubbing-contact seals which limit radially-inward leakage of buffer water at a higher pressure than ambient for both ambient-side and vacuum-side interfaces.
- Solar source-control drawing RSK 230833 (Appendix II-2) shows the finalized design including interface details with the rig test seal chamber. A single runner and two pairs of stationary seals with instrumentation passages were procured. Figure 11 shows a labelled cross-section of this assembly complete with instrumentation.

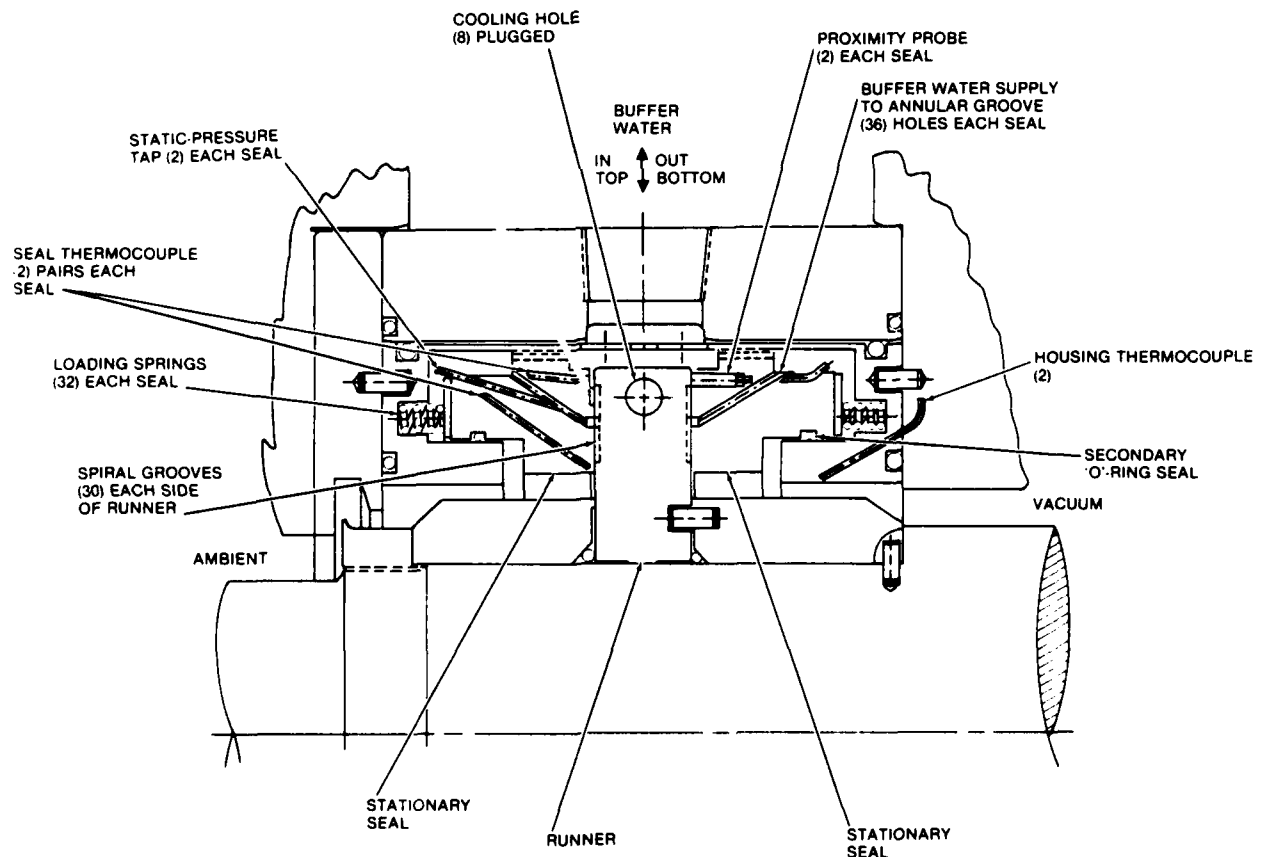


Figure 10. NASA-Solar Crane Design Spiral Groove Face Seal Assembly

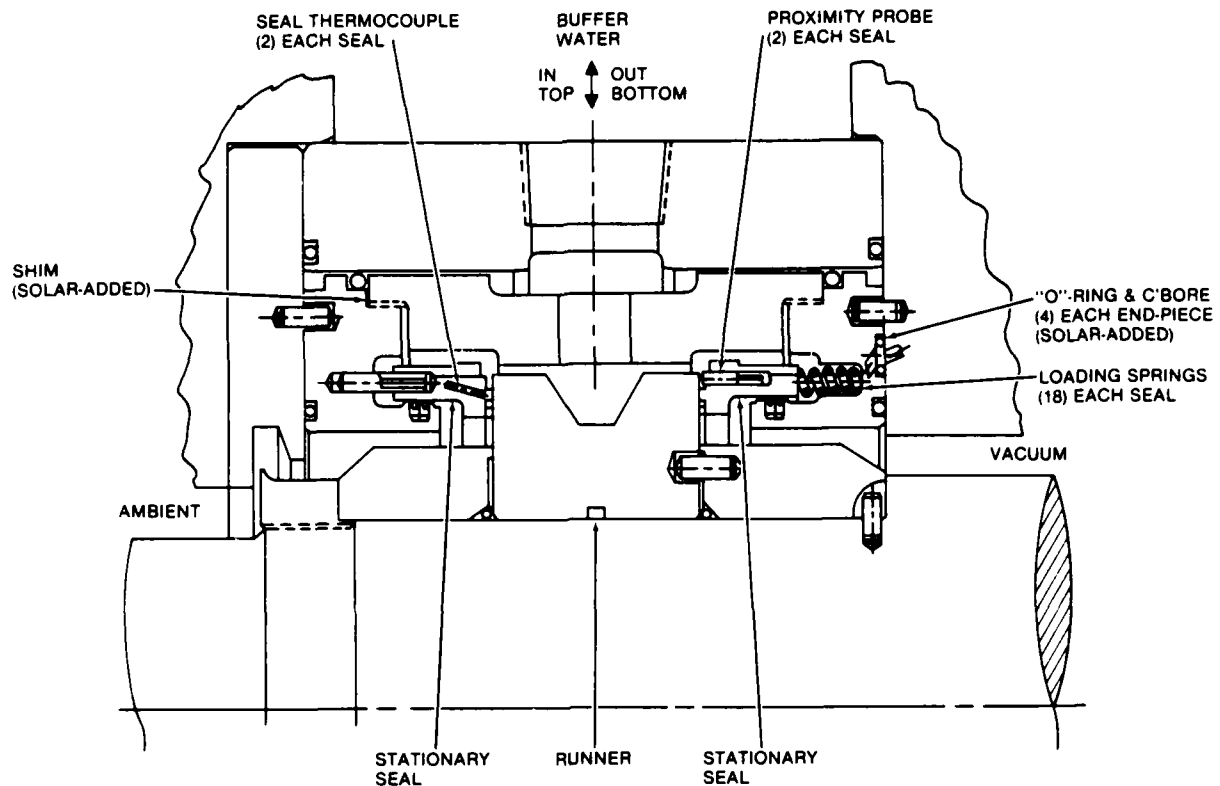
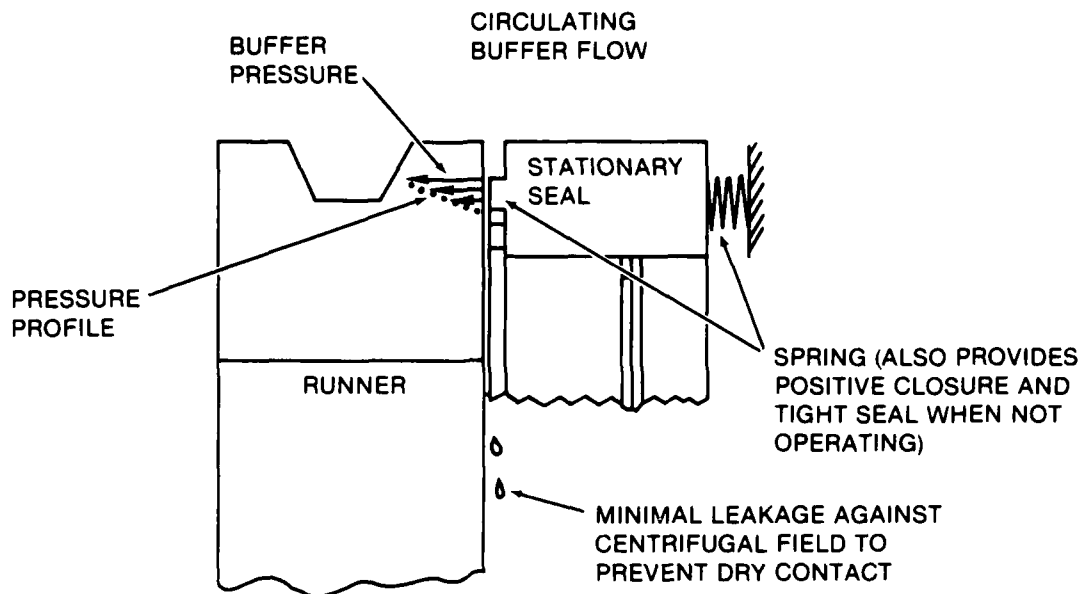


Figure 11. Koppers Face Seal Assembly

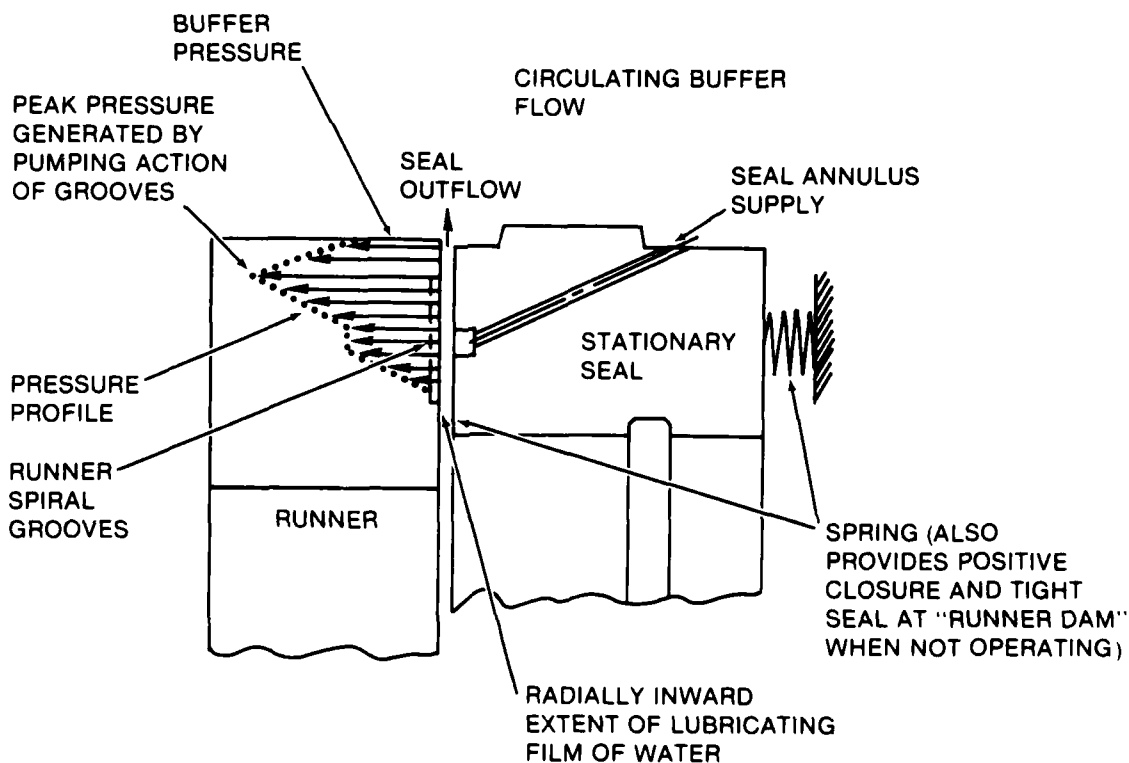
4.5 DESIGN CHARACTERISTICS OF NASA-SOLAR AND KOPPERS SEALS

Figure 12 shows the generalized pressure profile at the interface between the runner and the stationary member of the NASA-Solar spiral-groove and Koppers seals under evaluation. The NASA-Solar configuration (pioneered for liquid sodium applications in water-lubricated testing by NASA) can produce true zero leakage at turbomachinery speeds over a wide range of operating conditions, as demonstrated in oil-lubricated testing conducted previously by Solar at least. Also, operating lubricant film thicknesses can be somewhat greater than with other face seal types, thereby reducing sensitivity to foreign material and/or component accuracy requirements and tending to reduce heat generation. All of these factors, of course, would augur well for the extended lives intended for these seals.

Within the envelope size of the Crane-design components, the NASA-type seal was configured to operate (i.e., produce zero leakage) at least up to a pressure differential of 345 kPa (50 psi) at 15,000 rpm at a minimum film thickness (separation of rotating runner and stationary member) of 0.023 mm (0.0009 in.) and temperature rise of 5.5-11°C (10-20°F) due to shear losses in the interface water lube film. At 5,000 rpm the pressure differential capability would be at least 170 kPa (25 psi) at a film thickness of 0.015 mm (0.0006 in.). With a different (higher) spring loading, the maximum



**INTERFACE AREA OF KOPPERS
FACE SEAL**



**INTERFACE AREA OF NASA — SOLAR
SPIRAL GROOVE FACE SEAL**

Figure 12. Seal Interface Pressure Profiles

pressure differential at 15,000 rpm could be increased to at least 585 kPa (85 psi) at a film thickness reduced to about 0.017 mm (0.00065 in.) and with a temperature rise of about 14C° (25F°). Operation at a film thickness of 0.017 mm (0.00065 in.) would still be as intended, at values similar to the minimum film thicknesses in standard oil-lubricated journal bearings. Figures 13, 14 and 15 and Tables 1, 2 and 3 show sample results from a Solar-developed computer program for the analysis of this type of spiral groove seal.

The Koppers "rubbing contact" face seal design also features two stationary carbon members lightly loaded with 96 N (21.6 lb) against either side of a rotating runner but with a comparatively narrow annular sealing land on each. The operating film thickness with this type was expected to be of the order of 0.0025 mm (0.0001 in.), i.e., in or close to the "boundary" lubrication regime. The leakage rate was estimated to be 3.3-5 cc/min (1-2 gal. per day) at the 586 kPa (85 psig) pressure differential and was the lowest of all the outside-vendor proposals.

It is believed that the selected candidate test seals, together with the water buffer system, provided an excellent spectrum of possible approaches to the long-life low leakage sealing requirements of advanced combined cycle steam turbomachinery. Furthermore, it was anticipated that this investigation would provide design choices rather than be simply an elimination process.

4.6 TEST SET-UP

4.6.1 Test Rig

Figure 16 illustrates the test rig drive assembly. Figure 17 shows the whole test rig with the 37 kW (50 hp) motor procured for this program when it was found that the original 10 kW (13 hp) motor was inadequate.

Wetted stationary parts were made of AISI 304 stainless steel and shaft components of 17-4 PH stainless steel. Other parts were made of black-oxidized AISI 4340 steel.

The variations in test rig speed, simulated condenser vacuum, and buffer water temperature for untended operation were produced by a Research Inc. Model 73211 microprocessor programmer as follows:

- . rig drive motor speed variations by "ramped" millivolt signal to appropriate input in motor SCR controller.
- . vacuum variations by opening and closing solenoid valves in parallel lines with vacuum regulators at appropriate settings leading to vacuum pump inlet.

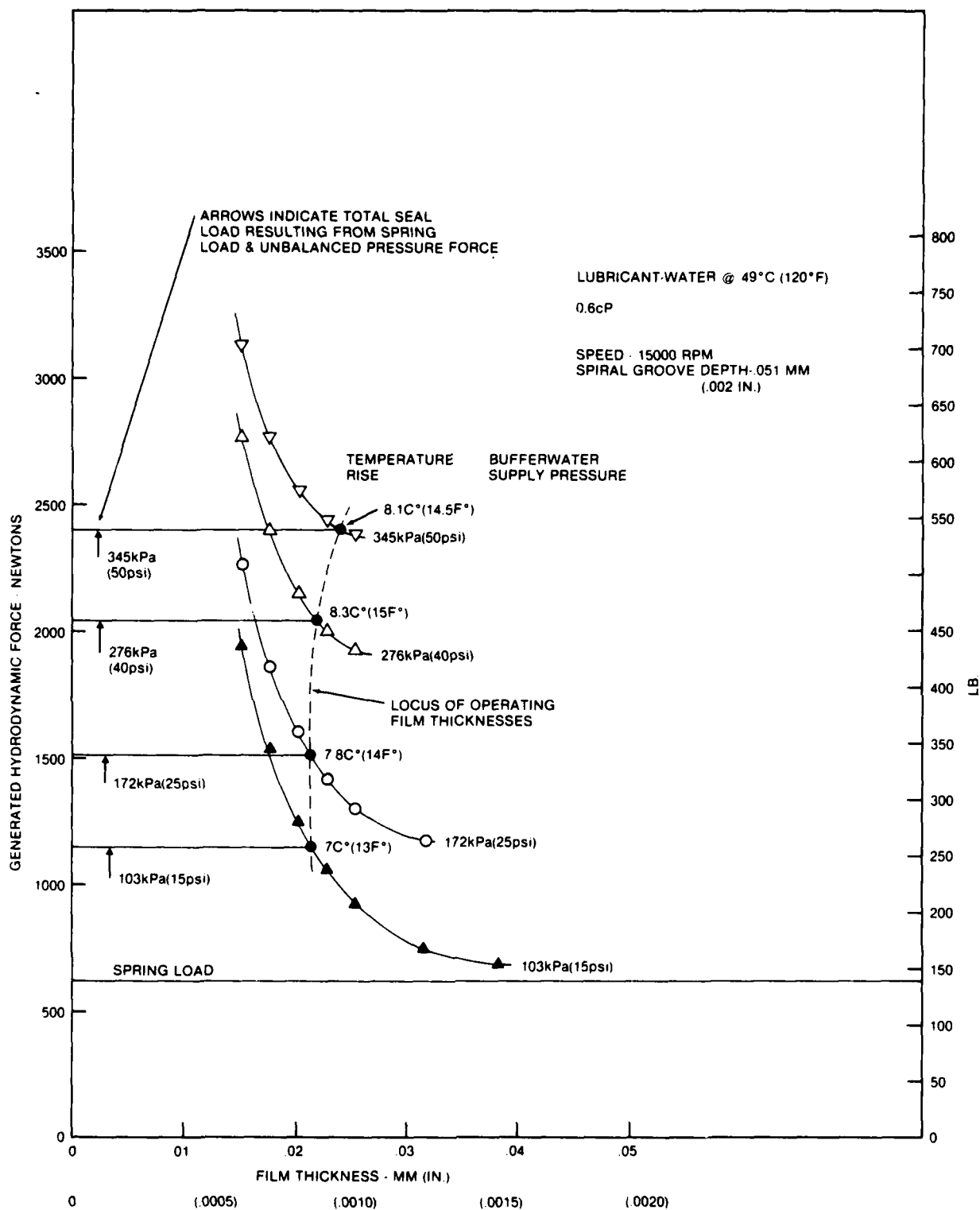


Figure 13. Computed Performance of NASA-Solar Spiral Groove Face Seal

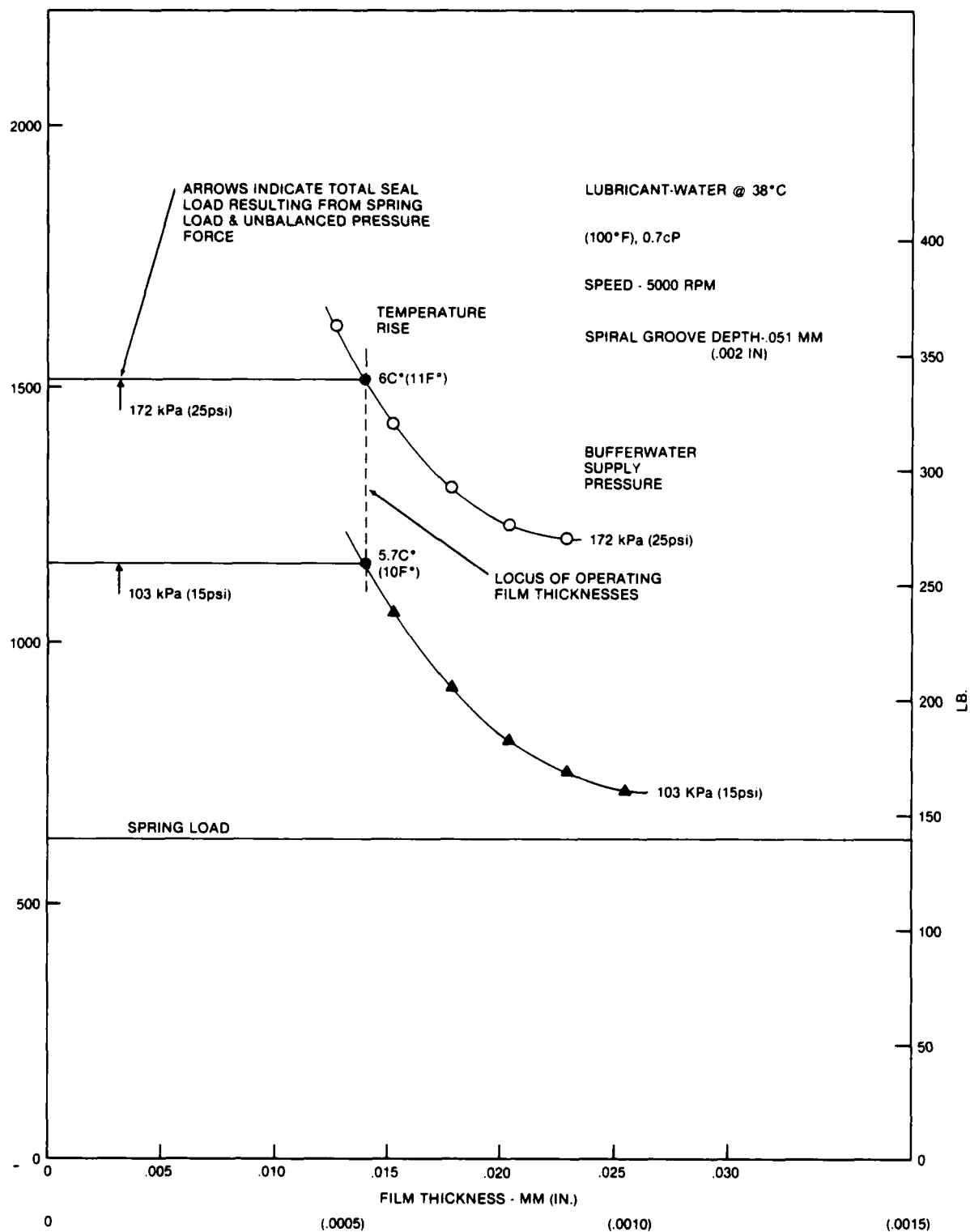


Figure 14. Computed Performance of NASA-Solar Spiral Groove Face Seal

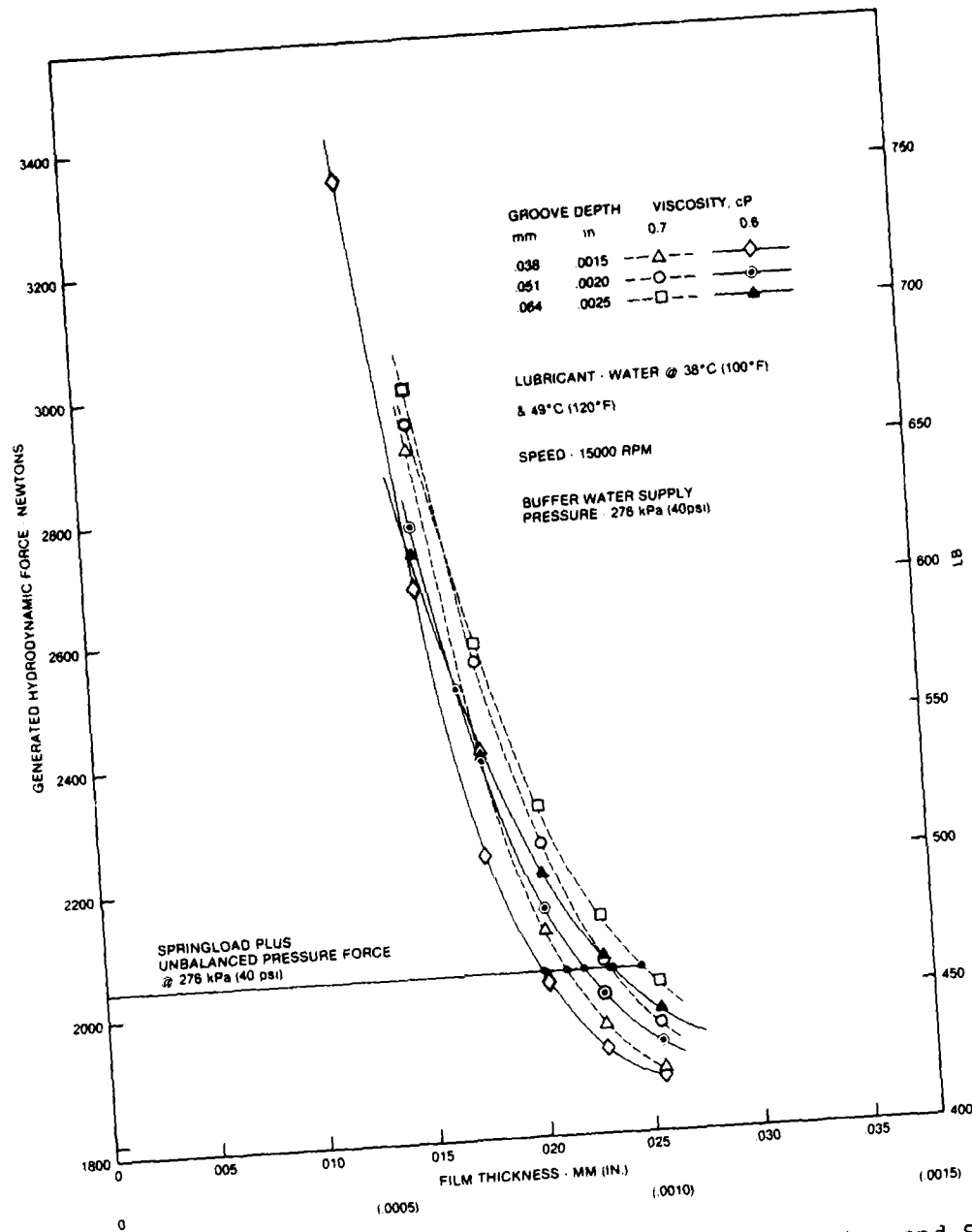


Figure 15. Effects on Computed Performance of Viscosity and Spiral Groove Depth - NASA-Solar Face Seal

- buffer water temperature variations by opening and closing solenoid valves in parallel lines with valves at appropriate settings leading to heat exchanger.
- Buffer water pressure variations by "ramped" millivolt signal to a Fischer pneumatic valve feeding the dome of the system pressure regulator.

Sample Computer Program Output for NASA-Solar
Spiral-Groove Face Seal

PLOT

Table 2

Sample Computer Program Output for NASA-Solar
Spiral-Groove Face Seal

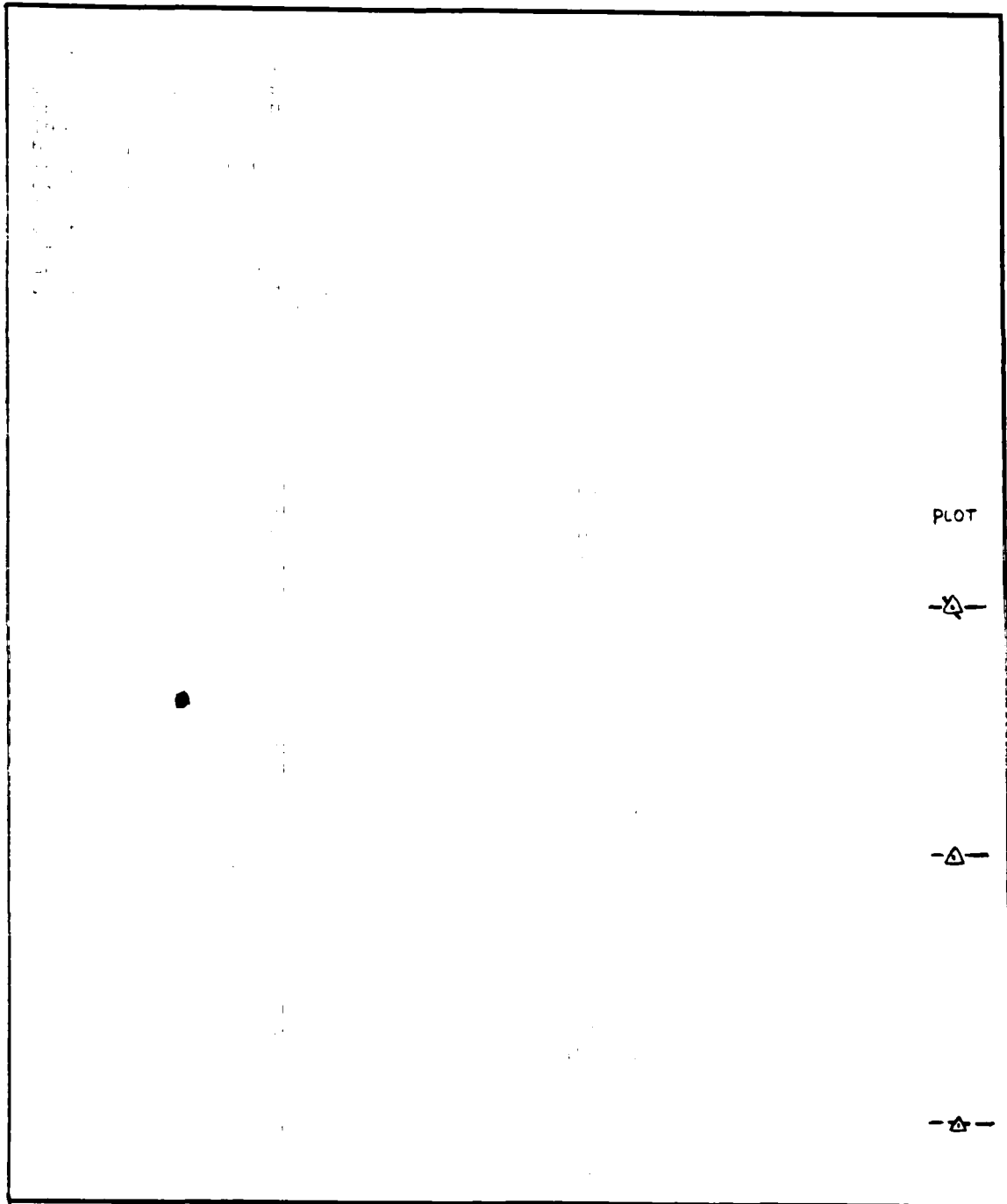
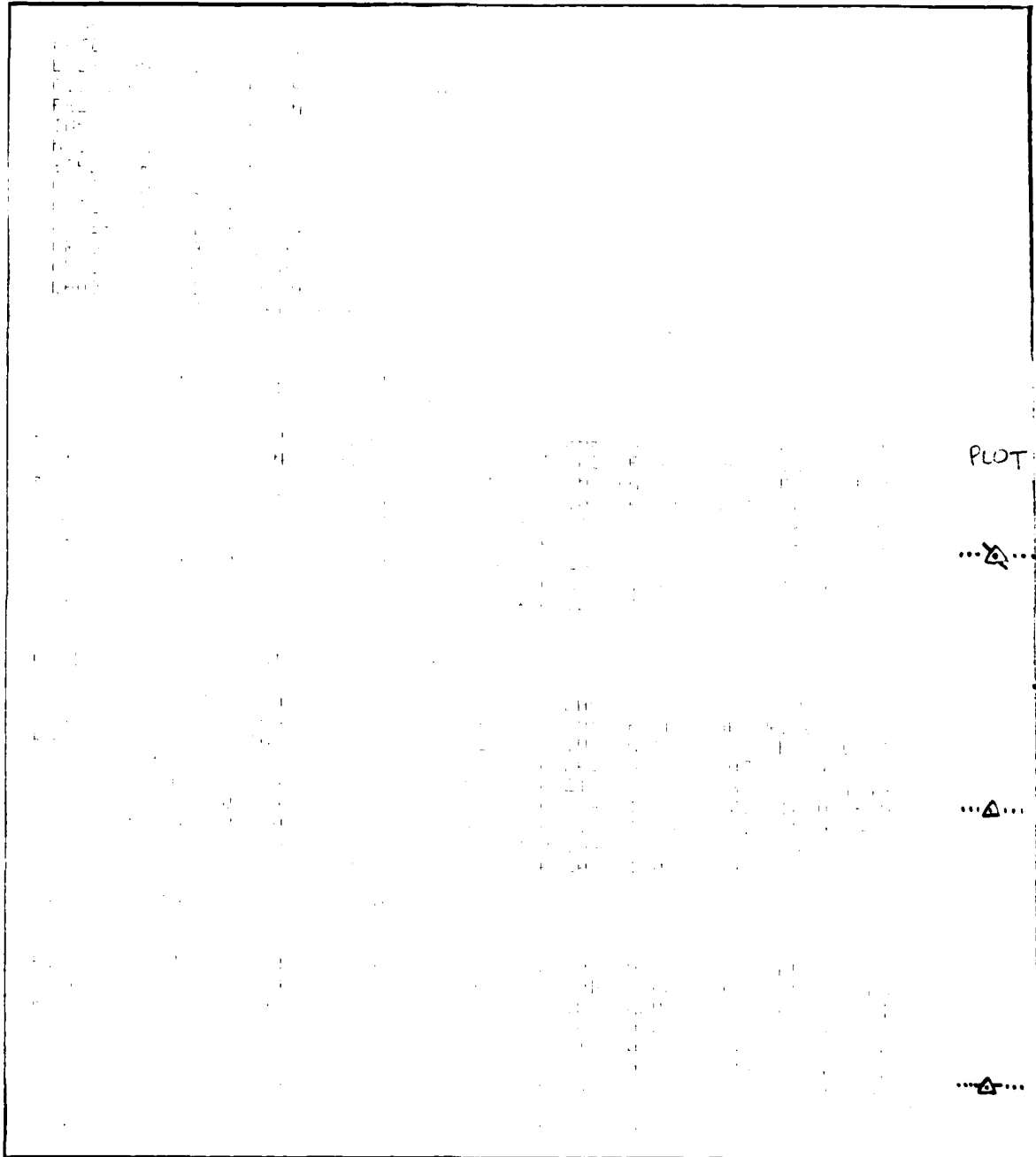


Table 3

Sample Computer Program Output for NASA-Solar
Spiral-Groove Face Seal



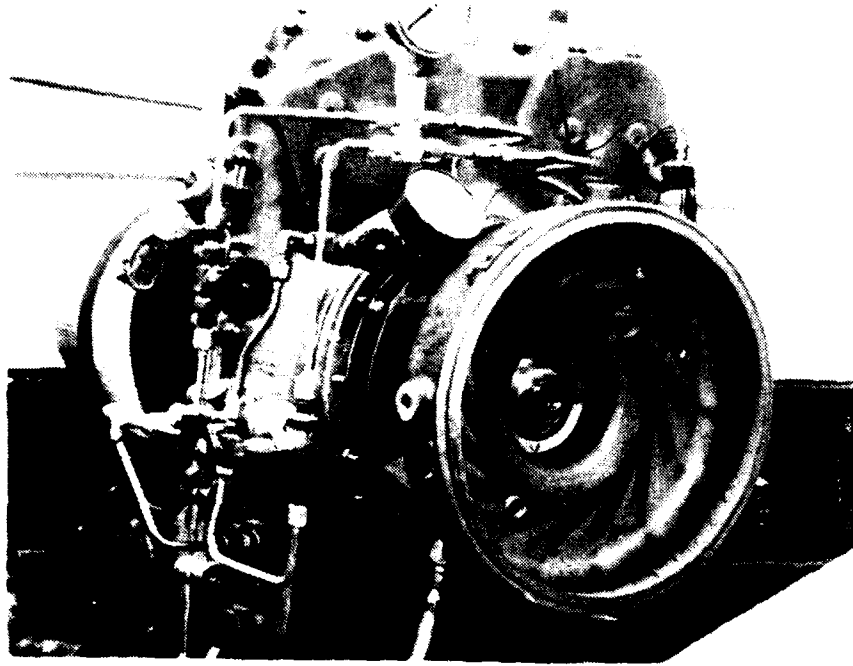


Figure 16. Test Rig Drive Assembly

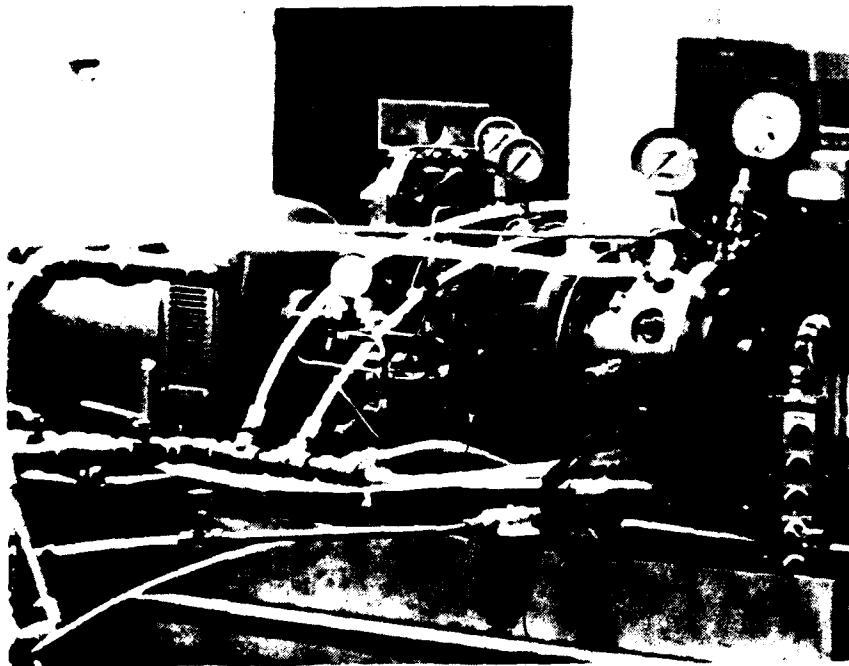


Figure 17. Face Seal Test Rig With Solar-Furnished 37 kW (50 HP) DC Motor
(SCR unit on wall in background at right edge of picture)

An automated data acquisition system, Monitor Labs Model 9300 S/N 260 Data Logger, provided temperature and voltage transducer output records at programmable intervals. An automated shutdown system provided protection against overspeed, underspeed at high speed, seal and water over-temperature, excessive proximity probe (vibration) amplitude, low oil pressure, low buffer water pressure, electrical failure. Included in the latter system were Action Instruments Inc. Model 1200-2253 thermocouple relays (4), a Model 1720-2854L frequency relay and a Model 1010-7070M voltage relay.

4.6.2 Buffer Water Supply System

A schematic of the Solar-furnished water supply system, including flowmeter connections, is shown in Figure 18. Figure 19 shows the overall system, notably comprising non-corrodable plastic, nylon, and stainless steel components. In addition to provision for automatic control of pressures and temperatures during untended endurance testing, much of the system complexity arose because of the necessity to monitor water quantity and flows by diversion of most of the lines through the flowmeters (one visible at the extreme right of Figure 19).

4.6.3 Test Plan

Parameters for the experimental testing were derived from the following data supplied by NAVSEA:

- "Typical 8000 Ton Destroyer - Power vs Speed Characteristic" (anon.)
- "Standard NAVSEC Destroyer Profile" NAVSEA Code 614B, 18 March 1975
- "Typical LM-2500 Operating Conditions During Emissions Studies," NAVSECPHILADIV Project A-1584 Report Table A-1

Since the steam turbine would be geared to the LM 2500 power turbine, performance of the seals was to be established from zero upwards to the rig 100 percent speed of 15,000 rpm, which gave a seal mean surface speed of 89.4 m/sec (300 fps). Inasmuch as an insignificant amount of actual turbine operating time was expected below 10-15 percent speed, the minimum rig speed at which performance would be established in any detail was 1800 rpm. At least four speed points would be investigated, at each speed various buffer supply pressures would be applied, with and without the condenser vacuum simulated, in order to determine the range of pressures over which satisfactory or minimal leakage rates were obtained. Testing would also include static leakage tests.

The foregoing results were to be used to determine optimum operating parameters for each of the two leading seal assembly candidates for a subsequent endurance test. The purpose of this test was to simulate as closely as

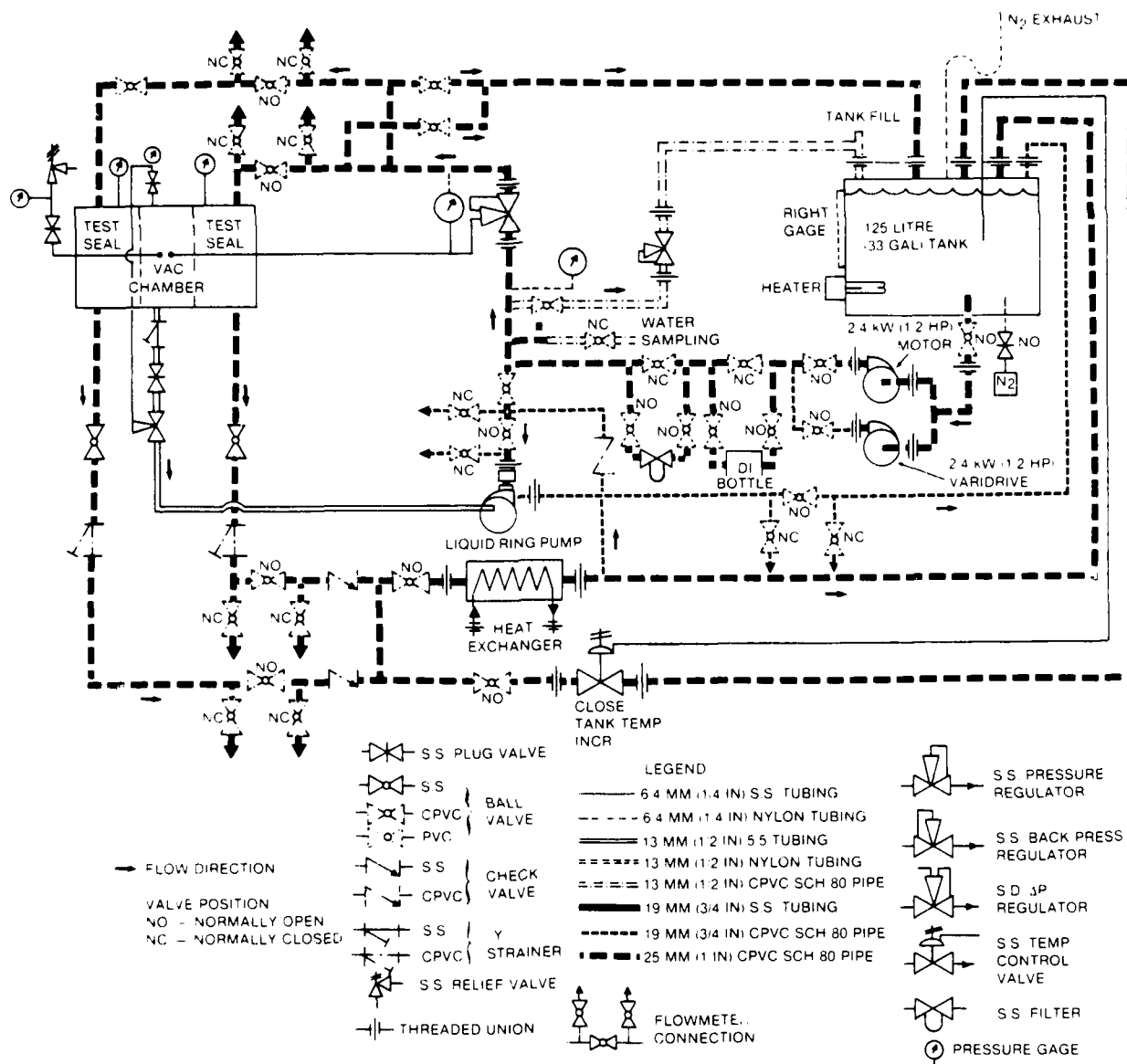


Figure 18. Water System Schematic

possible the actual turbine application for a period long enough to permit, primarily, leakage rate projections over the 15,000 hour intended life so that water treatment system requirements could be defined. Secondly, but of equal importance, it was desired to determine what effects, if any, long-term operation had on the seals, e.g., wear.

The above-mentioned ship operating characteristics were used to derive the endurance-test cycle shown in Figure 20. Once-per-week total shutdown of adequate duration to allow all components to cool to ambient was included.

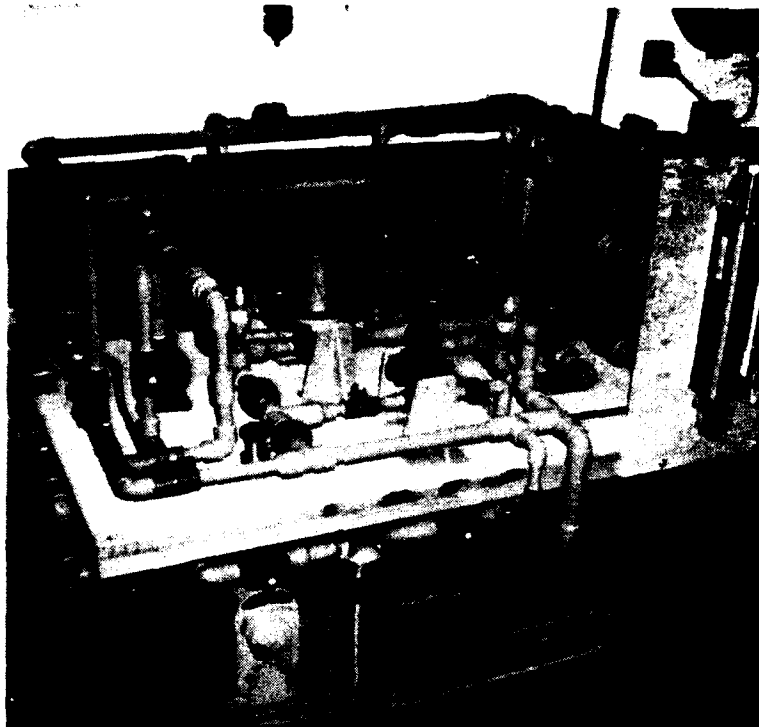


Figure 19. Seal Rig Buffer Water Supply System

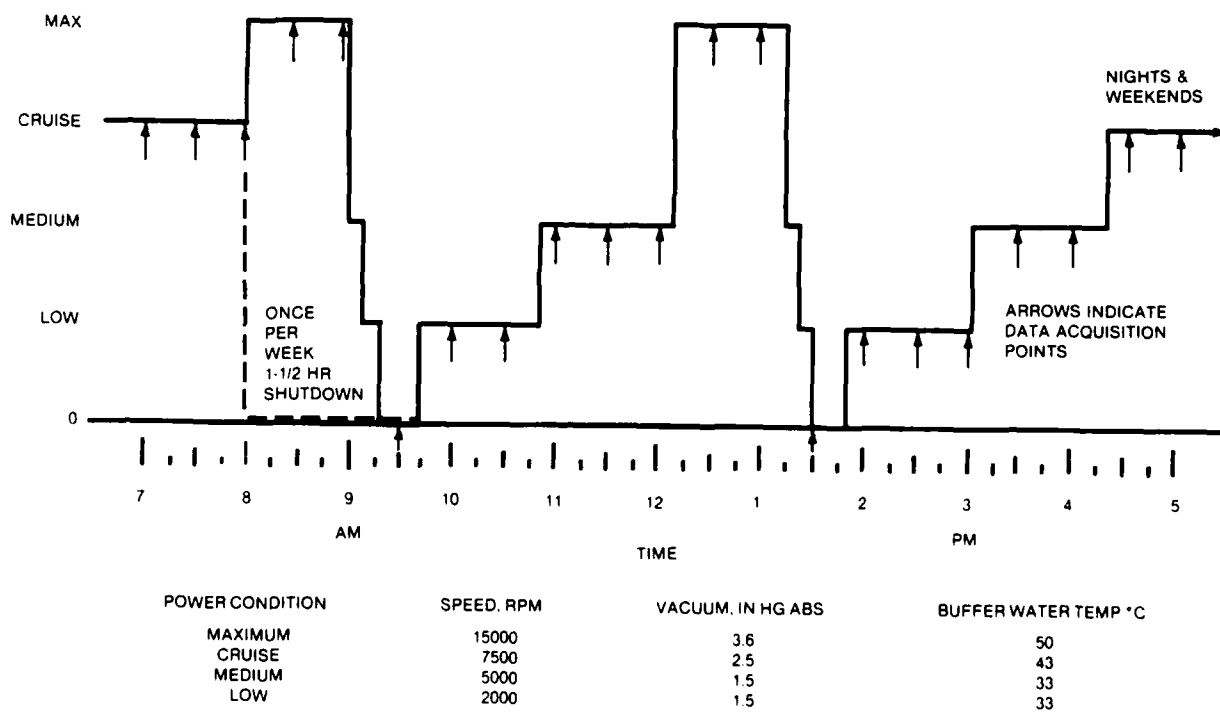


Figure 20. Endurance Cycle Test

4.7 EXPERIMENTAL TESTING

4.7.1 Crane-Design Seals (Type 1 above)

The stationary seals were instrumented with proximity probes and thermocouples. The runner was assembled with the other rotor components and dynamic-balanced. Figures 21 and 22 illustrate the components also shown in cross-section in Figure 9.

During testing the drive torque requirements exceeded anticipated values. The maximum speed run was 7,000 rpm. Test data were obtained at 4,000 and 5,000 rpm. Figure 23 shows the leakage at the 4,000 and 5,000 rpm speed points. Variations in pressure differential across the forward seal were obtained simply by setting the buffer water pressure (see Figure 9) at values above ambient. Additional variations in pressure differential across the aft seal (again in Figure 9) were obtained by raising the chamber ("steam/vacuum") pressure to various values above the buffer pressure.

Careful calibration of the two proximity probes installed in each carbon stationary seal taking into account temperature and "electrical runout", the latter arising from the chromium plating on the runner, failed to permit discrimination of any constant separation (film thickness) between the runner and either stationary seal during operation as may be seen in the Figure 24 probe output voltages during running. Any operating film thicknesses would have resulted in probe output voltages greater than the calibration "bands", between the straight lines. The maximum seal temperatures recorded during testing were consistently at the inner periphery of the seal interfaces.

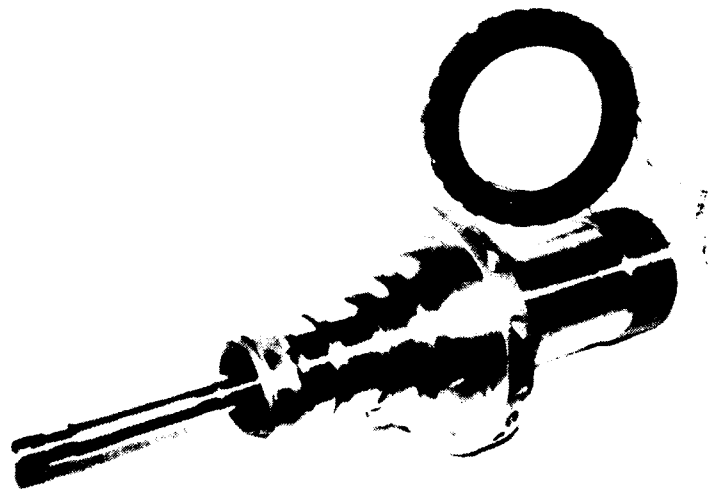


Figure 21. Seal Testing Rig Rotor Shaft in "Performance Test" Configuration With Crane-Design Spiral Groove Runner and One Stationary Seal



Figure 22. Crane-Design Stationary Seal and Housing Components

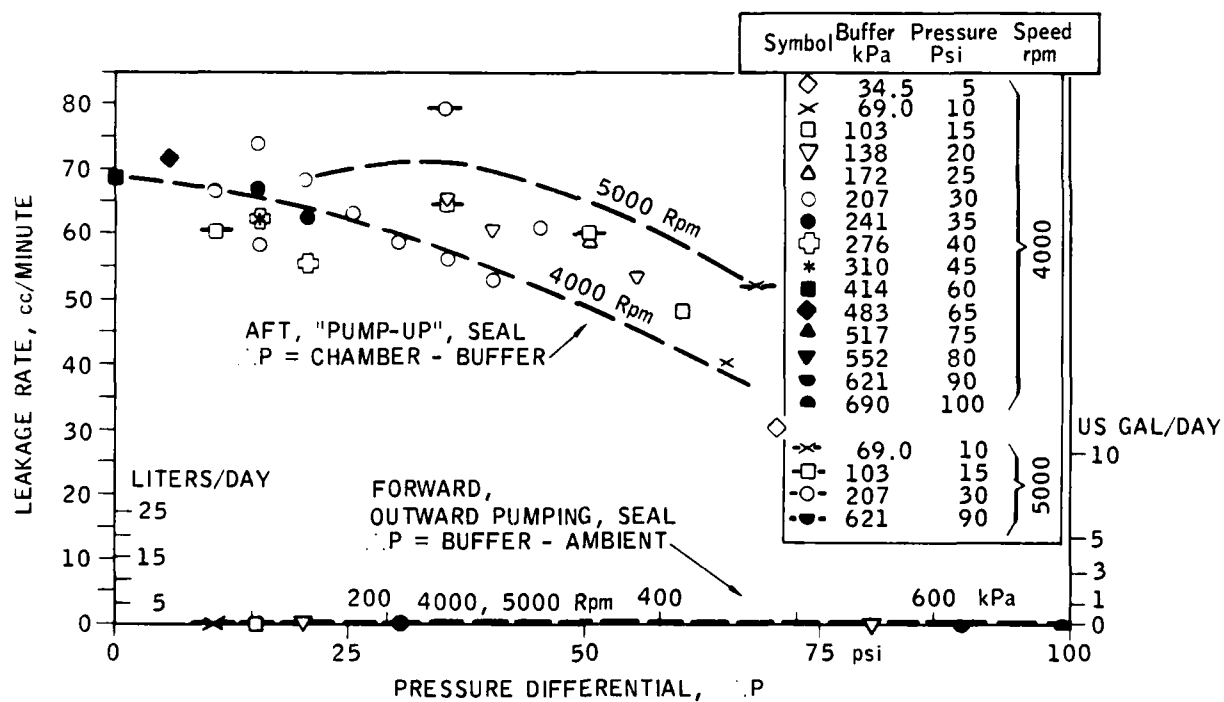


Figure 23. Opera' - Leakage - Crane Spiral Goove Seals
 (Incorrectly Assembled)

It was decided at this point to disassemble the rig for substitution of the NASA-Solar (Crane-manufactured) spiral groove seal components, because of the high leakage of the aft seal.

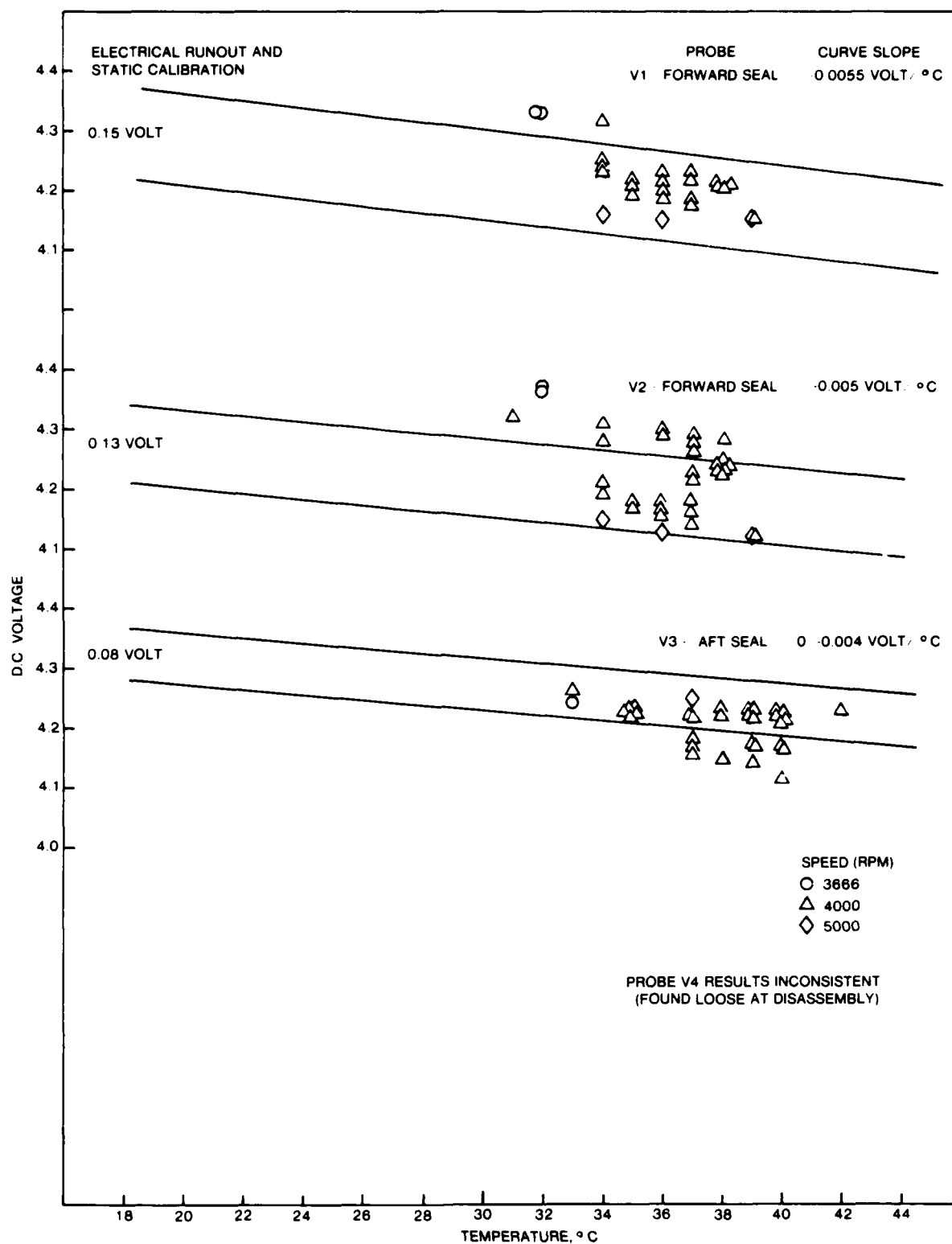


Figure 24. Operating Proximity Probe Data Versus Temperature
Crane-Design Seals

One contributing factor to the high torque required was the pumping power losses from the chordal holes through the runner intended to promote cooling. To overcome the unwanted pumping losses, the identical holes in the NASA-Solar runner were plugged with a mixture of half epoxy and half pure aluminum powder.

Total rig operating time at disassembly was 18 hours. Disassembly revealed that the two carbon stationary seals had inadvertently been interchanged during assembly. They were quite similar in appearance but had a critical difference in sealing face diameter. It is therefore questionable how meaningful were the results derived in the foregoing testing.

4.7.2 NASA-Solar Seals (Type 2 above)

As the housing components of the Crane-design seals were utilized with the NASA-Solar assembly also, installation involved substitution of the stationary carbon seals, each with its 32 rather than 8 springs, and of the different runner. The chordal holes in the runner for cooling were plugged to reduce the pumping power loss. These components are shown in Figure 25 and also in cross-section in Figure 10. Re-balance of the rotor was carried out after installation of the new runner.

Static leakage checks showed initially, rather surprisingly, that slight leakage occurred at buffer supply pressures as low as 35-70 kPa (5-10 psi). This indicated minor but significant out-of-flatness at the inner diameter of the stationary seal-runner interfaces since, allowing for less-than-perfect



Figure 25. NASA-Solar Design Spiral Groove Runner and Stationary Seals (Manufactured by Crane)

interfaces, leakage would not have been expected below at least 205-240 kPa (30-35 psi). With increased "running-in", these threshold values increased somewhat, as would be hoped and expected, but the aft seal threshold dropped again as testing progressed. Figure 26 shows the static leakages recorded just prior to disassembly.

The same careful calibration as with the Crane-design seals was carried out of each pair of proximity probes mounted in the stationary seals. Operating data shown in Figure 27, over-printed on the calibration curves, indicated that the atmosphere-side mean seal film thicknesses varied from about 0.008 mm (0.0003 in.) to 0.025 mm (0.001 in.), in the anticipated range, but were at most about 0.012 mm (0.0005 in.) with the vacuum-side seal, somewhat low. The results also indicated that slight progressive wear, confirmed at disassembly occurred, particularly on the atmosphere-side seal. The proximity probes were rendered inoperable during rework of the stationary seals and could not therefore produce data during the subsequent high speed testing. Prior to disassembly, a torque of 21.5 N.m (190 lb-in.) was found required to rotate the shaft manually against the loading of the stationary seals. Disassembly of the rig revealed light wear outward from the annular groove on both carbon stationary seals and outward of the grooved area on both faces of the runner. Rust deposits were found on each face of the runner opposite the annular grooves in the stationary seals. As they easily wiped away, it was concluded that the rust particles had been buffer-water-borne. Microscopic examination of the worn areas on the stationary seals showed some embedding of rust particles. After low speed testing the seals were

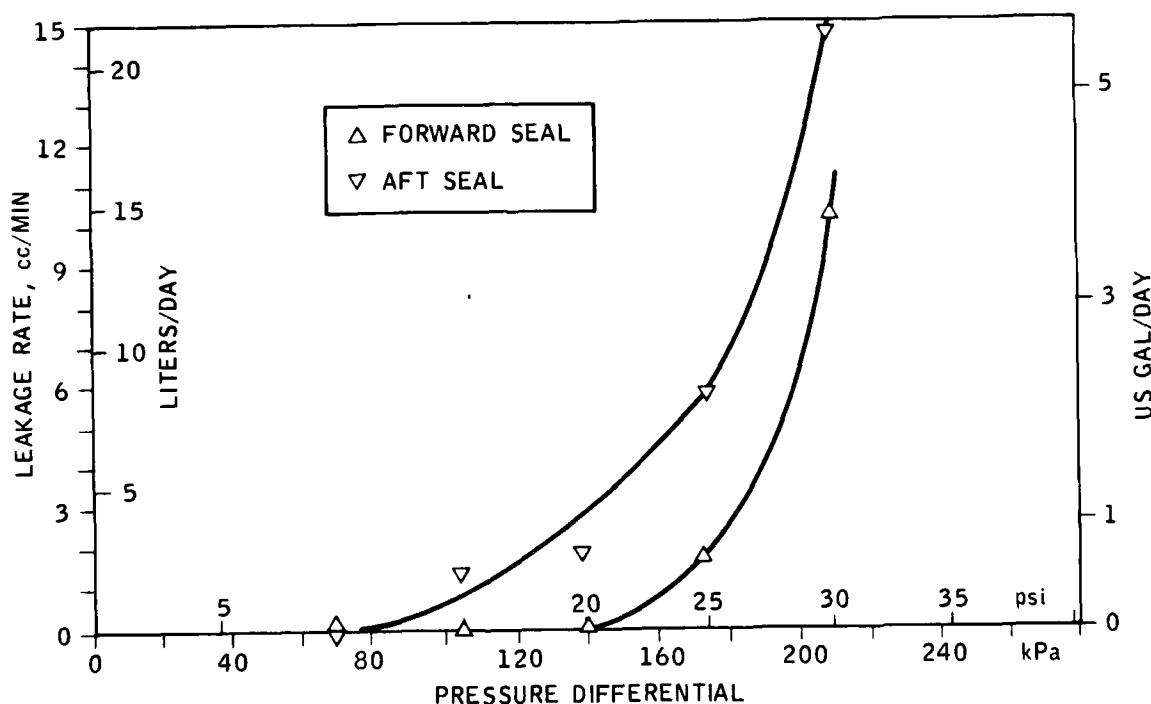


Figure 26. Static Leakage - NASA-Solar Spiral Groove Seals

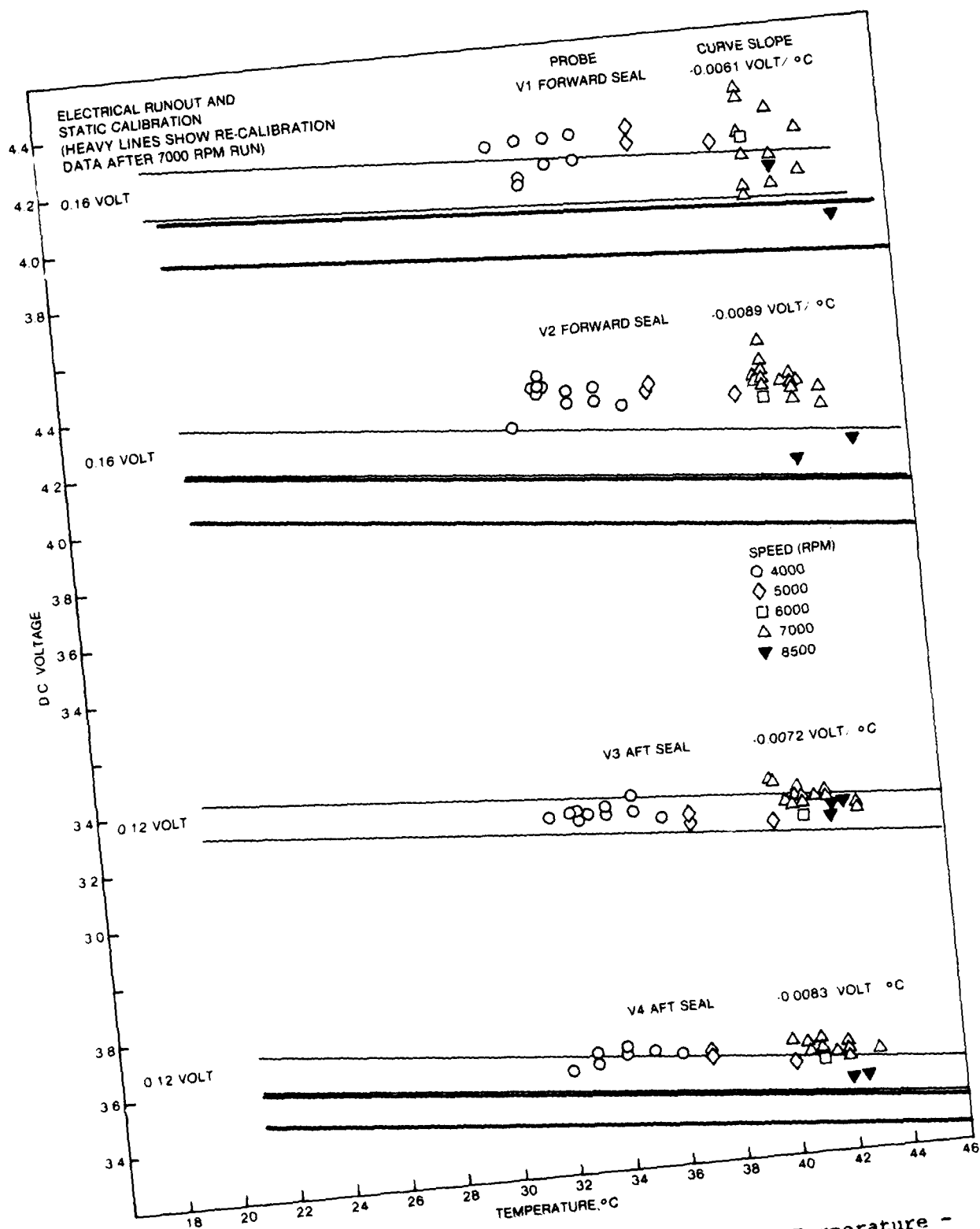


Figure 27. Operating Proximity Probe Data Versus Temperature -
NASA-Solar Seals

returned to Crane for refurbishment including re-application of the plating to improve the surface flatness of the runner.

Crane also offered the opinion that some of the wear could have been caused by residual chrome particles left in the bottom of the grooves after plating. The source of the rust was traced to buffer water supply system pressure regulators downstream of the filter. The rust had formed on interior, as-cast surfaces exposed to system water even though they were 316 stainless steel. The likely explanation is discussed in the "Design Guidelines" section, item 5. For the initial high speed testing, in an attempt to reduce the parasitic drag, the buffer water inlet and outlet flows and housing configuration were altered as shown in Figure 28.

In the course of high speed testing it was noted that the torque requirements at each speed were progressively increasing. At 1200 rpm, for example, the rig power requirement rose from 24.8 kW (33.2 HP) to 32.8 kW (44.0 HP). Investigation revealed that the epoxy plugging the runner cooling holes was coming out in pieces and collecting in the water line strainers. Also, the atmosphere-side seal leakage rates were, while on the whole within program goals, considered somewhat high. Disassembly was carried out to remove the epoxy and raise the spring load on the atmosphere seal by about 220 N (50 lbs). Rather severe cavitation erosion pitting was found on the components illustrated in figures 21, 22, and 25: on the runner outer diameter between the cooling holes, as shown in Figures 29 and 30, and on the outer diameter of the stationary carbon seals, as shown in Figures 31 through 34, particularly near the outlet ports. The damage extended just onto the seal faces near

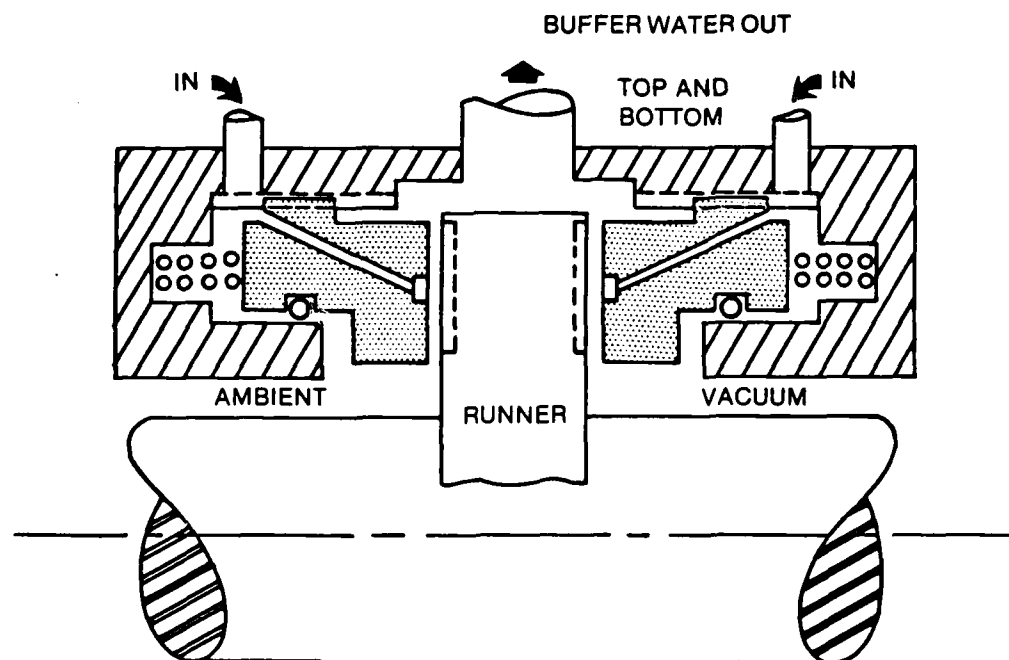


Figure 28. Crane (NASA-Solar) Spiral Groove Seal

Figure 29.

Outer Diameter of NASA-Solar Seal Runner, Also Shown in Figure 21, Illustrating the Location of Cavitation Erosion Damage After Initial High Speed Testing (see also Fig. 30).

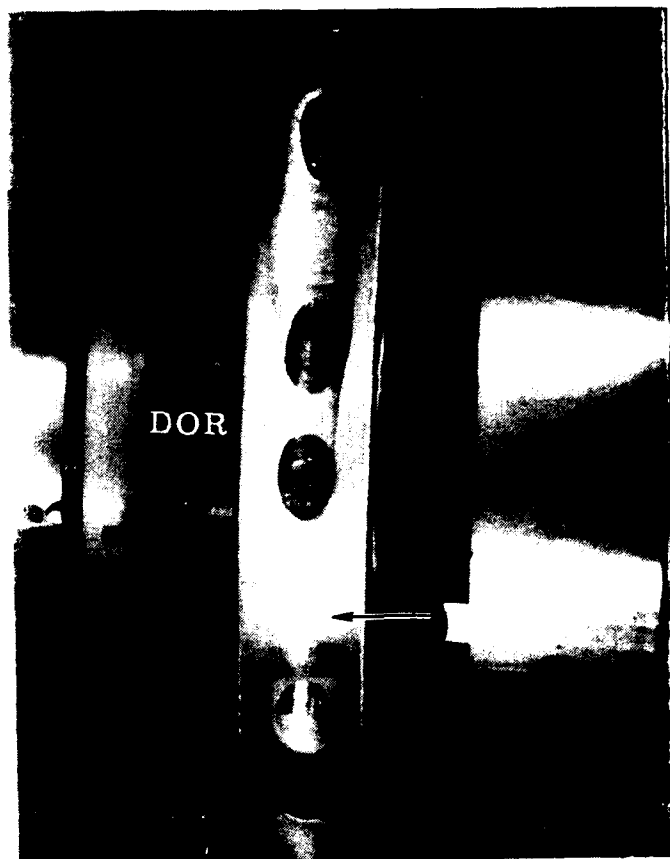


Figure 30.

NASA-Solar Seal Runner After Initial High Speed Testing: Closeup of the Area Between Cooling Holes Showing Cavitation Erosion

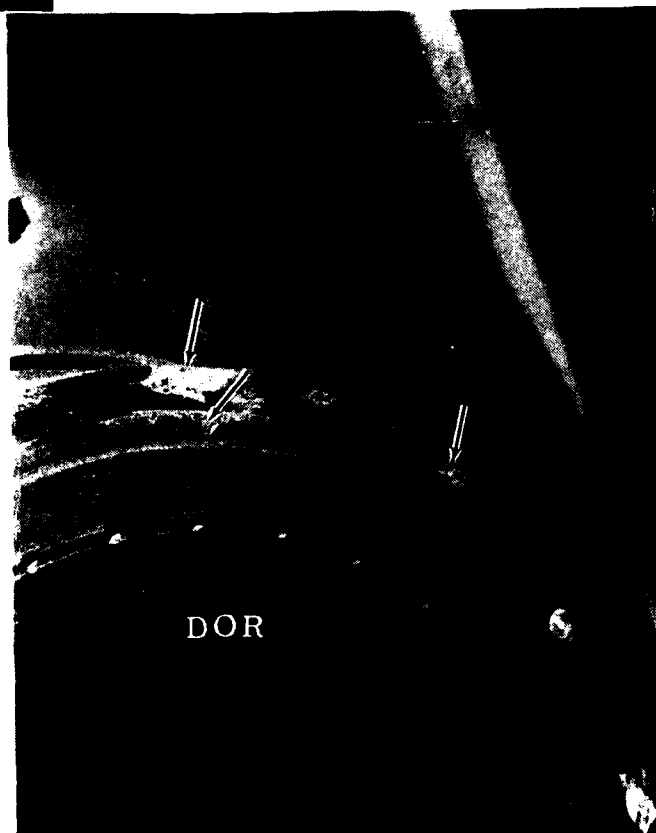


Figure 31.

NASA-Solar Atmosphere-Side
Stationary Seal Showing Cavitation
Erosion After Initial High Speed
Testing

Figure 32.

NASA-Solar Seal After Initial
High Speed Testing. Closeup of
12 o'clock area of atmosphere
side stationary seal showing
cavitation erosion.



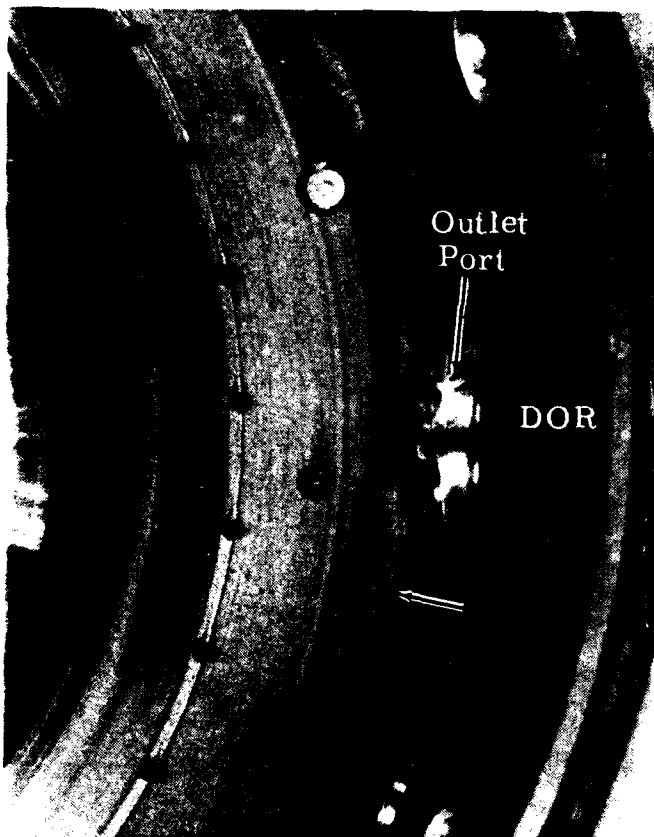
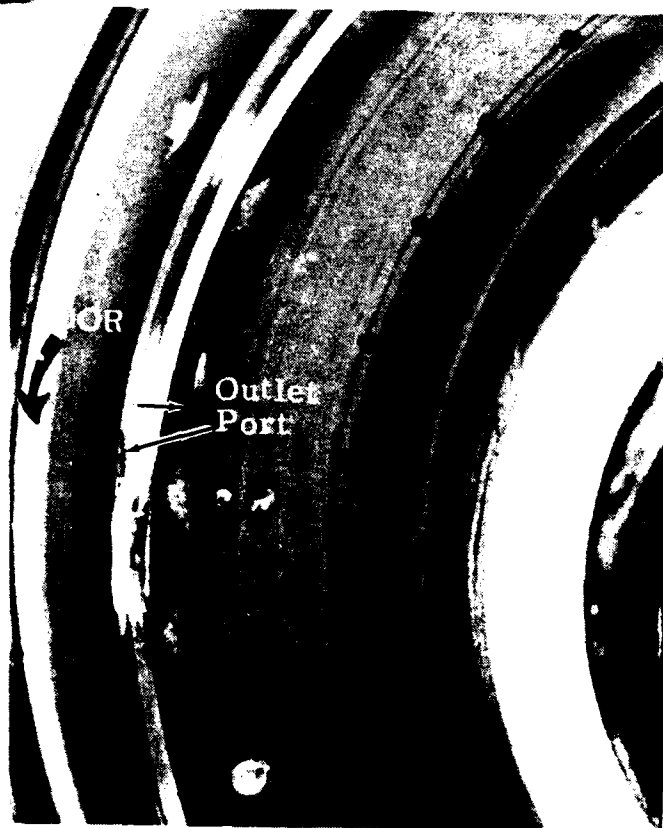


Figure 33.

NASA-Solar Seal After Initial High Speed Testing. Closeup of 12 o'clock area of vacuum-side stationary seal showing cavitation erosion.

Figure 34.

NASA-Solar Seal After Initial High Speed Testing. Closeup of 6 o'clock area of vacuum-side stationary seal showing cavitation erosion



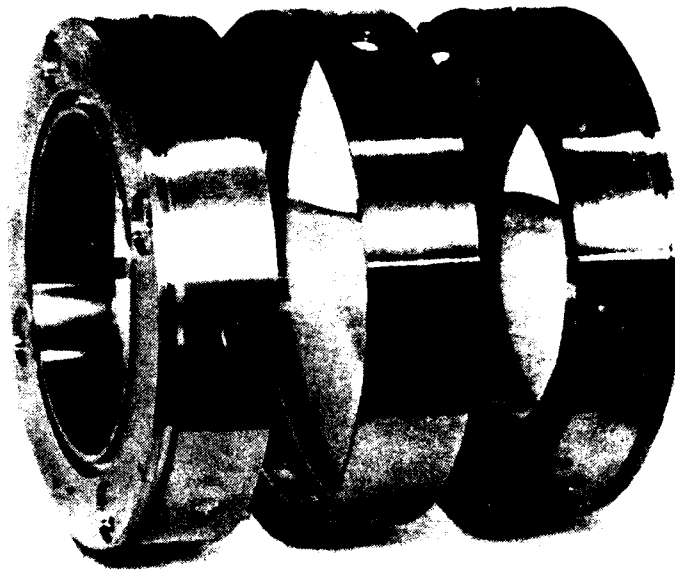


Figure 35. General Arrangement of Modified Crane Housings and New Center Housing for NASA-Solar Seal Assembly

these spots. The "plumbing" was therefore restored to the original configuration and a central housing (Fig. 35) was inserted to shroud the runner in an effort to suppress cavitation.

Retesting indicated that shrouding of the runner and/or re-routing of the water flow did suppress the cavitation erosion of the stationary seals but it did appear that further erosion occurred on the runner, as can be seen in Figures 36 and 37 (corresponding to Figs. 32 and 33). The power requirement was reduced somewhat too. It was also noted, however, that the runner had begun to contact the center housing, as can be seen in Figure 36. Also, some small pieces of epoxy had remained in the housing and migrated into the seal face, apparently causing slight scoring wear outboard of the annular supply groove, as can be seen in Figure 38. The contact of runner and center housing caused a vibration and noise that prompted disassembly. Experimental data sheets are shown in Appendix III.

The operating temperatures increased with speed and were greater than theoretical estimates at a speed of 15,000 rpm. The buffer water temperature rises (i.e. heating), could be equated approximately to the rig drive power levels. Calculations made of the frictional drag on the outside diameter of the runner arising from its "immersion" in the buffer water explain temperature rise. For the 19 mm (0.75 in.) wide, 146 mm (5.75 in.) diameter Crane runner this was found using a Crane-supplied method (included as Appendix IV) to amount to 8 kW (11 HP) at 15,000 rpm. To improve agreement of theory with experimental data a second approach to estimating the applicable coefficient of friction was located (also reported in Appendix IV) in NASA CR1774, A Review of Confined Vortex Flows. At 15000 rpm the second analysis yielded



Figure 36.

NASA-Solar Seal Runner After
Testing, Close-up of the Area
Between Cooling Holes Showing
Cavitation Erosion

(Same area as Figure 30)

Figure 37.

NASA-Solar Seal After
Testing, Close-up of
12 o'clock Area of
Atmosphere Side
Stationary Seal Showing
Cavitation Erosion

(Same Area as Figure 32)





Figure 38.

NASA-Solar Seal After Testing,
Close-up of Atmosphere-Side Station-
ary Seal Showing Presence of Small
Pieces of Epoxy (Impregnated With
Aluminum)

a frictional drag of about 20 kW (26 HP). Inasmuch as these figures accounted for most of the actual power measured the conclusion can be drawn that most of the seal power loss was caused by the flooded runner and accounted for most of the heat generation. By plotting maximum recorded seal temperature rise over buffer water outlet temperature, values much more in line with theoretical estimates of about 5-10C° (approximately 10-20F°) resulted as can be seen in Figure 39. These maximum temperatures always occurred at the inner diameters of the seals. Figure 40 shows the power levels mentioned above. Figure 41 depicts the incidence of leakage during operation. It can be seen that zero leakage occurred over a range of buffer pressure at each speed. At low buffer pressures the presence of air in the buffer outflow, evidenced by a "milky" appearance as it passed through the glass tube of the flowmeter, was detected. This is believed to indicate that air (at the atmosphere-side seal) can be "pumped" by the spiral grooves into the buffer chamber when the buffer pressure is sufficiently low. This is a speed-related occurrence and control of buffer pressure can minimize if not eliminate it.

4.7.3 Koppers Seals (Type 3 above)

Figures 42 and 43 show the components prior to assembly. In contrast to the Crane assemblies the runner had a considerably smaller outside diameter but

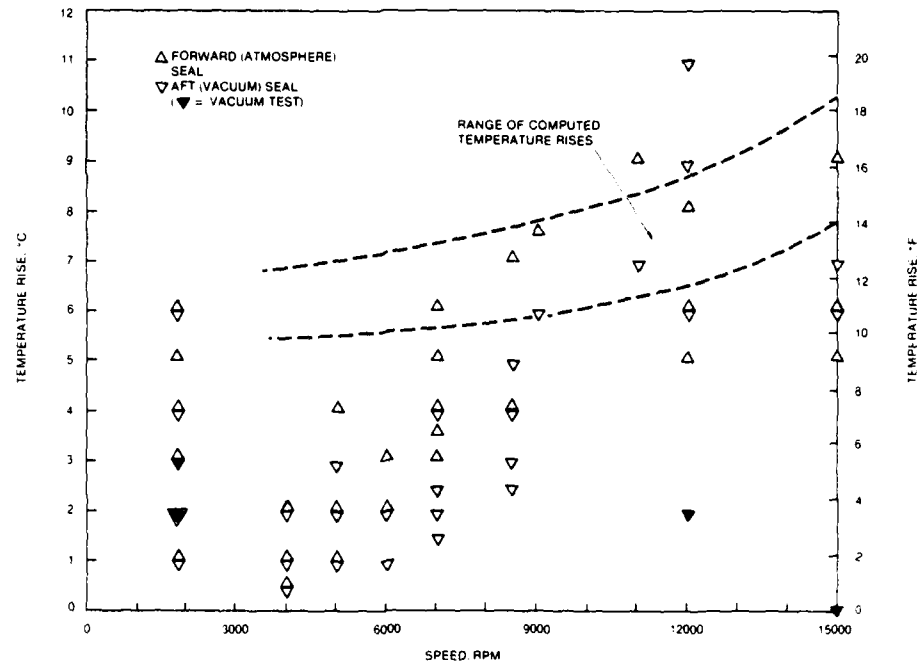


Figure 39. Maximum Seal Temperature Rise From Buffer Outflow (NASA-Solar Spiral Groove Seals)

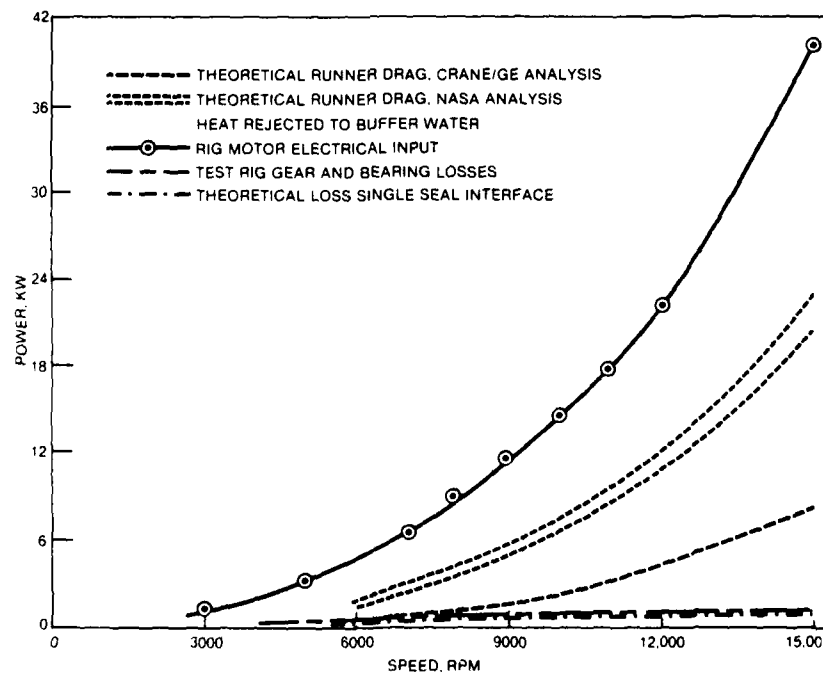


Figure 40. Power Characteristics - Crane NASA-Solar Seals

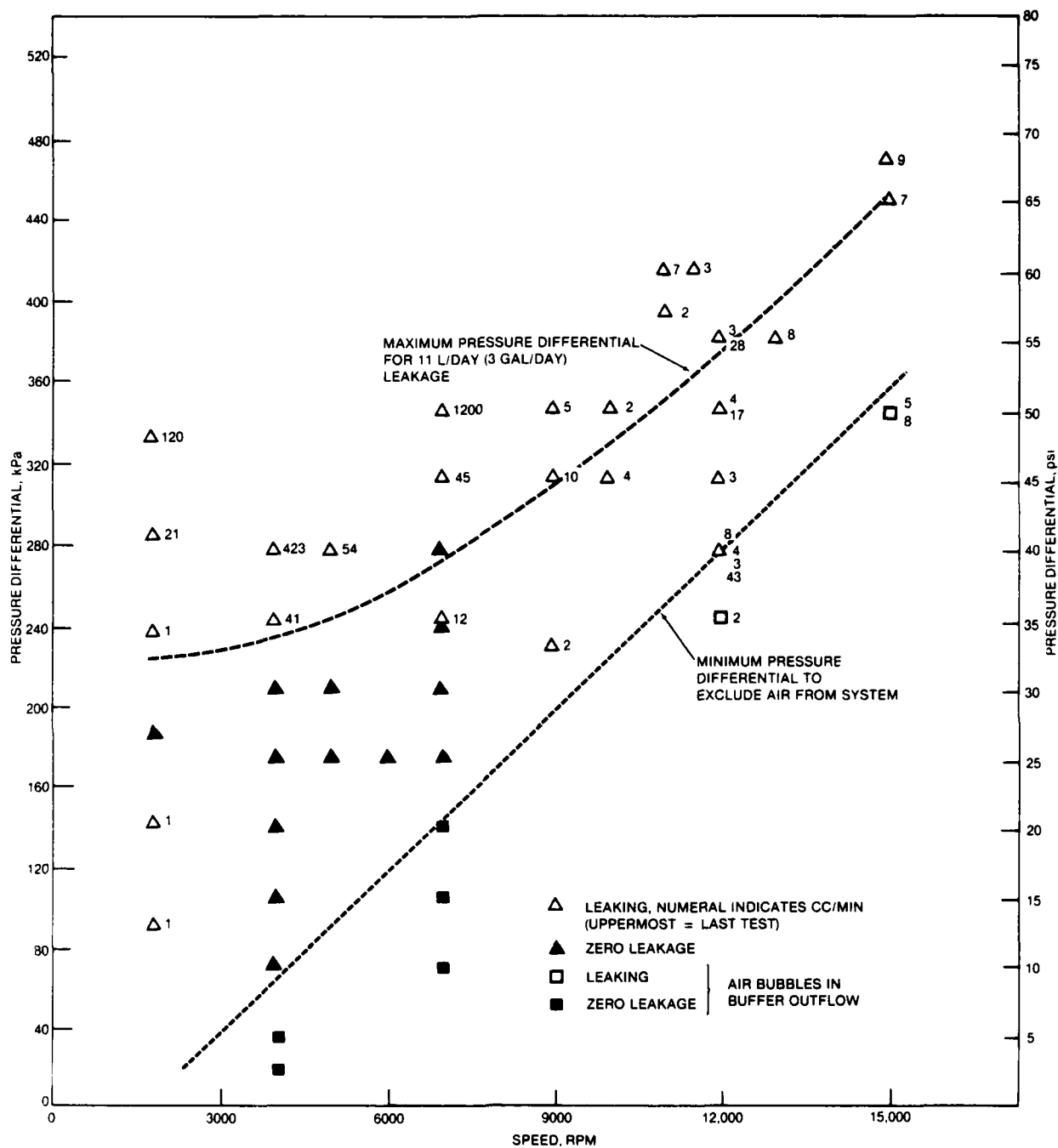


Figure 41(A). Operating Leakage as a Function of Pressure, Differential and Speed-Forward (Atmosphere) NASA-Solar Seal

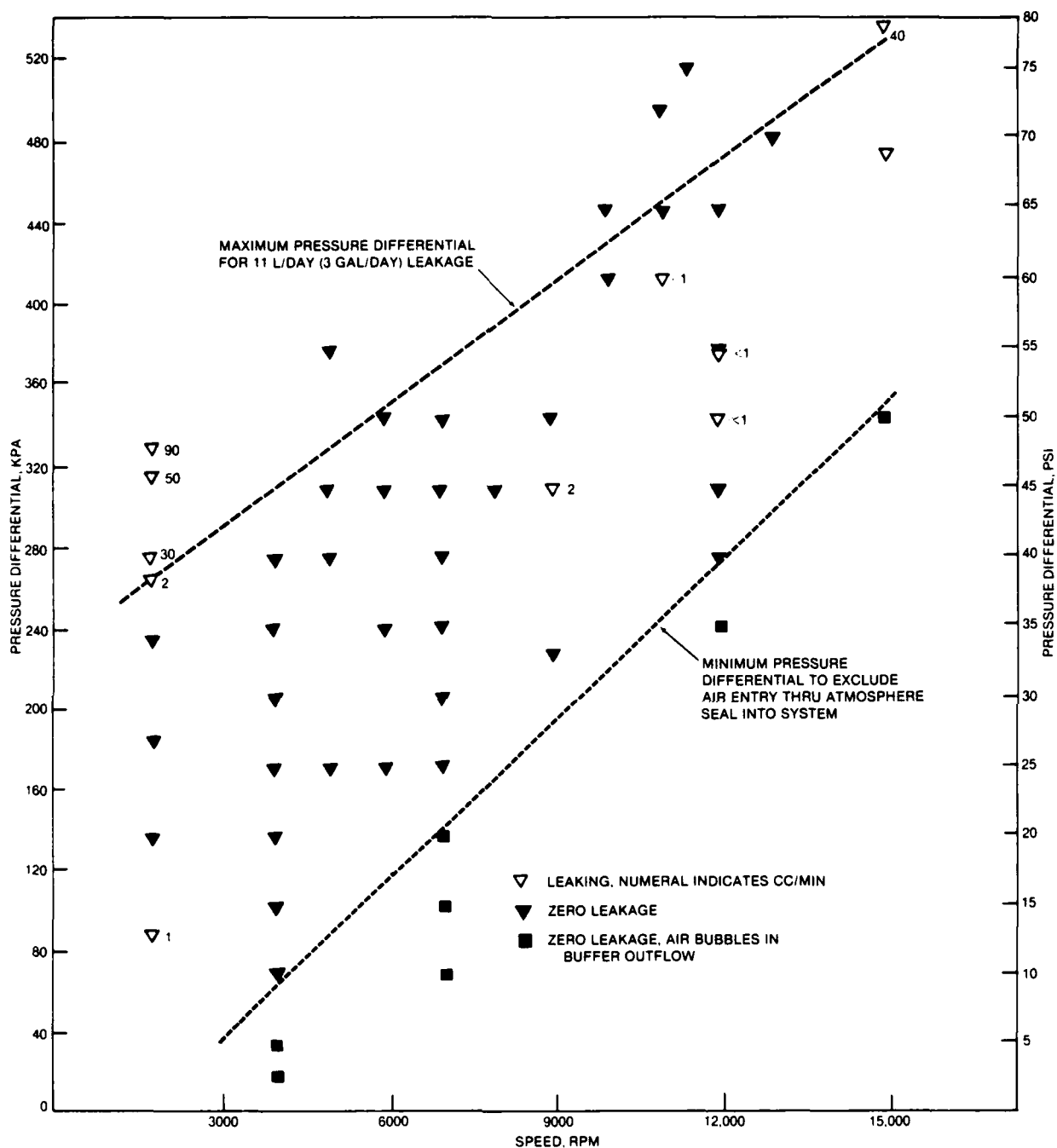


Figure 41(B). Operating Leakage as a Function of Pressure Differential and Speed - Aft (Vacuum) NASA-Solar Seal

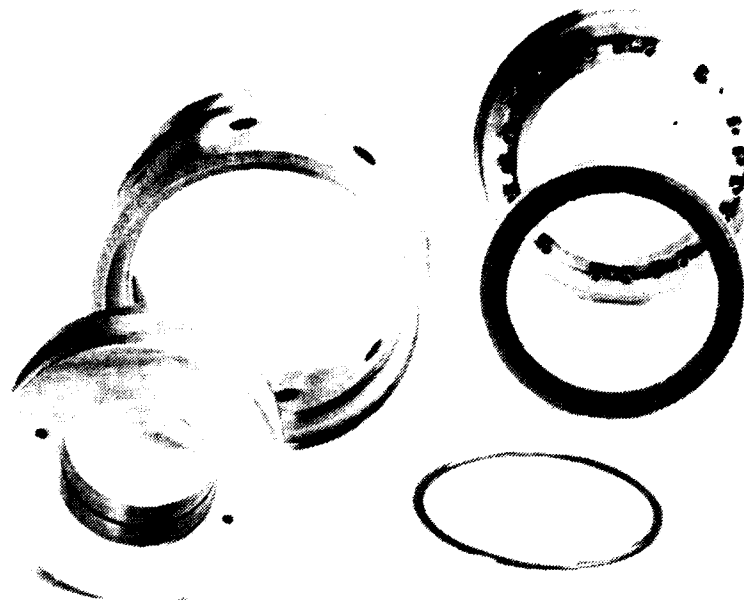


Figure 42. Koppers Test Seal Assembly Components Showing Runner, Housing and One of Two Stationary Seals



Figure 43. Close-Up of Koppers Carbon Stationary Seal and Secondary Seal (Positioned for Illustrative Purposes Only) Comprising L-Shaped Split Rings and Teflon Sealing Rings

was about twice as thick and had a large V-notch rather than holes to promote cooling. The stationary seals each comprised a 400-series stainless steel ring shrunk over a carbon ring. There were 18 springs per stationary seal compared to eight with the Crane and 32 with the NASA-Solar designs. The spring loading at the installed deflection was 96 N (21.6 lb) according to the vendor. The housing structure comprised a central portion threaded at either end to accept the end pieces. The latter, in addition to the spring pockets and groove for the secondary seal assembly, each had two dowels which fitted into holes in the stationary seal to provide circumferential retention. The dowels were flattened over the protruding portion in a triangular fashion so that circumferentially they contacted only the carbon part of the stationary seal.

Static leakage tests were carried out prior to running and periodically thereafter. Initially leakage was quite high, especially with the forward seal at about 100 liters/day (30 gal/day), but decreased with running-in to values in the target range, below 11 liters/day (3 gal/day). All operating leakage data are shown in Figures 44 and 45. Proximity probe calibrations indicated, again, slight progressive wear. Proximity probe oscilloscope traces showed very little stationary seal motion (instability). Careful control of temperature is deemed required to avoid boiling of the water in the seal interfaces at high speeds since the vendor estimated that film temperature could be up to approximately 30C° (50F°) higher than the seal temperatures recorded by the imbedded thermocouples.

Figure 46 shows the power characteristics of the Koppers seal assembly. Comparison with those of the Crane-manufactured seals shows that the Koppers seals required only about two-thirds the power. The theoretical drag curves for the Koppers seals, computed with both Crane and NASA analyses, showed better agreement with the actual results than did those for the Figure 40 Crane seals, particularly at high speed.

It can also be noted in the Koppers power characteristic that the vast majority of the power requirement showed up as heat rejection to the buffer water. Figures 47 and 48 show the maximum seal temperature rise over the buffer outlet water temperature. The previously mentioned dependence of leakage on temperature would in turn suggest caution in any attempt at substantial temperature reduction.

Figure 49 shows, overprinted on the proximity probe temperature calibration data, operating probe output voltages. These show as expected very little if any (0.005 mm or 0.0002 in. maximum) separation of the rotating and stationary surfaces, about as estimated.

Total performance-test running time with the Koppers seals was 19.5 hours. Experimental data sheets are shown in Appendix III. It was judged from the test results that 140 kPa (20 psi) buffer pressure could be used at all speeds eliminating the need for any added complexity of buffer pressure scheduling with changes of turbine speed. This would produce a pressure differential of up to 240 kPa (35 psi) across the vacuum-side seal.

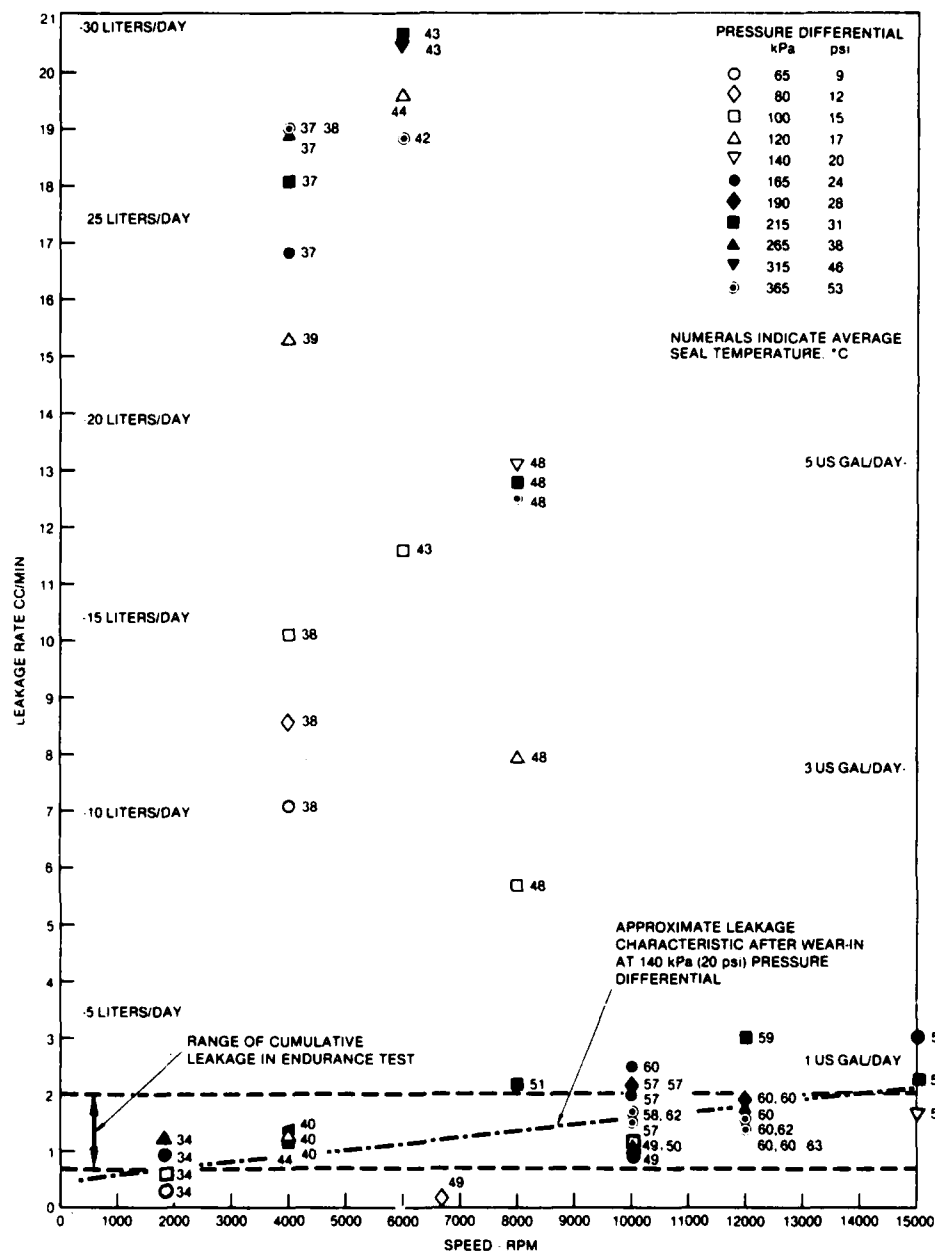


Figure 44. Operating Leakage Versus Speed, Pressure Differential and Temperature - Koppers Forward (Atmosphere) Seal

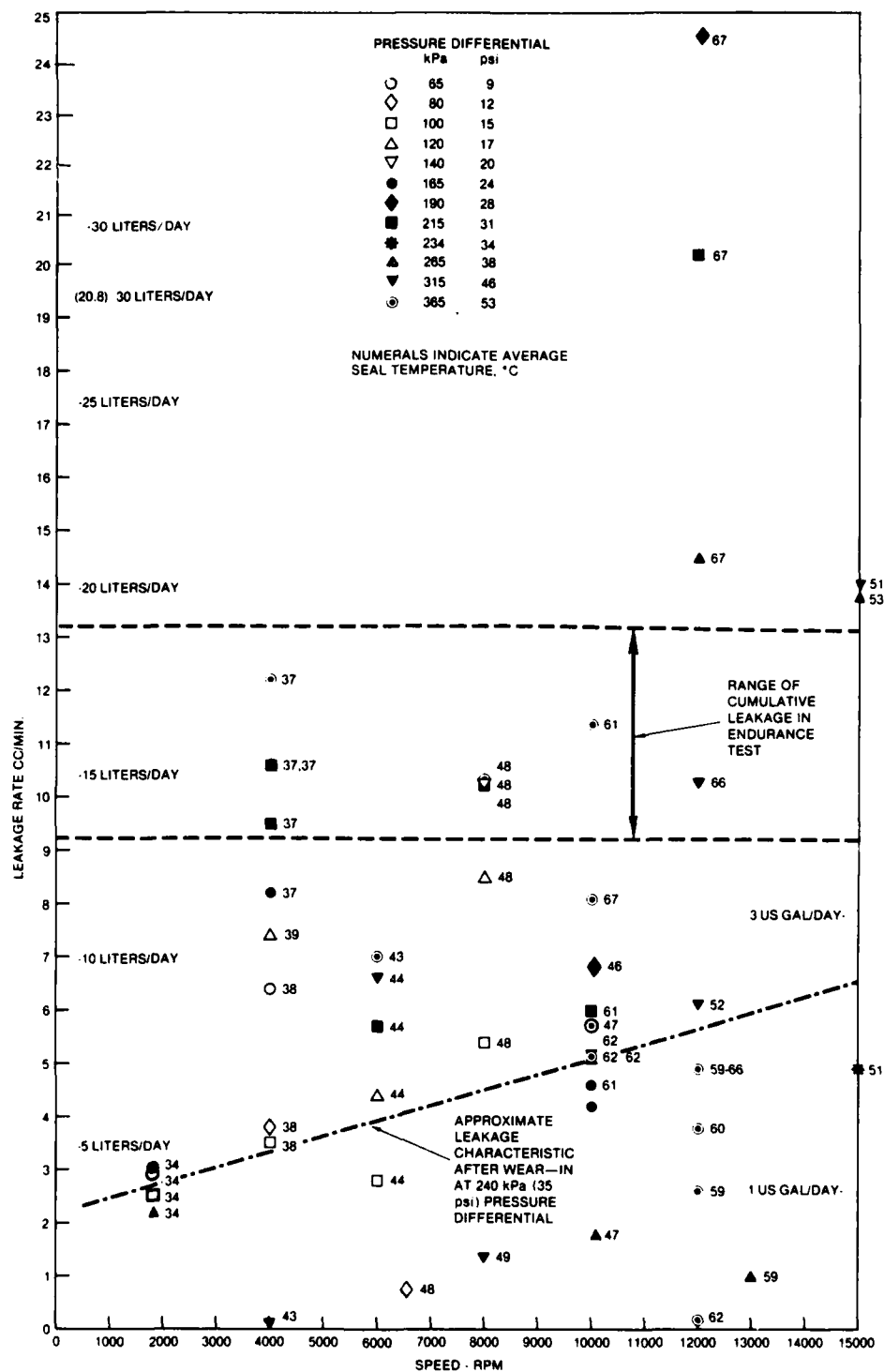


Figure 45. Operating Leakage Versus Speed, Pressure Differential and Temperature - Koppers Aft (Vacuum) Seal

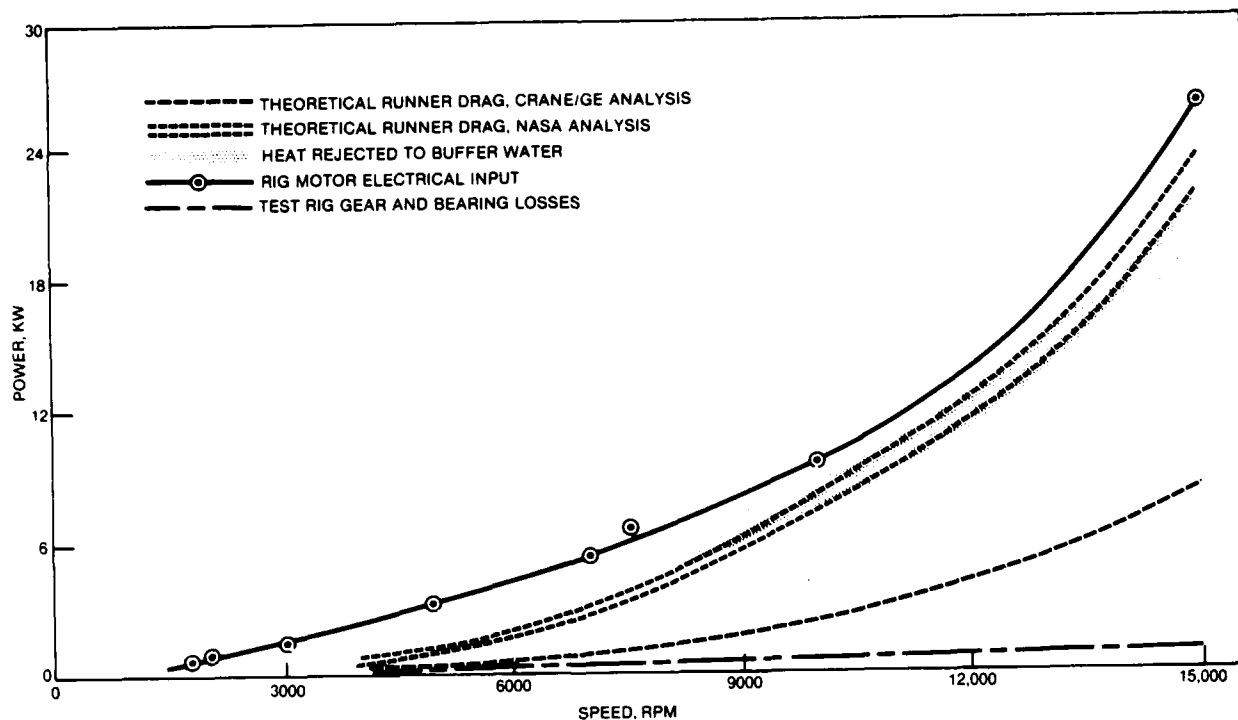


Figure 46. Power Characteristics - Kopper Seals

Figures 50 through 58 illustrate the condition of the Koppers seal components after running. Generally they were in excellent condition. One notable exception, however, was the corrosion evident on the outer diameter of the runner as may be seen in Figure 58. The AMS 6322 steel runner was chrome plated on the faces but corrosion protection on the OD had inadvertently been omitted. Prior to further testing the components were returned to Koppers for evaluation and application of electroless nickel plating to the runner OD.

Use of 440 C stainless steel runners has been successful in some Koppers water applications but their experience has indicated that the 6322 material is preferable for high speed applications because of its higher thermal conductivity, lesser tendency to warp in long term service, and reduced brittleness.

As the parasitic drag power requirement was not insignificant, some effort was devoted to devising means of reducing it. Revision of water inlet and outlet flows was carried out as shown in Figure 59 prior to endurance testing with the intention of promoting freer water outflow particularly.

4.7.4 Endurance Testing

Cyclic endurance testing was carried out on the Koppers seals in accordance with the schedule shown in Figure 20. Between 68 and 71 hours into the planned 500 hour test a large increase in leakage of the (aft) vacuum-side

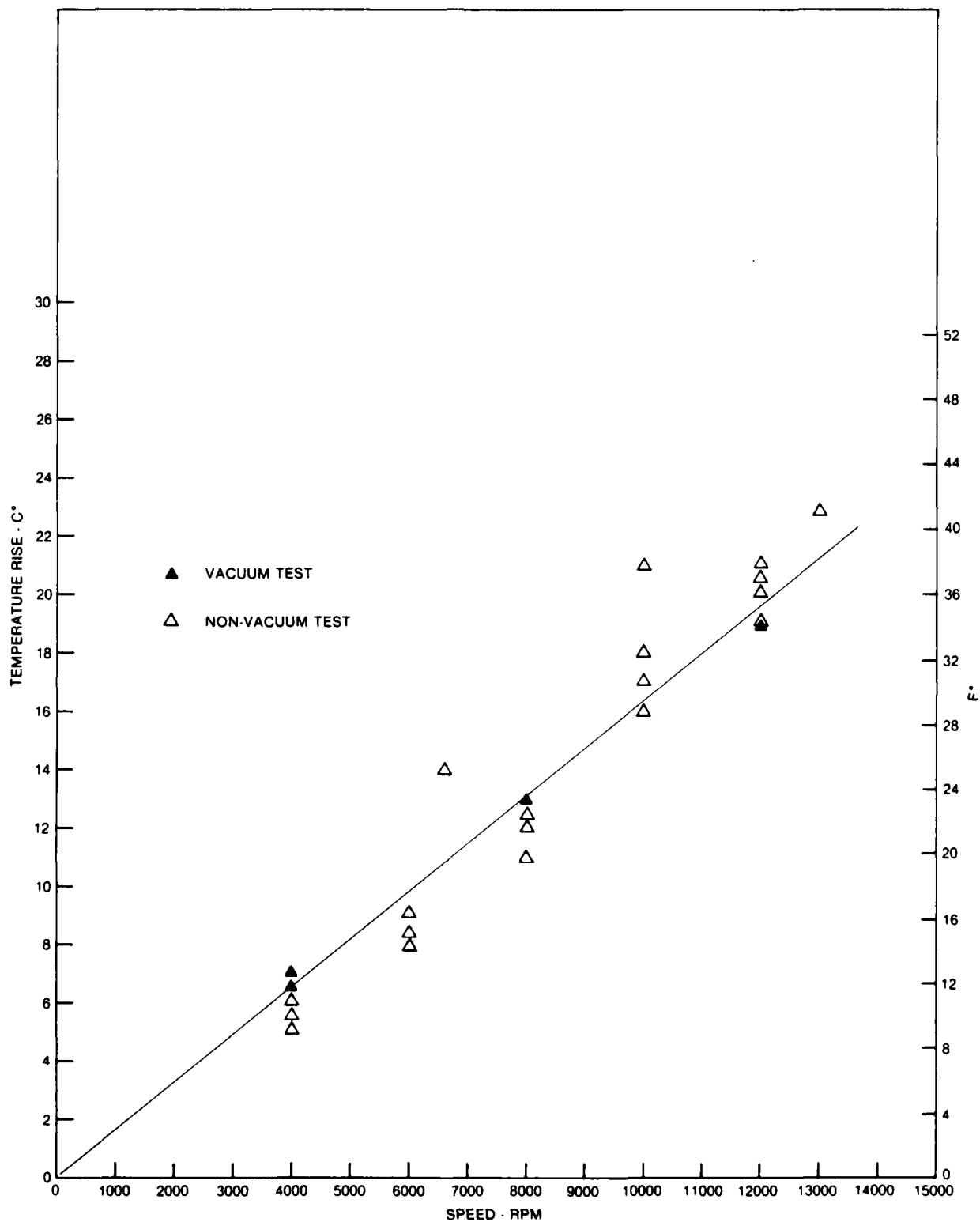


Figure 47. Maximum Seal Temperature Rise From Buffer Outflow
(Koppers Forward Seal)

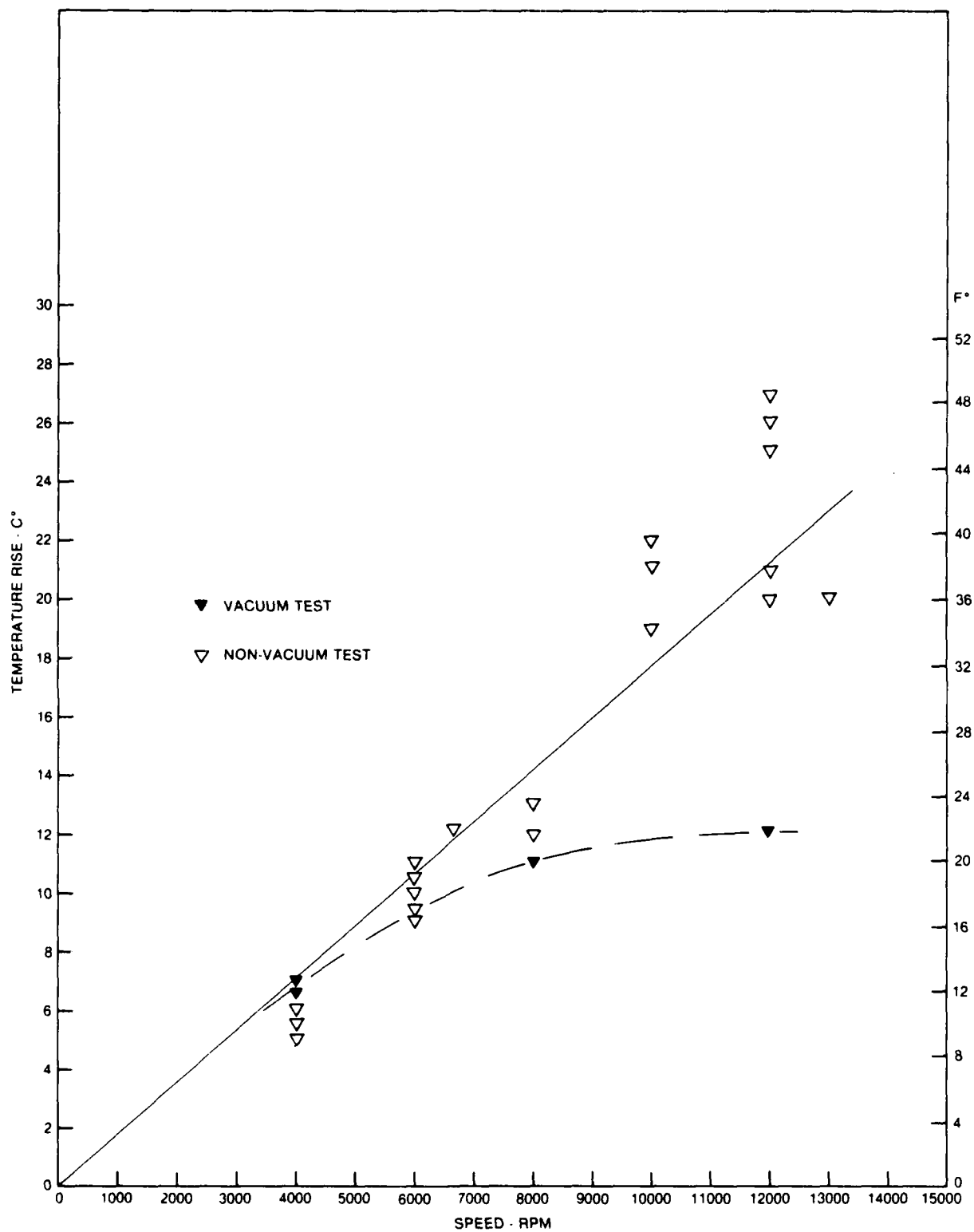


Figure 48. Maximum Seal Temperature Rise From Buffer Outflow (Koppers Aft Seal)

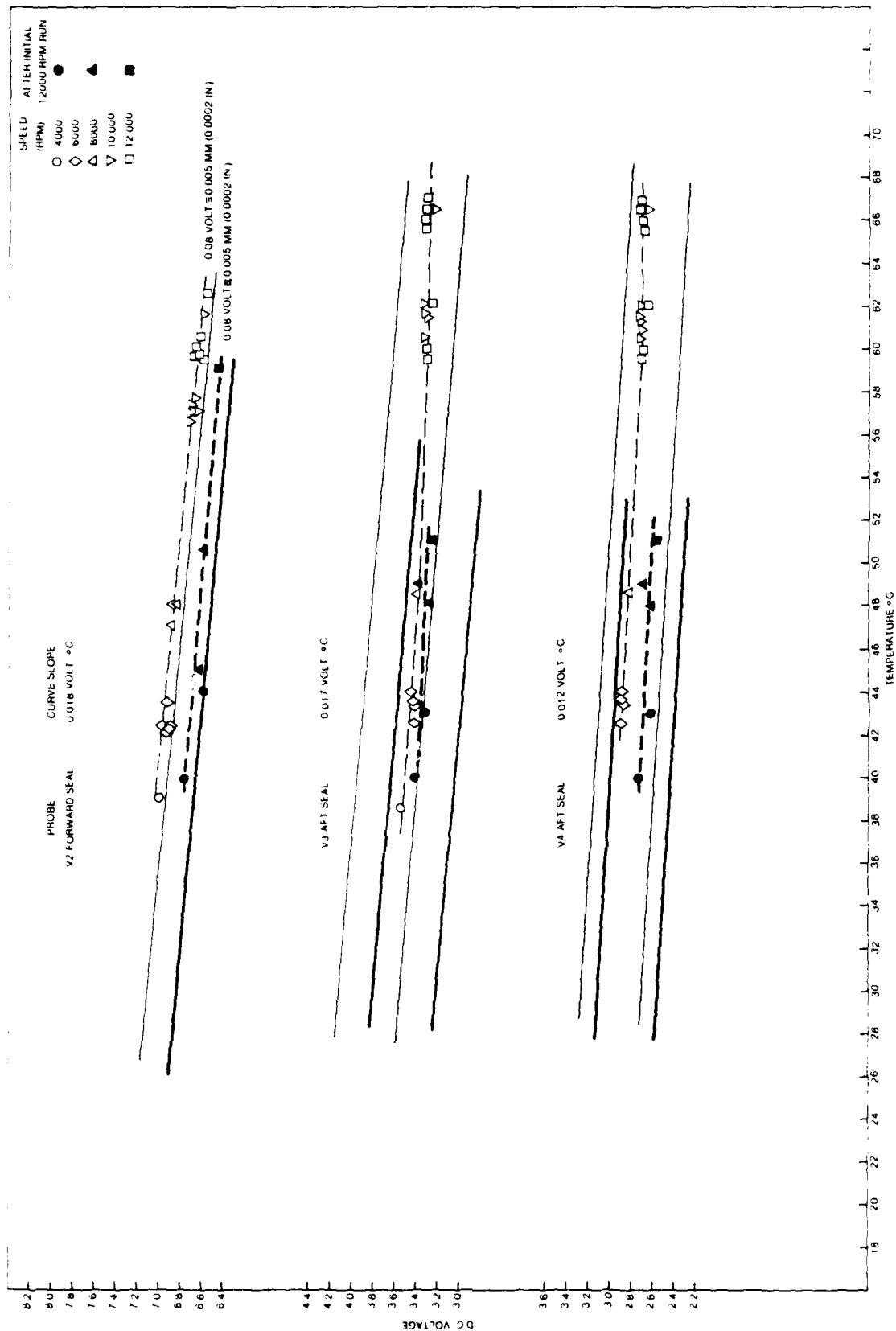


Figure 49 Operating Proximity Probe Data Versus Temperature - Koppers Seals

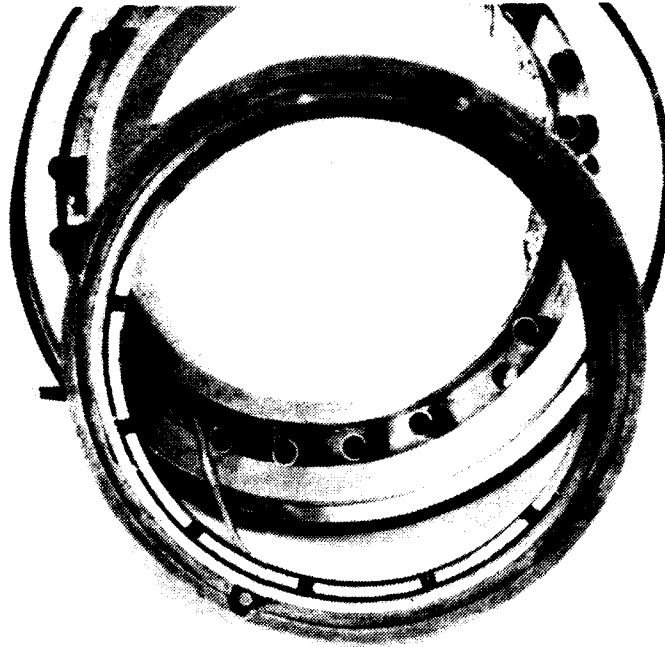


Figure 50. Koppers Forward Stationary Seal Components After Performance Testing

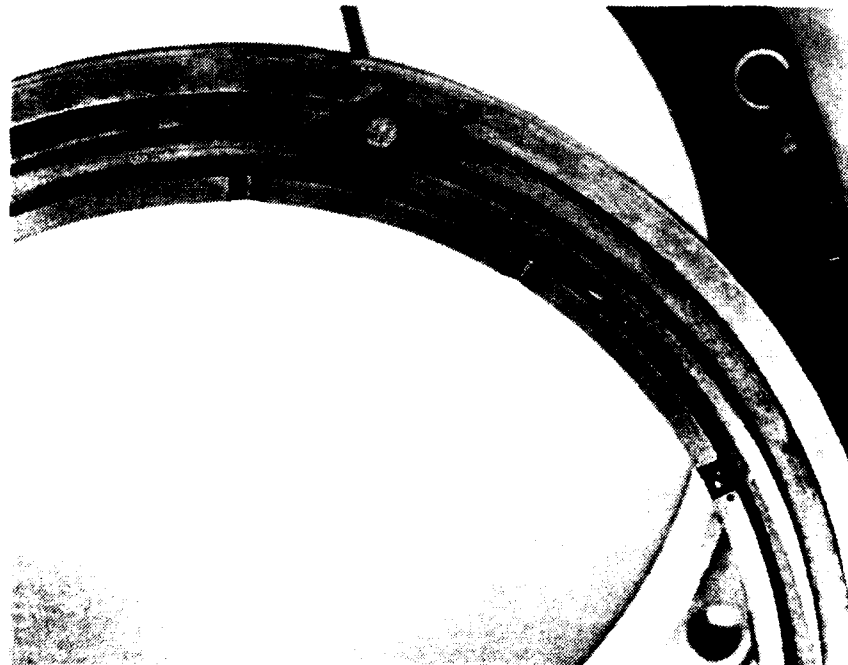


Figure 51. Close-Up of Koppers Forward Stationary Carbon Seal Sealing Interface After Performance Testing

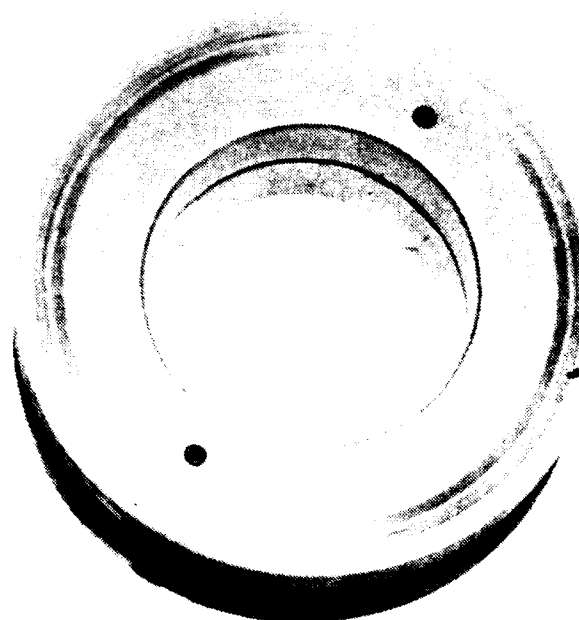


Figure 52 Forward Side of Koppers Runner After Performance Testing



Figure 53. Close-Up of Forward Face of Koppers Runner After Performance Testing

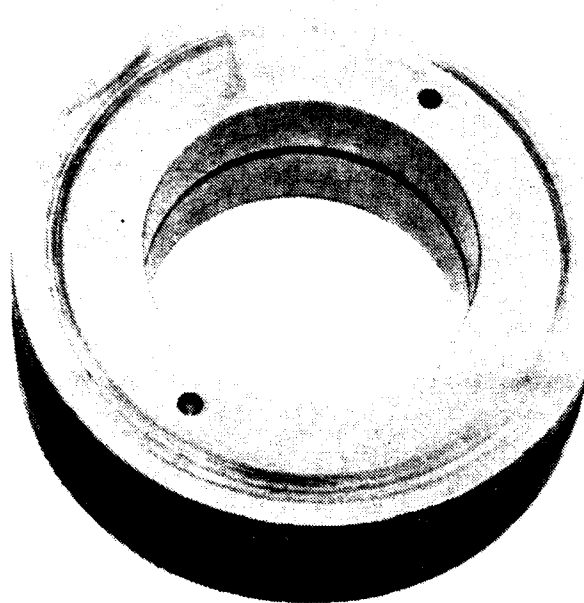


Figure 54. Aft Side of Koppers Runner After Performance Testing



Figure 55. Close-Up of Koppers Aft Stationary Seal Sealing Interface After Performance Testing

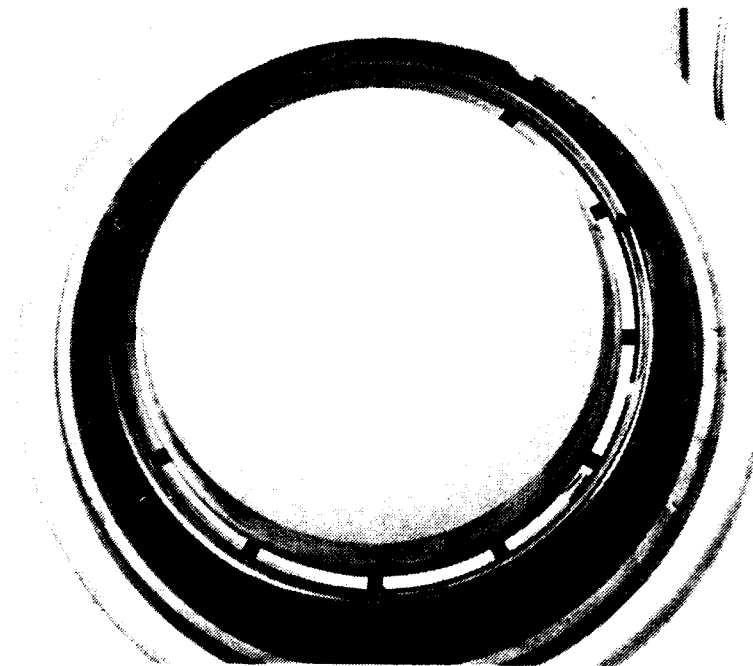


Figure 56. Koppers Aft Stationary Seal Components and Center Housing After Performance Testing

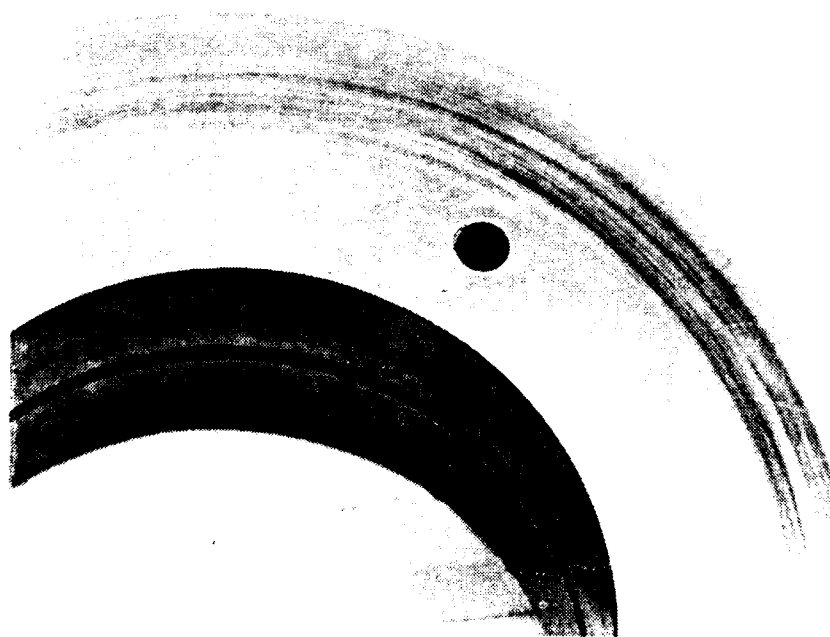


Figure 57. Close-Up of Aft Face of Koppers Runner After Performance Testing



Figure 58. Corrosion on Outside Diameter of Koppers Running After Performance Testing

seal was noted. This seal had been replaced at build-up for the endurance test because of assembly damage. Total running time on that seal at test cessation was therefore 71 hours while the other had 90.5 hours. Table 4 shows a summary of the leakage results recorded during the endurance testing.

Disassembly revealed that both anti-rotation dowels in each housing member had failed in multi-origin fatigue at the runouts between the triangular-shaped and round sections of the dowels. Without circumferential restraint the stationary seals rotated, dislodging and damaging some of the loading springs and thermocouples. Typical views are shown in Figures 60 through 62. As can be seen in Figure 63 the faces of the seals had suffered cavitation erosion pitting over short arcs extending (in the direction of runner rotation and water circulation) from the proximity probes utilized for gap measurements during the performance testing. Evidently the protrusion of the probe tips provided turbulent wakes which promoted cavitation. Pitting was also noted on the runner outer diameter as shown in Figure 64. This was located only in depressions formed by material removal for rotor dynamic balance.

Investigation of the dowel failures, unprecedented in Koppers' experience, indicated a number of possible causes, in order of greatest likelihood:

- (1) high torsional vibration due to failure of circuit board in drive motor SCR during performance testing
- (2) excessive torques arising from inadvertent very high acceleration and deceleration of the rotor during performance testing

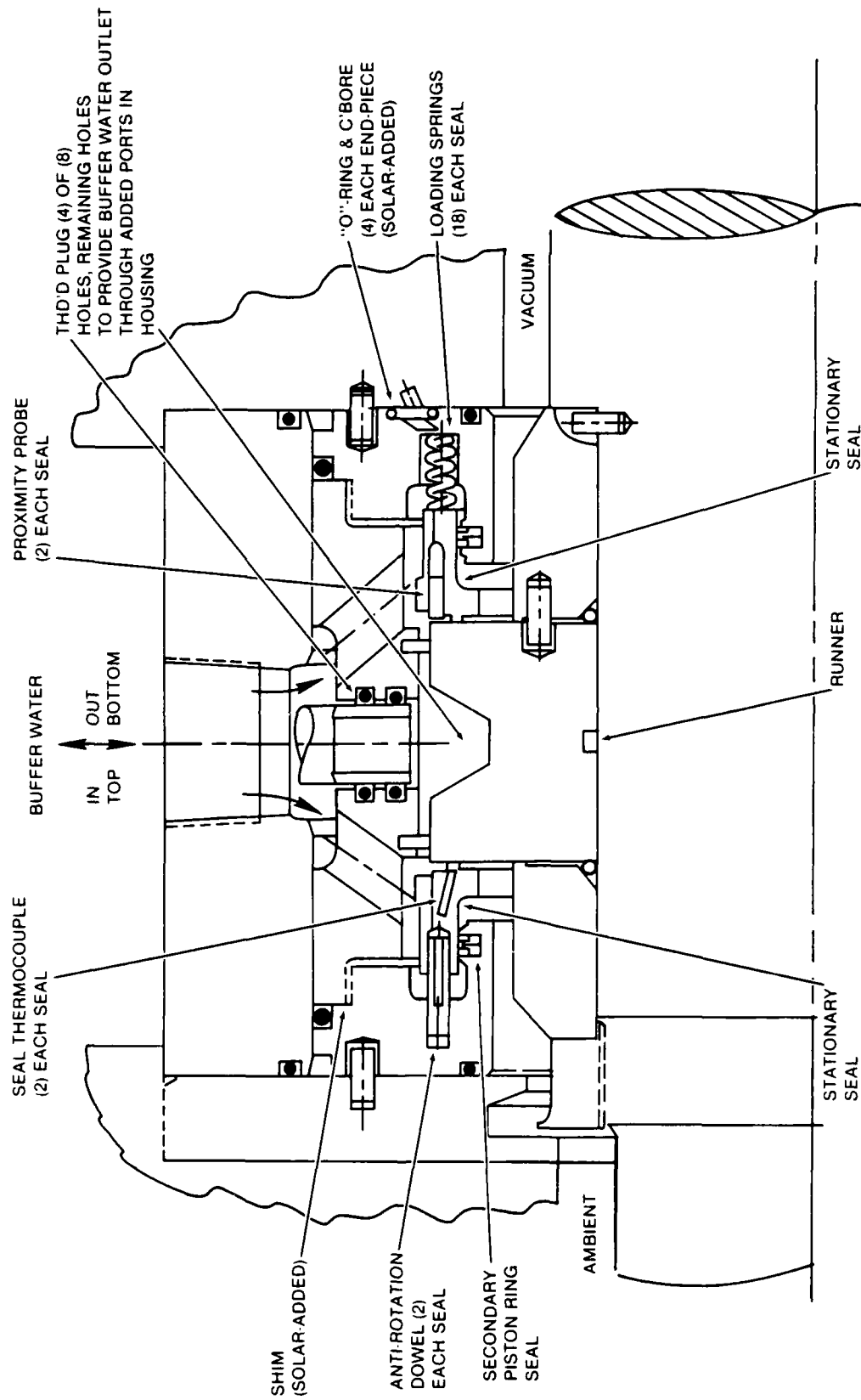


Figure 59. Koppers Face Seal Assembly, Modified

Table 4

Endurance Test Running Time ~ Hr.	Atmosphere-Side (Forward)				Seal Leakage			Vacuum-Side (AFT) Seal Leakage		
	Interval Hr.	Vol. Liters	Rate L/Hour	Cumulative Rate (Gal/Day)	Interval Hr.	Vol. Liters	Rate L/Hr	Cumulative Rate (Gal/Day)		
7.0	6.7	0.248	0.037	0.037	6.7	4.5	0.67	0.67	4.3	
11.8	4.8	0.379	0.079	0.055	4.0	1.36	0.34	0.55	3.5	
18.5	6.7	0.520	0.078	0.063	6.7	4 +	0.60	0.57	3.6	
24.0	5.5	0.051	0.009	0.051	5.5	9.7	1.76	0.68	4.3	
32.6	8.6	0.634	0.074	0.057	8.6	9.5	1.10	0.79	5.0	
51.0	11.2	1.2	0.107	0.070	11.2	11.2	0.73	0.78	4.9	
67.0	16.0	3.5	0.219	0.110	16.0	5.6	0.35	0.66	4.2	
71.0	4.0	1.0	0.250	0.119	4.0	36.2	9.05	1.20	7.6	
71.1	N/R				5 min.	7.6	91.2	1.30	8.2	

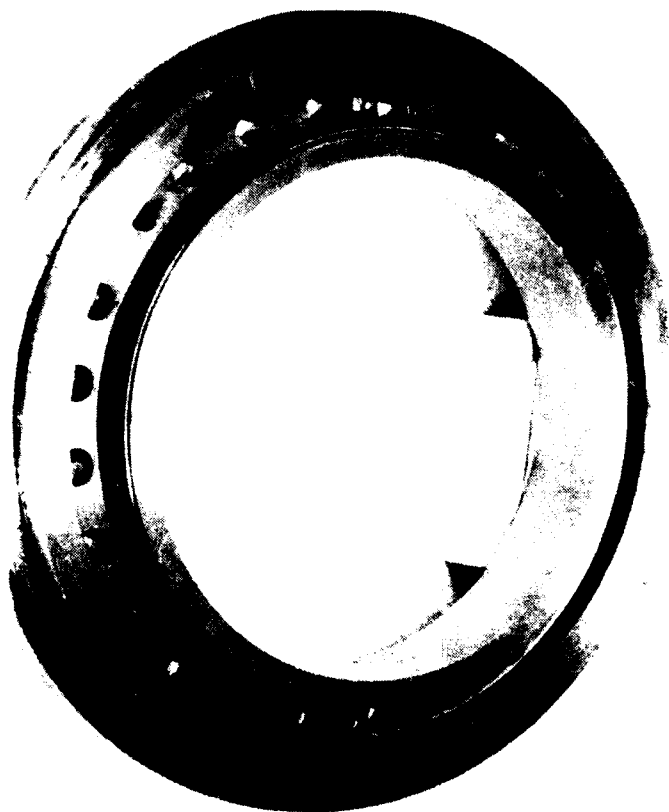


Figure 60.

Koppers Atmosphere-Side (Forward)
End Housing After Failure at 71
Hours of Endurance Test

Figure 61.

Close-Up of Figure 60 Housing
Showing Failed Anti-Rotation
Dowell and Typical Secondary
Damage

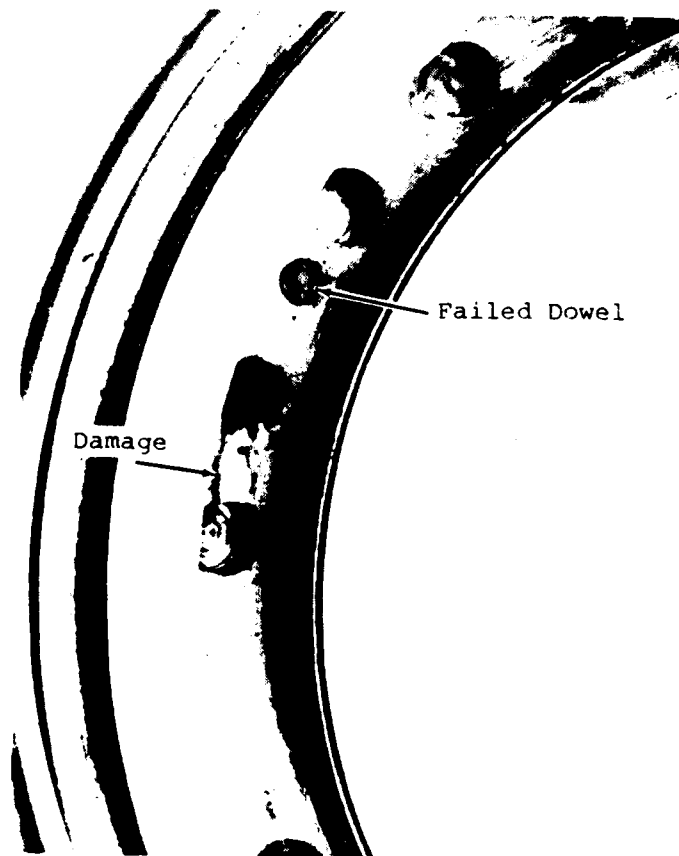


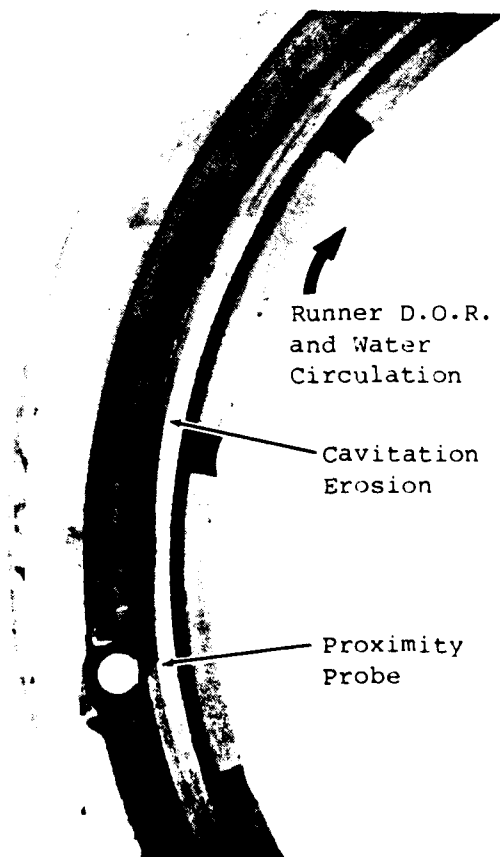


Figure 62.

Close-Up of Figure 60 Housing Showing Multi-Origin Fatigue on Fracture Surface of One Failed Anti-Rotation Dowel

Figure 63.

Close-Up of Figure 61 Seal Showing One of Two Areas of Pitting on Land Near Proximity Probe



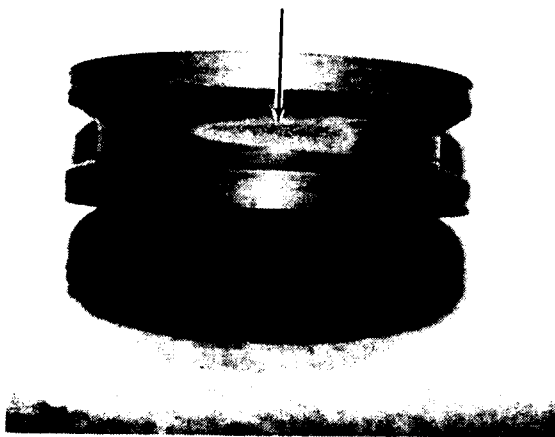


Figure 64.

Koppers Runner Showing Severe Corrosion and Erosion Pitting at Area of Material Removal (for Rotor Dynamic Balancing)

- (3) sharp radius on dowels at position of fractures
- (4) radial forces associated with localized cavitation on runner OD

All of the above factors could be eliminated by operating procedures and/or revised design features. In summation, the dowel failures did not constitute an impasse to the satisfactory operation of the Koppers seal but may be considered strictly mechanical failures with typical design engineering solutions.

Three factors demand mention relative to the cavitation erosion:

- . The proximity probes, which evidently each provided a turbulent wake to "trigger" cavitation, would not be present in production-type seals.
- . The runner was slightly larger in diameter than otherwise required so as to present a "target" surface for the proximity probes.
- . The localized depression where the erosion occurred on the runner outer diameter (material removed for rotor balancing) should be located on an unwetted surface.

Thus, with design modifications, avoidance of cavitation erosion might be possible with the Koppers assembly.

The Crane NASA-Solar seals were not endurance tested on the automated cycle schedule primarily because cavitation appeared during the first 29 hours of performance evaluation. Total running time on these seals was 29 hours.

4.8 SEAL BIBLIOGRAPHY

A partial bibliography, with emphasis on face seals, is included as Appendix V.

5

DISCUSSION OF RESULTS

The NASA-Solar seal assembly performed about as intended demonstrating zero leakage or leakage below the target value of 11 liter/day (3 gal/day) over a range of buffer pressures at each speed tested. At low buffer pressures air bubbles, of increasing volume as pressure was reduced, were observed in the buffer water outlet flow as it passed through the glass tube of the flowmeter. Zero water leakage was, however, still obtained under these circumstances. The pressure at which bubbles were no longer formed was found to increase with speed. While computed seal performance included satisfactory operation at low buffer pressures at all speeds, it seemed that actual pumping action of the runner spiral grooves on air was sufficient to overcome low buffer water pressures. This speed-related effect could in tests be eliminated by operating at slightly higher buffer pressures. Higher buffer pressures also aid in suppression of cavitation.

Cavitation-erosion was found to occur at the higher speeds tested. This can be minimized by keeping all surfaces as smooth as possible and no larger than necessary (particularly diameter), and minimizing the changes in direction the water is required to make, as for example by tangential entry and exit.

Demonstration of operation in accordance with analytical predictions was confirmed by measurement of separation of the sealing interfaces (Figure 27). It is believed that the aft seal did operate at somewhat lower film thicknesses than the forward seal because of the wear noted at first disassembly, particularly at the outer periphery of the runner and the outer half of the stationary seal. A cause for the wear could have been waterborne rust particles, however, the aft seal suffered significantly greater wear than the forward seal. Crane offered a possible explanation for this difference, suggesting hard particles of chrome left in the groove bottoms coming loose from that side of the runner. The second plating job resulted in much improved grooving with no residual particles.

The Koppers seals, once "run-in", produced low leakage rates. Also, separation of the sealing interfaces of about the estimated magnitude was detected during operation with the proximity probes.

During all the testing no seal behavior was encountered which would prevent turbine operation in the usual gas turbine fashion, i.e., typical start-up and shutdown acceleration and deceleration. The seal operating temperatures, for example, were found to reach near-equilibrium values within 2-3 minutes.

The Koppers parasitic drag losses were somewhat greater than they might otherwise have been with production-type seals. This was because the test seal runner diameter was slightly larger than necessary to provide target

surfaces for the 3.2 mm (0.125 in.) diameter proximity probes in the stationary seals. (The proximity probes in the NASA-Solar seals were "buried".) Ignoring other factors and assuming the same seal inner diameter, the differing radial width requirements of the sealing faces would rank the seals Koppers then NASA-Solar in order of increasing parasitic losses, mainly because those losses vary as the fourth power of the diameter of the surface in contact with the water. Since the losses vary only directly with the length of that surface, however, a wider but profiled runner such as the Koppers design should, generally, be considered by evaluation with the analyses in Appendix IV of this report. The Crane runner had chordal holes intended to promote cooling: they created pumping losses of about 3 kW (10.5 HP) at 12000 rpm.

Much experience was obtained with the use of water as a lubricant and in the application of face seals to the turbine. This has been collated in a self-sufficient form and presented in the section entitled "Design Guidelines".

Finally but very significantly, a development of the NASA-Solar seal was devised which overcomes both the factors which presented difficulties for the tested seals. The new type is shown in Figure 3 of the Summary. The area at the outer diameter of the runner is vented to vacuum rather than flooded with buffer water. The buffer water for lubrication and cooling is supplied separately through two sets of internal passages. Confidence that this type will not suffer cavitation erosion damage is, it is believed, offered by the test results of both seal assemblies - no erosion was found on the vacuum side of the sealing interfaces. Additionally, it may be seen by comparison of Figures 1 and 3 that one of the stationary seals has been eliminated further reducing parasitic losses. A similar adaptation of the Koppers seal would demand addition of a second sealing surface radially outwards of the first and an intervening annulus for the water buffer supply. Whether such a drastic revision to the original design, particularly involving as it would more than doubling the face area which must remain square and flat within very stringent limits during operation, would be viable is considered doubtful.

In summary, it is believed that the performance of the NASA-Solar and Koppers seals was as intended. Leakage rates varied from zero to about 11 liters/day (3 gal/day) at buffer system pressures which can readily be supplied and controlled. The seal static leakages were also low enough to permit continuous, moderate-level buffer system pressurization without exceeding target leakage even though the turbine is not operating.

6

DESIGN GUIDELINE

1. Seal performance and life can be enhanced by venting the seal at the high pressure (steam) end of the turbine rotor also to the condenser hot well (vacuum). The primary advantage of such a configuration is that it provides an essentially isothermal environment for the seals. Face seals have stringent requirements for flatness and squareness which would be difficult to maintain with the potentially large temperature gradients arising from the close proximity of steam. With the seals at both ends of the turbine having the same sealing environment and at least similar requirements, commonality of seal assemblies might be possible.
2. Carefully integrate the seal assembly into the turbine detail design. The seal vendor(s) should be required to submit fully dimensioned component and assembly drawings with recognized military, aerospace, or industry material specifications, including coatings and plating with thickness(es) and area(s) of coverage, and loading spring data. It should not be possible for the stationary seal loading springs to be compressed to their solid height in order to prevent distortion damage as might occur during build-up. Provision of a retention feature to hold the stationary seals against the loading springs past the subassembly stage is recommended. Where the stationary seals on either side of the runner have detail differences, "Murphy-proofing" to prevent interchanging them at assembly is mandatory. Assembly and subsequent in-service repair/replacement are greatly facilitated by configuring the seal assembly as a "plug-in" unit. It is recommended that provision be made to allow checking after complete assembly that the runner is properly located axially. That is, the spring deflection must produce loading of each stationary seal against the runner within acceptable (vendor-supplied) limits.
3. Minimize parasitic friction drag losses resulting from contact of rotating surfaces with the buffer water by minimizing rotating component exposed diameters (power \propto diameter⁴), speed (power \propto speed³), axial dimensions (power \propto length) and by minimizing the operative coefficient of friction (power \propto friction coefficient), consistent with optimum seal operating temperature requirements. (In the absence of applicable experimental experience, the theoretical analyses in Appendix IV of this report may be used.)
4. Arrange buffer water inlet and outlet flows so as to maintain as uniform a circumferential temperature distribution as possible in the stationary seals. If possible, avoid porting arrangements, etc. which tend to promote development of turbulent wakes or require changes in direction of

flow in favor of those which tend to reduce the relative velocity of the water flow and any rotating surfaces the water contacts. Multiple tangential inlets and outlets, for example, could be considered along with the absence of protruberances and interruptions in surfaces so as to minimize the chances for cavitation erosion. This applies particularly to instrumentation and includes localized removal of material for rotor balance.

5. Eliminate as far as practical the possibility of corrosion of wetted components. (Corrosion products and any other abrasive foreign material are extremely detrimental to both seal performance and life.) Machined AISI 304, 316 and 17-4 PH stainless steels, nylon, and CPVC plastic components can be recommended, based on successful use in this development program, with due consideration of limitations imposed by temperature and water-induced dimensional change of non-metallics.
6. During initial turbine build-up minimize seal lube water system contamination by an appropriate scrupulous cleaning procedure. Provision of water lube system filtration with capability to remove contamination including corrosion products is essential.
7. Ethylene propylene and nitrile material "O"-rings are, based on experience in this program, considered superior to Viton A for lube system use with water at temperatures under 90°C (200°F) because of a lesser tendency to take on a permanent set.
8. The use of teflon coatings and components and, at assembly, silicone grease (e.g., Dow Corning Stopcock or #11 silicone greases) as means to reduce static friction should be considered especially in the secondary seal area. With "O"-ring secondary seals loading hysteresis resulting from turbine rotor axial movements due to thrust bearing clearance and/or differential thermal expansion may have to be taken into account or avoided. Grease, however, must not be allowed to enter the sealing interface either by handling or, subsequently, in operation when increased temperatures may allow it to flow more readily.
9. During development testing of the actual steam turbine provision should be made for measurement of seal static leakage and, during operation, for varying buffer water pressure and flow and measuring seal leakages and temperatures and buffer flows and temperatures. This would permit optimization of the seal system design. The installation of proximity probes in each stationary seal to detect the gap between it and the runner would be desirable. The purpose would be to determine whether any instability occurred indicating the necessity for greater spring loading and/or stiffness. Observe guideline 4 above in determination of transducer location.
10. The seals in production turbines should be run-in by operating step-wise at progressively higher speeds.

7

CONCLUSIONS

1. An optimum mainshaft bearing and seal system for advanced US Navy COGAS steam turbines is a buffered system utilizing as the buffer fluid system feedwater obtained from the condensate boost pump and returned via the condenser hot well.
2. Face-type seals offer the most promise for achieving target overall system external leakage rates of 11 liters/day (3 gal/day) over the intended 15,000 hour turbine (TBO). Significant overall water treatment system simplification is feasible and attractive with their use.
3. Face seal performance and life can be enhanced by venting, through an appropriate labyrinth seal for example, the turbine high pressure end also to the condenser vacuum. This would provide, with no additional system water external loss, an essentially isothermal environment for the seals. High thermal gradients which can be detrimental to face seals and which would accompany sealing of steam would be eliminated.
4. Experimental evaluation of specially designed and manufactured candidate seals in a test rig showed that target leakage rates could be achieved with two vendor-supplied seal assemblies, Crane and Koppers.
5. Parasitic friction drag power losses can be substantial. They can be fairly closely estimated, and therefore minimized, by careful seal assembly design in accordance with existing theoretical treatments.
6. Cavitation-erosion damage was found to occur at the upper end of the tested speed range. This can be minimized by ensuring that wetted surfaces are as small in diameter and as smooth as possible and that water trajectories are as straight as possible, with tangential entry and exit for example.
7. A modified Crane NASA-Solar spiral groove seal was devised with the outer diameter vented to vacuum, circumventing the parasitic drag and cavitation problems. A similar approach with the Koppers seal appeared to be much more difficult if possible at all.
8. The experimental testing also showed that the water-lubricated face seals, once "run-in", could safely be operated in typical gas turbine fashion, i.e., did not require complex, slow start-up procedures.
9. Some scoring damage was encountered in the testing of the sealing interfaces from foreign material inadvertently admitted to the water system downstream of the filter.

8

RECOMMENDATIONS

1. Incorporate the modified Crane NASA-Solar spiral groove seal with its outer diameter vented to vacuum in the RACER COGAS steam turbine. Verification testing is recommended.
2. Determine the filtration requirements for the seal lube water supply system to prevent scoring damage to the seal interface from corrosion products or other contamination.

APPENDIX I

VENDOR PROPOSED DESIGNS

DISTR.		DATE		BY	
ARGEN.					
AUST.					
CAN.					
HOLL.					
JAPAN					
MEX.					

RELEASE TO MFG				BY	
REVISIONS					
LTR	E.C.N.	BY	DATE	CK	
A	2A	DK	13 Jun 78		

THIS MATERIAL IS THE PROPERTY OF BORG WARNER CORPORATION AND IS FURNISHED ONLY FOR THE PURPOSE INDICATED ANY AND ALL CONFIDENTIAL, PROPRIETARY, PATENT AND OTHER RIGHTS IN THE SUBJECT MATTER BEING RETAINED INCLUDING ANY RIGHT TO REPRODUCE THIS MATERIAL IN WHOLE OR IN PART OR MANUFACTURE THE SUBJECT MATTER SHOWN THEREIN OR USE THE CONFIDENTIAL OR PROPRIETARY INFORMATION THEREON. SUCH PERMISSION TO BE GRANTED ONLY BY SPECIFIC AUTHORIZATION IN WRITING SIGNED BY AN OFFICER OR OTHER AUTHORIZED AGENT OF BORG WARNER CORPORATION ITS DIVISIONS OR SUBSIDIARIES.

4.565 BONE
4.560 DEPTH

320 (TYP)
300

I DRILL 1 DEEP
32 ONE PLACE
ON 4 8 BC
BOTH ENDS
IN SAME
ANGULAR PLANE
(ANY POSITION)

36
5.250
5.253 (2 PLCS)

2.750
2.748
3.062
3.059
2.755
2.754
3.062
3.059
.065
.075
2 PLCS

SCALE - FULL

CK BR

S- APP DATE 9 MAY 78

REV

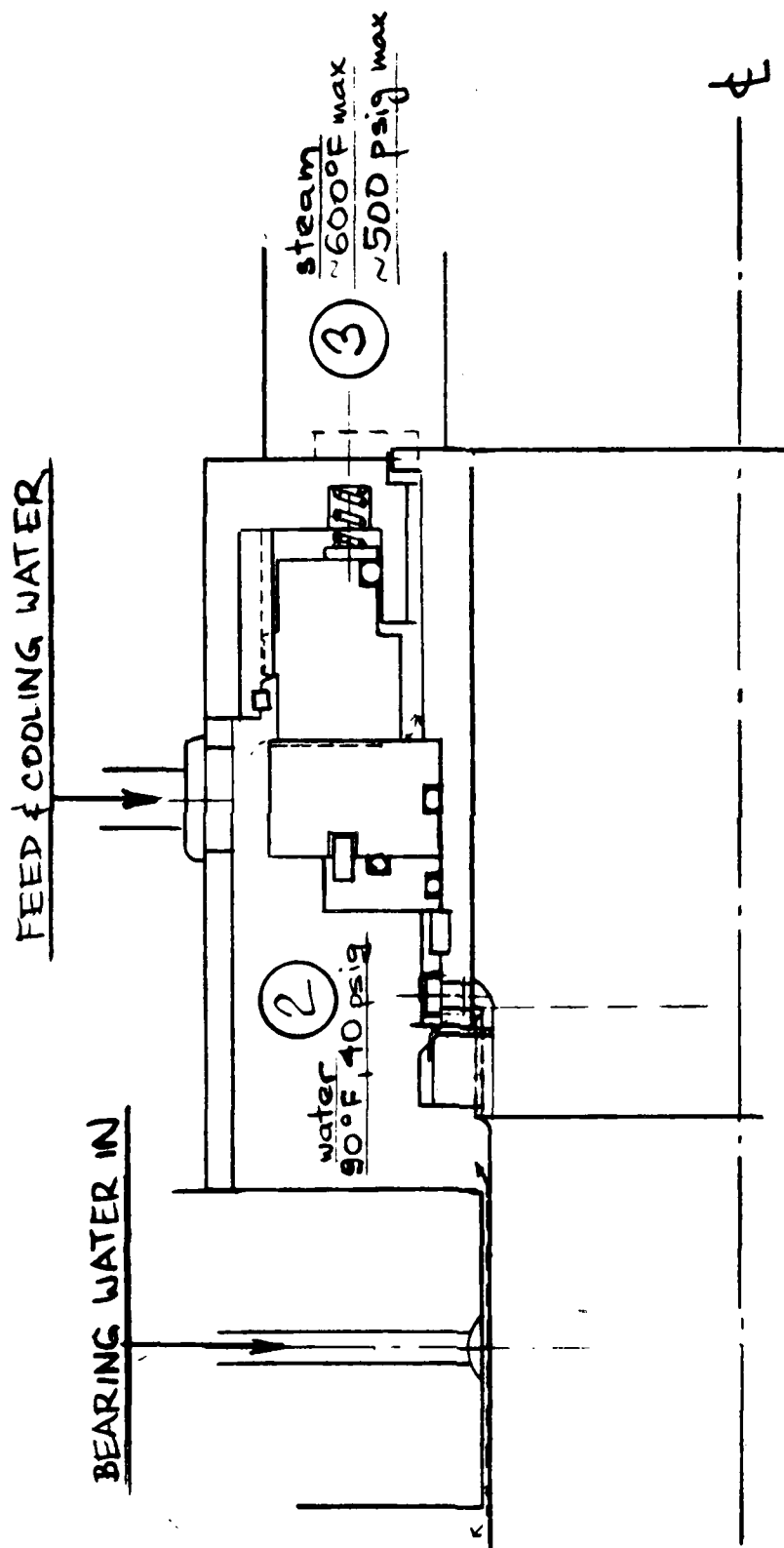
PROP 78064-R

GW 300
DOUBLE 50PL

Mechanical Seal Division
BORG WARNER CORPORATION TENCLE, CA 92390

UNLESS OTHERWISE SPECIFIED
BREAK OR DEBURR SHARP EDGES
INTERNAL CORNERS .000 R40 H
SURFACE FINISH 125 PER ANSI B46.1
DIMENSIONAL TOLERANCES
ANGLES ±3°
HOLES ±.010 DIA
OTHER .000 FROM MMC
INTERPRET PER ANSI Y14.5

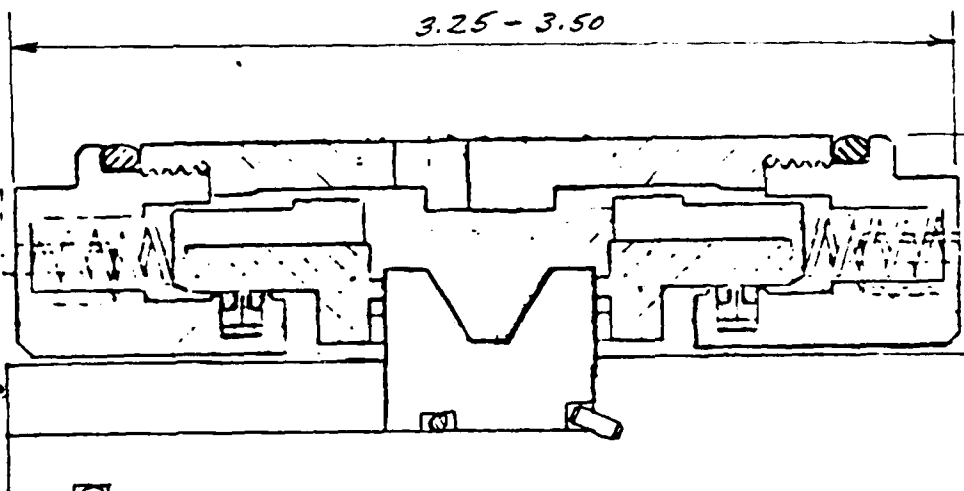
Copy available to DTIC does not
permit fully legible reproduction



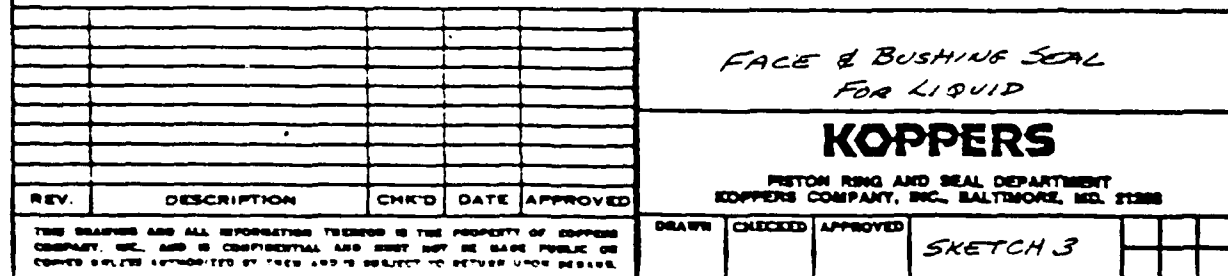
WATER BEARING & REVERSE T20 SEAL - SOLAR

py ... to DMC does not
 permit fully legible reproduction

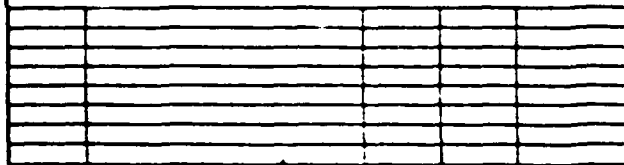
J. SEDY
 5-24-78

				
3.25 - 3.50 2.8 6.12				
DOUBLE FACE SEAL				
KOPPERS PISTON RING AND SEAL DEPARTMENT KOPPERS COMPANY, INC., BALTIMORE, MD. 21205				
REV.	DESCRIPTION	CHK'D	DATE	APPROVED
THIS DRAWING AND ALL INFORMATION THEREON IS THE PROPERTY OF KOPPERS COMPANY, INC. AND IS CONFIDENTIAL AND MUST NOT BE MADE PUBLIC OR COPIED UNLESS AUTHORIZED BY THEM AND IS SUBJECT TO RETURN UPON DEMAND.				
DRAWN		CHECKED	APPROVED	SKETCH 1 <div style="display: flex; justify-content: space-around;"> <div style="border: 1px solid black; width: 20px; height: 20px;"></div> <div style="border: 1px solid black; width: 20px; height: 20px;"></div> </div>

Copy available to DTIC does not permit fully legible reproduction



84



KOPPERS

REV.	DESCRIPTION	CNCD	DATE	APPROVED
------	-------------	------	------	----------

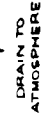
DRAWN	CHECKED	APPROVED
-------	---------	----------

85

The Draftboard Inc

88

10. FOR SHIP, USE IN ONE COLUMN 11. FOR SHIP, USE IN TWO COLUMNS 12. FOR SHIP, USE IN THREE COLUMNS	13. SHIP NAME 14. SHIP TYPE 15. SHIP NO. 16. SHIP CODE 17. SHIP CLASS 18. SHIP TYPE 19. SHIP NO. 20. SHIP CODE 21. SHIP CLASS 22. SHIP TYPE 23. SHIP NO. 24. SHIP CODE 25. SHIP CLASS 26. SHIP TYPE 27. SHIP NO. 28. SHIP CODE 29. SHIP CLASS 30. SHIP TYPE 31. SHIP NO. 32. SHIP CODE 33. SHIP CLASS 34. SHIP TYPE 35. SHIP NO. 36. SHIP CODE 37. SHIP CLASS 38. SHIP TYPE 39. SHIP NO. 40. SHIP CODE 41. SHIP CLASS 42. SHIP TYPE 43. SHIP NO. 44. SHIP CODE 45. SHIP CLASS 46. SHIP TYPE 47. SHIP NO. 48. SHIP CODE 49. SHIP CLASS 50. SHIP TYPE 51. SHIP NO. 52. SHIP CODE 53. SHIP CLASS 54. SHIP TYPE 55. SHIP NO. 56. SHIP CODE 57. SHIP CLASS 58. SHIP TYPE 59. SHIP NO. 60. SHIP CODE 61. SHIP CLASS 62. SHIP TYPE 63. SHIP NO. 64. SHIP CODE 65. SHIP CLASS 66. SHIP TYPE 67. SHIP NO. 68. SHIP CODE 69. SHIP CLASS 70. SHIP TYPE 71. SHIP NO. 72. SHIP CODE 73. SHIP CLASS 74. SHIP TYPE 75. SHIP NO. 76. SHIP CODE 77. SHIP CLASS 78. SHIP TYPE 79. SHIP NO. 80. SHIP CODE 81. SHIP CLASS 82. SHIP TYPE 83. SHIP NO. 84. SHIP CODE 85. SHIP CLASS 86. SHIP TYPE 87. SHIP NO. 88. SHIP CODE 89. SHIP CLASS 90. SHIP TYPE 91. SHIP NO. 92. SHIP CODE 93. SHIP CLASS 94. SHIP TYPE 95. SHIP NO. 96. SHIP CODE 97. SHIP CLASS 98. SHIP TYPE 99. SHIP NO. 100. SHIP CODE 101. SHIP CLASS 102. SHIP TYPE 103. SHIP NO. 104. SHIP CODE 105. SHIP CLASS 106. SHIP TYPE 107. SHIP NO. 108. SHIP CODE 109. SHIP CLASS 110. SHIP TYPE 111. SHIP NO. 112. SHIP CODE 113. SHIP CLASS 114. SHIP TYPE 115. SHIP NO. 116. SHIP CODE 117. SHIP CLASS 118. SHIP TYPE 119. SHIP NO. 120. SHIP CODE 121. SHIP CLASS 122. SHIP TYPE 123. SHIP NO. 124. SHIP CODE 125. SHIP CLASS 126. SHIP TYPE 127. SHIP NO. 128. SHIP CODE 129. SHIP CLASS 130. SHIP TYPE 131. SHIP NO. 132. SHIP CODE 133. SHIP CLASS 134. SHIP TYPE 135. SHIP NO. 136. SHIP CODE 137. SHIP CLASS 138. SHIP TYPE 139. SHIP NO. 140. SHIP CODE 141. SHIP CLASS 142. SHIP TYPE 143. SHIP NO. 144. SHIP CODE 145. SHIP CLASS 146. SHIP TYPE 147. SHIP NO. 148. SHIP CODE 149. SHIP CLASS 150. SHIP TYPE 151. SHIP NO. 152. SHIP CODE 153. SHIP CLASS 154. SHIP TYPE 155. SHIP NO. 156. SHIP CODE 157. SHIP CLASS 158. SHIP TYPE 159. SHIP NO. 160. SHIP CODE 161. SHIP CLASS 162. SHIP TYPE 163. SHIP NO. 164. SHIP CODE 165. SHIP CLASS 166. SHIP TYPE 167. SHIP NO. 168. SHIP CODE 169. SHIP CLASS 170. SHIP TYPE 171. SHIP NO. 172. SHIP CODE 173. SHIP CLASS 174. SHIP TYPE 175. SHIP NO. 176. SHIP CODE 177. SHIP CLASS 178. SHIP TYPE 179. SHIP NO. 180. SHIP CODE 181. SHIP CLASS 182. SHIP TYPE 183. SHIP NO. 184. SHIP CODE 185. SHIP CLASS 186. SHIP TYPE 187. SHIP NO. 188. SHIP CODE 189. SHIP CLASS 190. SHIP TYPE 191. SHIP NO. 192. SHIP CODE 193. SHIP CLASS 194. SHIP TYPE 195. SHIP NO. 196. SHIP CODE 197. SHIP CLASS 198. SHIP TYPE 199. SHIP NO. 200. SHIP CODE 201. SHIP CLASS 202. SHIP TYPE 203. SHIP NO. 204. SHIP CODE 205. SHIP CLASS 206. SHIP TYPE 207. SHIP NO. 208. SHIP CODE 209. SHIP CLASS 210. SHIP TYPE 211. SHIP NO. 212. SHIP CODE 213. SHIP CLASS 214. SHIP TYPE 215. SHIP NO. 216. SHIP CODE 217. SHIP CLASS 218. SHIP TYPE 219. SHIP NO. 220. SHIP CODE 221. SHIP CLASS 222. SHIP TYPE 223. SHIP NO. 224. SHIP CODE 225. SHIP CLASS 226. SHIP TYPE 227. SHIP NO. 228. SHIP CODE 229. SHIP CLASS 230. SHIP TYPE 231. SHIP NO. 232. SHIP CODE 233. SHIP CLASS 234. SHIP TYPE 235. SHIP NO. 236. SHIP CODE 237. SHIP CLASS 238. SHIP TYPE 239. SHIP NO. 240. SHIP CODE 241. SHIP CLASS 242. SHIP TYPE 243. SHIP NO. 244. SHIP CODE 245. SHIP CLASS 246. SHIP TYPE 247. SHIP NO. 248. SHIP CODE 249. SHIP CLASS 250. SHIP TYPE 251. SHIP NO. 252. SHIP CODE 253. SHIP CLASS
--	--



APPENDIX II-1

**SOLAR SOURCE CONTROL DRAWING
RSK 230832**

AD-A149 372

LOW LEAKAGE TURBINE SHAFT SEALS FOR ADVANCED COMBINED
CYCLE SYSTEMS(U) SOLAR TURBINES INC SAN DIEGO CA
G W HOSANG NOV 84 SR84-R-4622-36 N00024-78-C-5345

2/2

UNCLASSIFIED

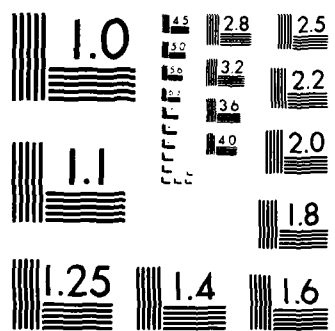
F/G 11/1

NL

END

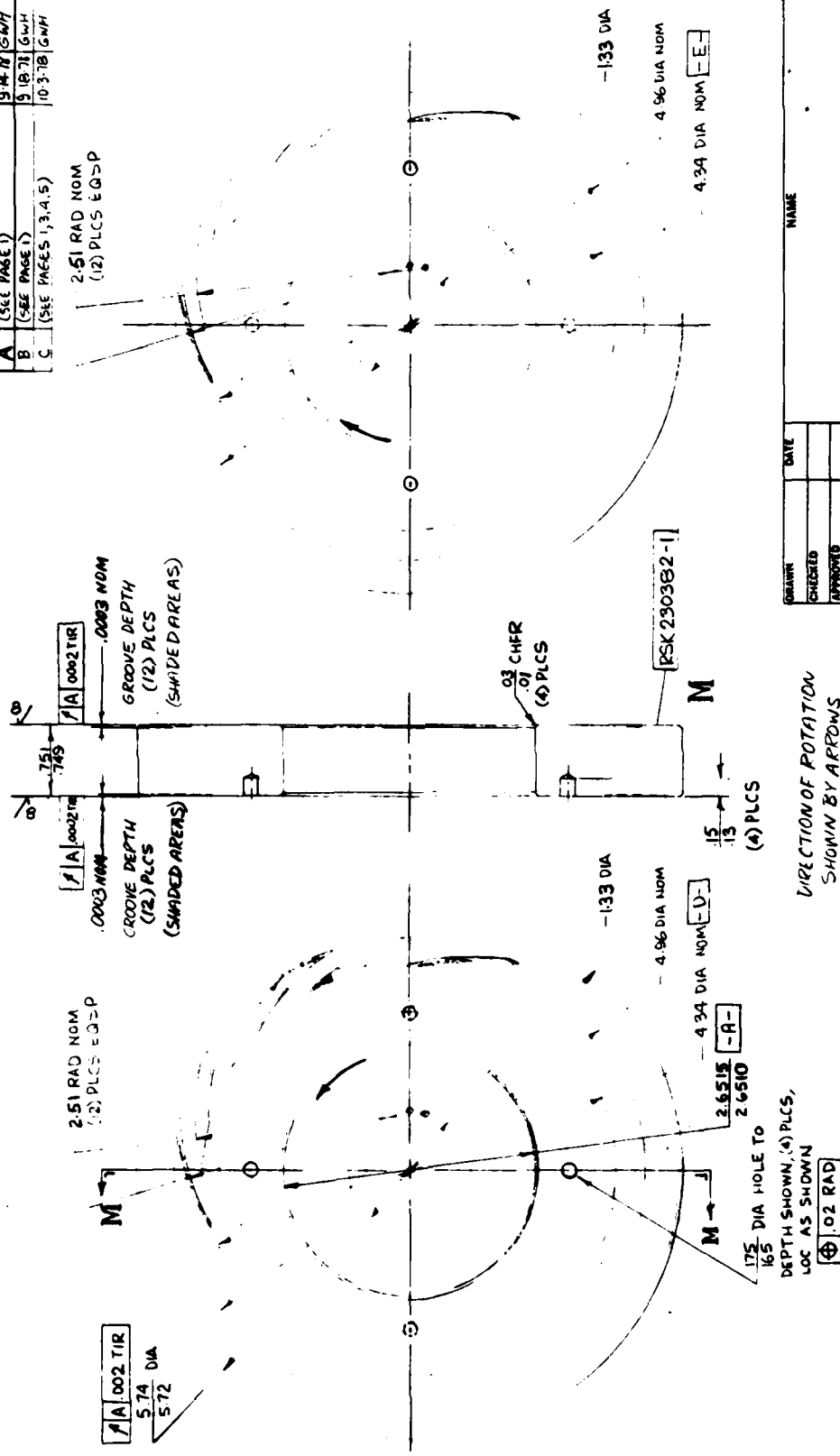
FILMED

DTIC



MICROCOPY RESOLUTION TEST CHART
NATIONAL BUREAU OF STANDARDS 1963-A

REV	DESCRIPTION	DATE	APP
A	(SEE PAGE 1)	9-14-78	GWH
B	(SEE PAGE 1)	9-18-78	GWH
C	(SEE PAGES 1, 3, 4, 5)	10-3-78	GWH

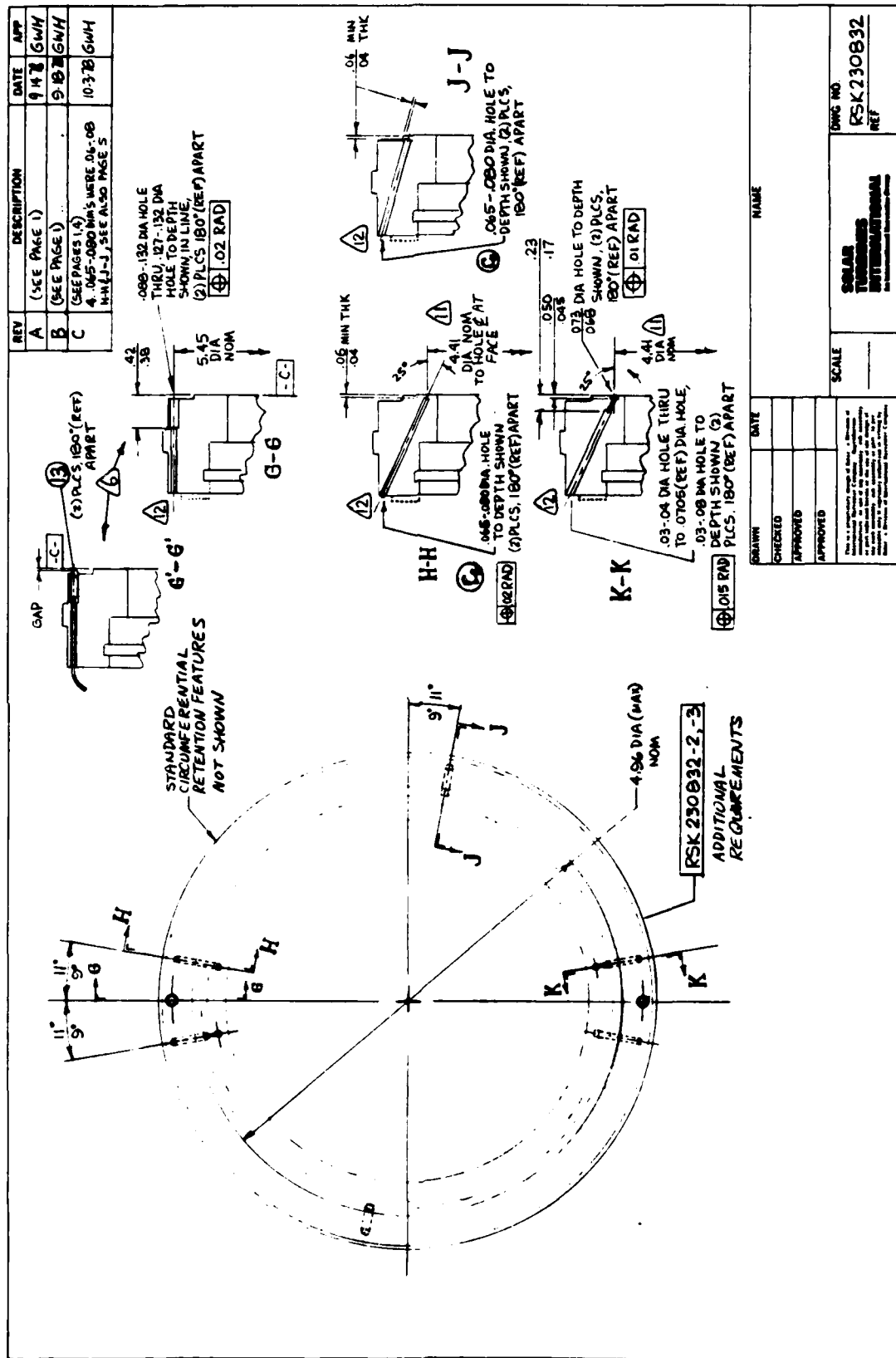


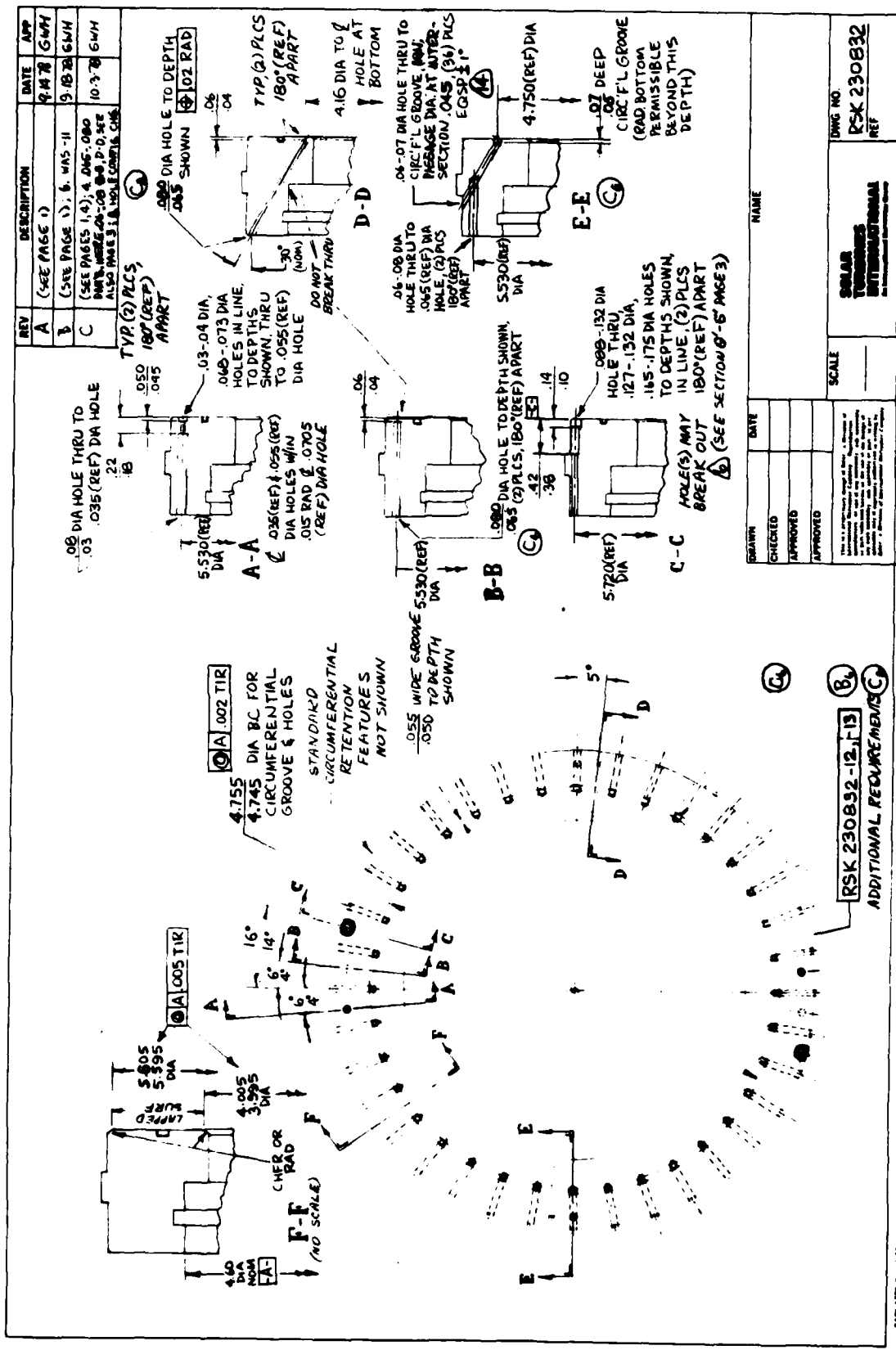
DIRECTION OF ROTATION
SHOWN BY ARROWS

DATE	NAME
CHECKED	
APPROVED	
APPROVED	
SCALE	
DRWG NO.	RSK 230382
REF	

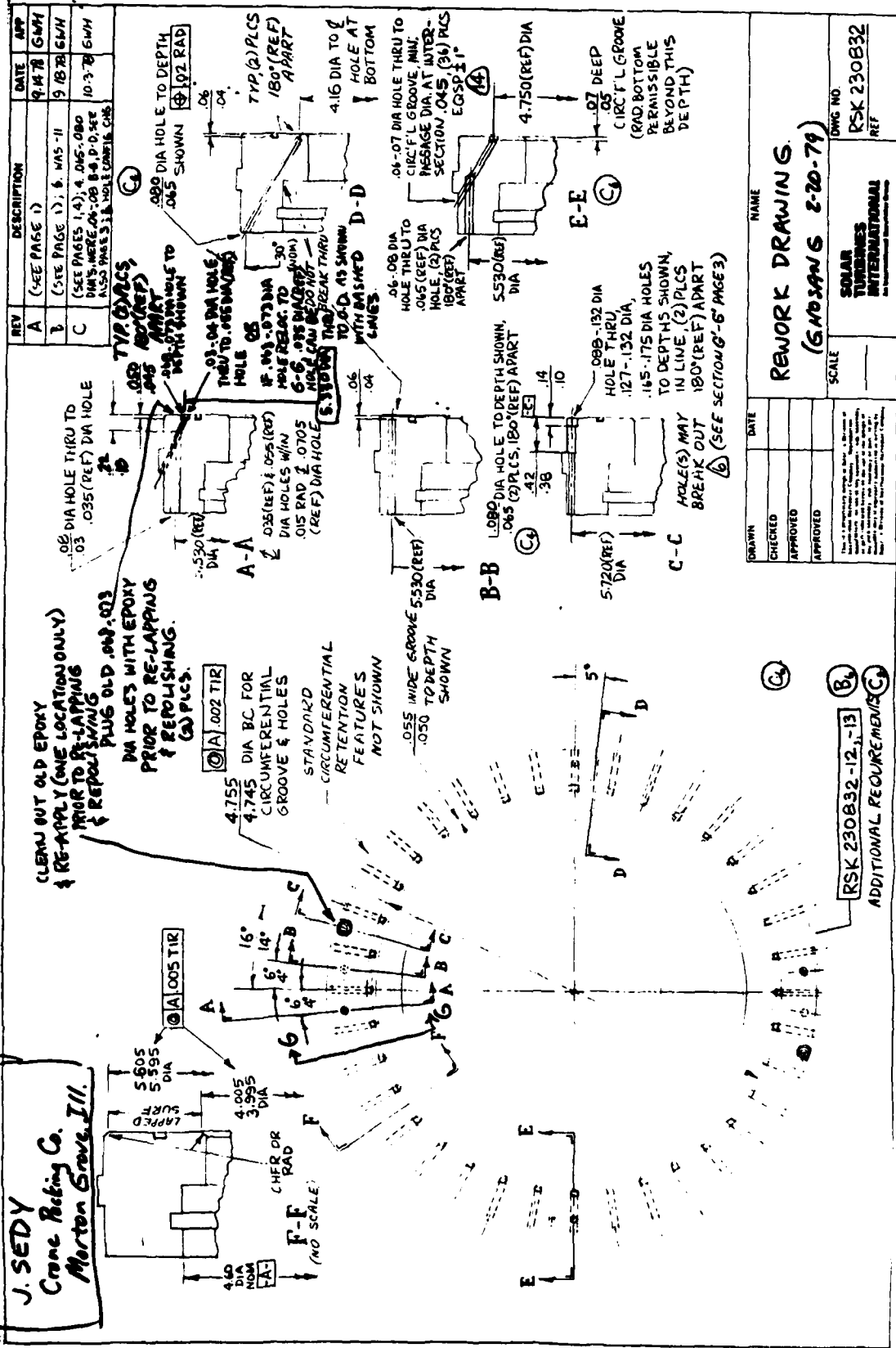
PAGE 2 OF 5

Scale 1:1.5





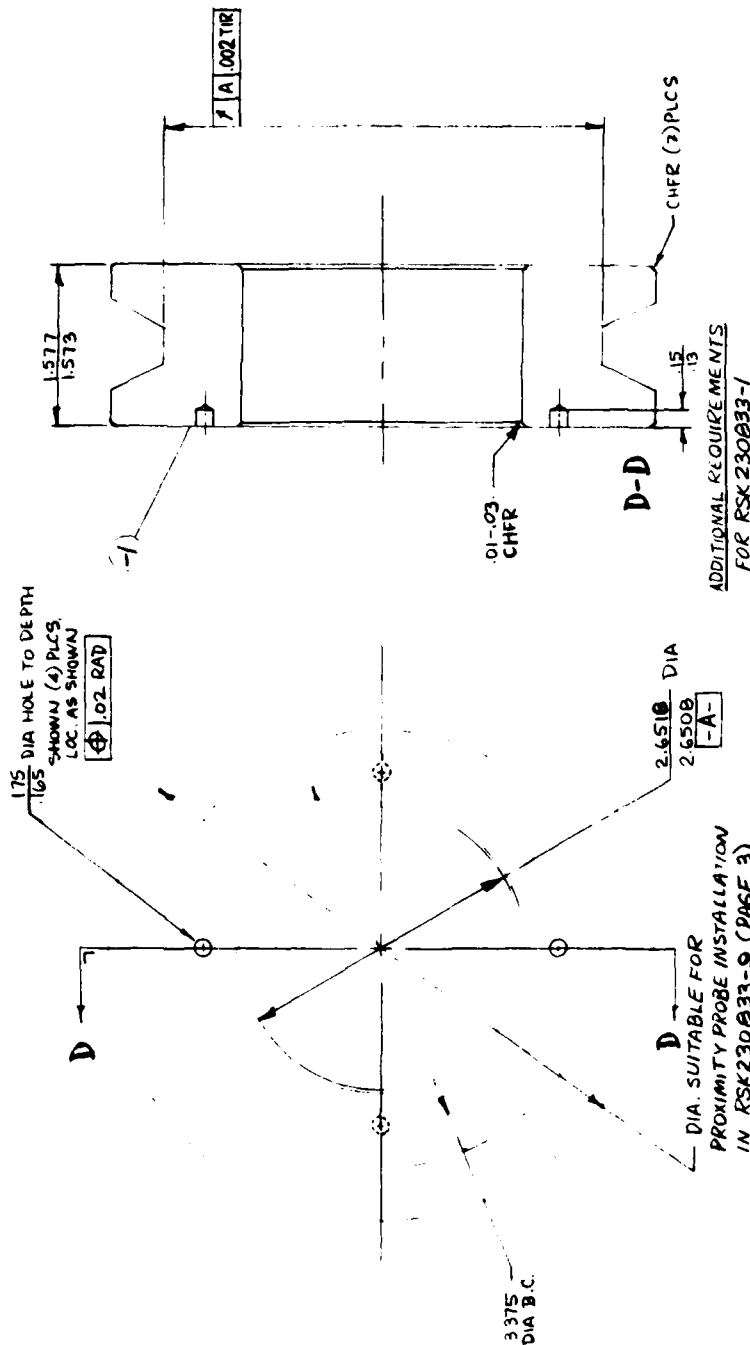
J. SEDY
Crane Raising Co.
Morton Grove, Ill.



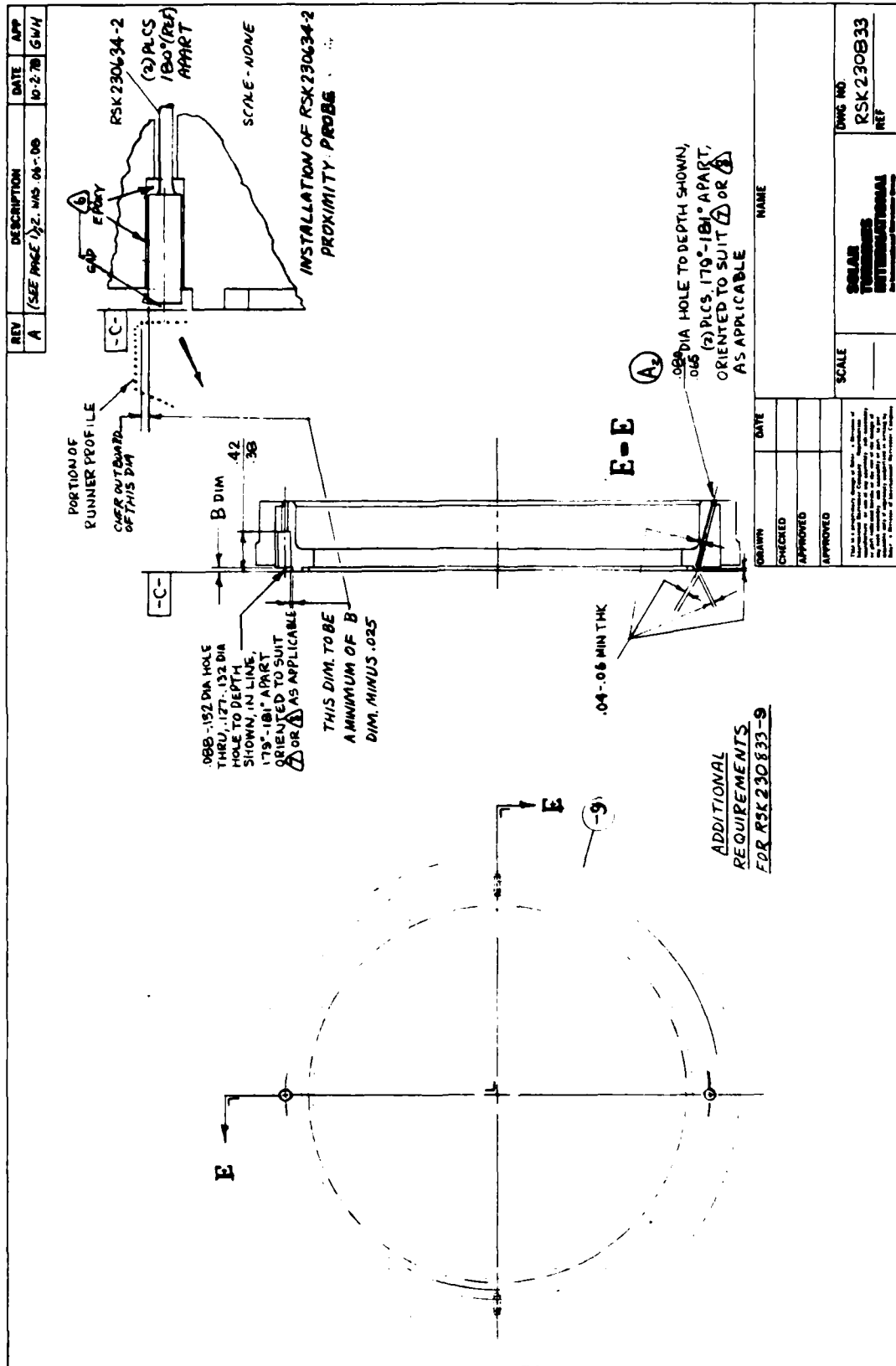
APPENDIX II-2

**SOLAR SOURCE CONTROL DRAWING
RSK 230833**

REV	DESCRIPTION	DATE	APP
A	(SEE PAGE 1, 3)	10-2-78	GAH



DRAWN	DATE	NAME
CHECKED		
APPROVED		
APPROVED		
THIS IS A PRELIMINARY DRAWING. It is subject to change without notice. It is not to be used for manufacturing purposes.		
SCALE	DWG NO.	REF.
	RSK230B33	
SOLAR TUNNERS INTERNATIONAL 10000 E. 10th Avenue, Suite 100 Denver, CO 80231		



APPENDIX III

EXPERIMENTAL DATA

App. Sub. Sec. 11

$\frac{1}{x^2} = x^{-2}$

NASA Solar H. Speed Perf. (3)

Large 0.0965 } Flow multiplier / 40 multiplier : 6 ft
Small 0.055 }

NASA Solar Hi-Speed Perf. (cont.)

Average 20565 { Power (top) / 80 factor = 2565 }
 25-11-0055

Functions	Vol Time Val	ATE Val	Temp										Vol Time Val	ATE Val	Cur rent	Oil Press Bar	Oil Temp Bar	Motor Temp Bar
			1	2	3	4	5	6	7	8	9	10						
7-22-81			Added 70's for motor 0.1 in. 0.1 in.															
9-40-81	2000	2000	40	52	51	51	50	40	40	30	30	31	39	56		55	58	30
9-40-81	1000	1000	41	53	52	52	52	40	40	33	33	34	40	39				35
10-40-81	1000	1000	41	53	53	53	53	39	39	33	36	40	39					35
10-05-81	1000	1000	42	58	54	53	53	39	39	33	35	41	40	60		56	60	35
10-13-81	1000	1000												60				35
10-24-81	1000	1000	41	55	55	53	53	40	40	34	43	43	42	60		57	62	35
10-26-81	1000	1000	41	57	57	56	56	41	41	34	44	44	42	62		57	62	35
10-35-81	1000	1000	42	58	58	56	56	41	41	34	44	44	42	62		57	62	35
10-40-81	1000	1000	43	59	58	57	57	41	41	36	47	49	42					35
11-00-81	1000	1000												65		56		35
10-27-81	1000	1000	43	61	60	58	58	41	41	36	48	50	43	69		58	68	35
10-30-81	1000	1000	43	61	61	60	59	41	41	35	50	50	42			58	68	35
11-00-81	11500	11500	43	63	63	60	60							73		60		35
11-10-81	11500	11500	44	64	64	61	61									60		35
11-20-81	11500	11500	44	64	64	61	61									60		35
11-30-81	11500	11500	44	64	64	61	61									60		35
11-40-81	11500	11500	44	64	64	61	61									60		35
11-50-81	11500	11500	44	64	64	61	61									60		35
11-55-81	11500	11500	44	64	64	61	61									60		35
11-56-81	11500	11500	44	64	64	61	61									60		35
11-57-81	11500	11500	44	64	64	61	61									60		35
11-58-81	11500	11500	44	64	64	61	61									60		35
11-59-81	11500	11500	44	64	64	61	61									60		35
12-00-81	11500	11500	44	64	64	61	61									60		35
12-01-81	11500	11500	44	64	64	61	61									60		35
12-02-81	11500	11500	44	64	64	61	61									60		35
12-03-81	11500	11500	44	64	64	61	61									60		35
12-04-81	11500	11500	44	64	64	61	61									60		35
12-05-81	11500	11500	44	64	64	61	61									60		35
12-06-81	11500	11500	44	64	64	61	61									60		35
12-07-81	11500	11500	44	64	64	61	61									60		35
12-08-81	11500	11500	44	64	64	61	61									60		35
12-09-81	11500	11500	44	64	64	61	61									60		35
12-10-81	11500	11500	44	64	64	61	61									60		35
12-11-81	11500	11500	44	64	64	61	61									60		35
12-12-81	11500	11500	44	64	64	61	61									60		35
12-13-81	11500	11500	44	64	64	61	61									60		35
12-14-81	11500	11500	44	64	64	61	61									60		35
12-15-81	11500	11500	44	64	64	61	61									60		35
12-16-81	11500	11500	44	64	64	61	61									60		35
12-17-81	11500	11500	44	64	64	61	61									60		35
12-18-81	11500	11500	44	64	64	61	61									60		35
12-19-81	11500	11500	44	64	64	61	61									60		35
12-20-81	11500	11500	44	64	64	61	61									60		35
12-21-81	11500	11500	44	64	64	61	61									60		35
12-22-81	11500	11500	44	64	64	61	61									60		35
12-23-81	11500	11500	44	64	64	61	61									60		35
12-24-81	11500	11500	44	64	64	61	61									60		35
12-25-81	11500	11500	44	64	64	61	61									60		35
12-26-81	11500	11500	44	64	64	61	61									60		35
12-27-81	11500	11500	44	64	64	61	61									60		35
12-28-81	11500	11500	44	64	64	61	61									60		35
12-29-81	11500	11500	44	64	64	61	61									60		35
12-30-81	11500	11500	44	64	64	61	61									60		35
12-31-81	11500	11500	44	64	64	61	61									60		35

NASA-Solar Hi-Speed Perf.(8)

45005
 45005

Impulsions 7.2.5	Leaf Vol Tm Val	Tm - Ps °C											Daily Pm Pm Pm	Vac Pm Pm Pm	OP Pm Pm Pm	Diff. In Pm Pm Pm	ATF Pm Pm Pm	Current Pm Pm Pm	Oil Pressure Pm Pm Pm	Power Pm Pm Pm			
		1	2	3	4	5	6	7	8	9	10	11											
11000 104		56	56	55	55	55	55	55	55	55	55	55	79	59	28	45	40	41	85	112	370	68	
400000		57	58	57	58	58	58	58	58	58	58	58	76	68	28	52	50	50	85	117	370	68	
411		58	58	58	58	58	58	58	58	58	58	58	76	68	28	52	50	50	85	117	370	68	
411		59	58	58	58	58	58	58	58	58	58	58	76	68	28	52	50	50	85	117	370	68	
411		SUSPENDED DURING ABRUPT STOP RUNNER 1000'S											CHECKED OUTLINE LIVE STRAINING'S CONFIRMED										
411		VACUUMING STRAINER CLIMATE																					

Flow multipliers / q_0 factor = 0.65

Copy available to DTIC does not permit fully legible reproduction

Flow multipliers / q_0 factor = GFA

115

$$(1) : \text{small number}$$

...valued
for learning tests

Copy available to DTIC does not
permit fully legible reproduction

SOLAR
KUPF - PER (1), EMPHATIC (1)
[OVER, (2)]

DATE _____

ARBINES INCORPORATED

NAVSEA SEMS-KORPERS ENVOUANCE (3)

↓ \$

1 NO. 0000

SPRINT 1957

DATE _____

ARBINES INCORPORATED

NAVSEA SEMS-KORPERS ENVOUANCE (3)

↓ \$

1 NO. 0000

SPRINT 1957

DATE _____

ARBINES INCORPORATED

NAVSEA SEMS-KORPERS ENVOUANCE (3)

↓ \$

1 NO. 0000

SPRINT 1957

DATE _____

ARBINES INCORPORATED

NAVSEA SEMS-KORPERS ENVOUANCE (3)

↓ \$

1 NO. 0000

SPRINT 1957

MAVSEA SEMS - KOPRITS BUDJANICE (4)

[illegible]

APPENDIX IV

DESIGN DATA

- | | |
|----------------------|----------|
| 1. Crane/GE Analysis | page 123 |
| 2. NASA Analysis | page 127 |

A. ENCLOSED CYLINDERS WITH ZERO AXIAL FLOW IN THE GAP**1. Basic Concepts and Definitions**

The drag torque, or moment, M , produced by fluid friction, often called "windage," of a rotating cylindrical surface is generally evaluated in terms of a friction factor, c_f , defined as follows:

$$c_f = \frac{T}{\rho(\omega r_i)^3 / (2g)} = \frac{M}{\pi r_i^4 L \omega^3 / g} \quad (1)$$

where the symbols are the conventional symbols defined in Section G408.1, p. 2, as well as in item B below. Subscripts i and o here refer to the rotor ("inner" surface of the rotor-stator gap) and stator ("outer" surface) respectively.

This relation excludes the contribution of the ends (which can be considered separately as "disks") and of the bearings. The power loss from "drag" or "windage" of the cylindrical surface is as follows:

$$\text{in mechanical units:} \quad P_w = M\omega \text{ ft lbs/sec} \quad (2)$$

$$\text{or, in watts:} \quad q_w = (1.358 M\omega) \text{ watts} \quad (3)$$

The evaluation of c_f is explained below.

B. STEP-BY-STEP PROCEDURE FOR EVALUATING FRICTION FACTOR, c_f **Step 1. Data**

From the given data, or estimates, evaluate the following quantities (one set of consistent units and numerical values are noted here as an example). For properties of gas and of liquids, see Section G513 and G514, respectively, but make sure to use, or convert to, the units chosen here.

		Units	Numerical Example
Fluid density	ρ	lb/ft ³	0.075 (air at 1 atm, 70°F)
Fluid viscosity	μ	lb/(sec ft)	1.223×10^{-4} (air at 70°F)
Radial gap between rotor and stator	b	ft	0.03
Radius of rotating cylinder	r_i	ft	0.30
Rev. per minute	n	rpm	3600
Rotational velocity	ω	rad/sec ($=2\pi n/60$)	377
Rotor axial length	L	ft	2.0

Step 2. Taylor Number

Evaluate, from the above data, the rotor Taylor number, $(N_{Ta})_i$, from its constituent factors, as follows:

Factor or Formula	Numerical Example
$\frac{\rho \omega r_i b}{\mu}$	$\frac{0.075 \times 377 \times 0.30 \times 0.03}{1.223 \times 10^{-4}} = 20,800$
b/r_i	$0.03/0.30 = 0.10$
$(N_{Ta})_i = \left(\frac{\rho \omega r_i b}{\mu}\right) \left(\frac{b}{r_i}\right)^{1/2}$	$20,800 (0.10)^{1/2} = 6.58 \times 10^3$

Eq. (4)

JOSEF SEDY
AUG 7 1979

DESIGN DATA
DRAG - ROTATING
CYLINDERS - ENCLOSED

Fluid Flow
Division

Step 3. Friction Factor

Evaluate c_f from whichever of the following formulas for c_f applies to the pertinent range of $(N_{Ta})_i$:

Range	Formula	Segments in Fig. 5-1
$0 < (N_{Ta})_i < 41$ (Laminar)	$c_f = \frac{2}{(\rho \omega r_i b / \mu)} \frac{(1 + b/r_i)^2}{(1 + 0.5b/r_i)} \quad \text{Eq. (5)}$	a-b
$41 < (N_{Ta})_i < 63$ (Transition)	$c_f = \frac{2(N_{Ta})_i^{1.0}}{\rho \omega r_i b / \mu} = 2 \left(\frac{\rho \omega r_i b}{\mu} \right)^{0.6} \left(\frac{b}{r_i} \right)^{0.76} \quad \text{Eq. (6)}$	b-c
$63 < (N_{Ta})_i < (N_{Ta})_i, V-T$ (Vortex Flow)	$c_f = \frac{0.476(N_{Ta})_i^{0.5}}{\rho \omega r_i b / \mu} = \frac{0.476(b/r_i)^{0.26}}{(\rho \omega r_i b / \mu)^{0.5}} \quad \text{Eq. (7)}$	c-d

For $(N_{Ta})_i, V-T$ see Note 1 below. This equation (7) applies when vortex-flow is dominant.

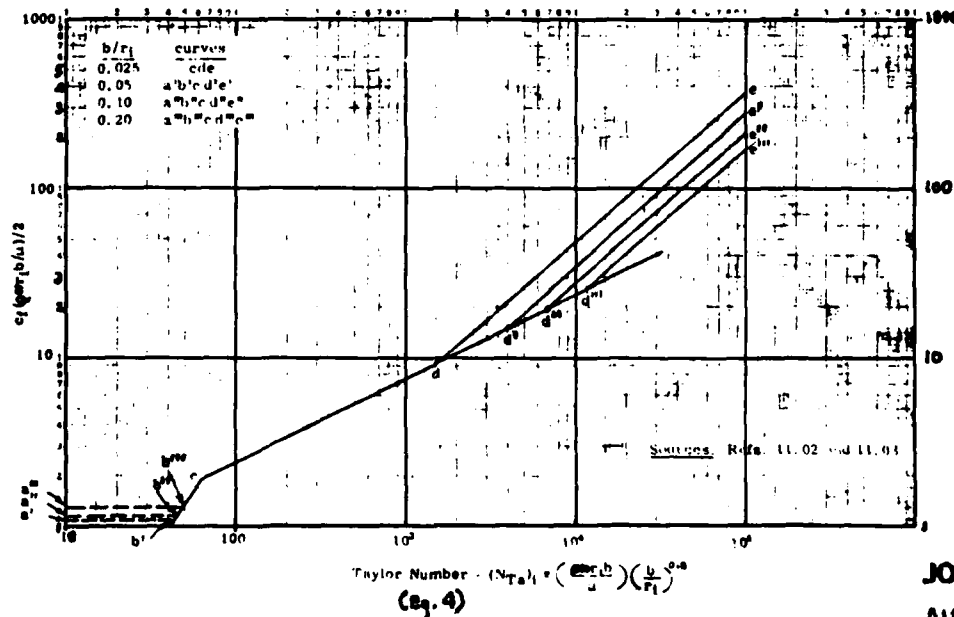
$(N_{Ta})_i, V-T < (N_{Ta})_i < \infty$
(Turbulent)

c_f in this range is related to $(\rho \omega r_i b / \mu)$ by the implicit relation:

$$(\rho \omega r_i b / \mu) = \exp \left\{ \frac{(1 + b/r_i)}{1.2/2c_f(1 + 0.5b/r_i)} - \log_e \left[\frac{\sqrt{c_f/2}}{2(1 + b/r_i)} \right] - 8.58 \right\} \quad \text{Eq. (8)}$$

d'-e'
d''-e'' etc.

Note 1: $(N_{Ta})_i, V-T$ is the value of $(N_{Ta})_i$ at transition from vortex-dominant flow to turbulence-dominant flow. Until better test evidence becomes available, the procedure here suggested is to evaluate c_f from Eq. (7) and also from Eq. (8) and use whichever of these values is the higher. The approximate value of $(N_{Ta})_i, V-T$, above which Eq. (8) is then applicable, can be judged, from inspection of Fig. 5-1, as the intersection of segments cd and de, selected for the chosen value of (b/r_i) .



JOSEF SEDY
AUG 7 1979

Figure 5-1. Friction Factor for Smooth Cylinder Rotating in a Smooth Coaxial Enclosure with Zero Axial Flow

SYMBOLS (with one set of consistent units as an example)

- a, Radius of rotating cylinder, or of edge of a disk, feet
- b, Thickness of disk, or radial gap between cylindrical rotor and the cylindrical stator surrounding the rotor, feet
- c, Disk radial-tip clearance, feet
- c_f , Friction factor, defined as $\tau / (\rho \omega^2 r_l^2 / 2g) \pm \tau / (\rho \omega^2 a^2 / 2g)$, i.e., based on the peripheral velocity, $\omega r_l \pm \omega a$, of the rotor
Note: If the force unit were not lb., but were newton or dyne, the factor g would be deleted.
- C_{mt} , Disk torque (or moment) coefficient, defined by
$$M_t = C_{mt} [\rho \omega^2 a^3 / (2g)] \text{ lb. ft.}$$

Note: The "note" on c_f above applies here also.
- f, Friction factor defined as $\tau (\rho V_{rel}^2 / 2g)$, i.e., based on relative velocity, V_{rel} , between the rotor surface and the average "bulk" velocity of the fluid in the rotor-stator gap. (See c_f for a definition of a different form of friction factor.) The "note" on c_f above applies here also.
- g, Gravitational acceleration, generally used here as a conversion factor between force units and mass units
- K, k = β / ω = ratio of angular velocities, called "core rotation coefficient"
- L, Axial length, feet
- M, Torque or moment in general, lb. ft.
- M_t , Disk frictional torque, for one side, lb. ft.
- n, Rotational speed expressed as rev. per minute = $60 \omega / (2\pi)$, rpm
- N_{Re} , Reynolds number as defined for the pertinent context; if not otherwise defined N_{Re} is Reynolds number defined as:
$$N_{Re} = \frac{\omega a^2}{\nu}$$
- p, Pressure, lb/ft² unless otherwise specified
- Q, Through flow as may be supplied from an external source, ft³/sec
- Q_p , Disk pumping capacity, ft³/sec
- r, Distance radially outward from axis, feet
- r_e , Radius at inlet (entrance) of ventilating air (for disks), ft.
- r_l , Radius of a cylindrical rotor, ft.
- r_o , Radius of cylindrical stator enclosing a rotor, so $r_o = (r_l + b)$, ft.
- s, Axial clearance between the disk and side wall, feet
- u, Absolute tangential velocity component, ft/sec
- u_{rel} , Tangential velocity component relative to the disk, ft/sec
- v, Absolute radial velocity component, ft/sec
- v_o , Reference radial velocity, ft/sec
- v_{rel} , Relative radial velocity component, ft/sec
- V, Resultant relative velocity, ft/sec
- w_o , Reference axial velocity, ft/sec
- z, Axial distance, measured from rotating disk surface unless otherwise specified, feet

GREEK LETTERS

- β , Angular velocity of fluid in the gap, rad/sec
- δ , Boundary layer thickness on the disk, feet, subscript t refers to tangential-velocity, subscript r refers to radial-velocity boundary layer; without subscript these thicknesses are assumed to be the same.
- ϵ , Grain size roughness, feet
- η , Dimensionless distance from solid boundary, y/s
- θ , Boundary layer thickness on the end wall adjacent to a disk, (θ_t , tangential, θ_r , radial-velocity boundary layer thickness when they differ), feet
- μ , Dynamic viscosity, lb-sec/ft²
- ν , Kinematic viscosity, ft²/sec
- ρ , Density, lb/ft³
- τ , Shear stress of fluid friction (windage), lb/ft²
- γ , $Q/(\omega a^3)$ = coefficient of through flow based on area a^2
- γ_t , $Q/(2\pi \omega a^2 s)$ = coefficient of through flow based on area $(2\pi a s)$
- γ_r , $Q/(2\pi \omega r_o s)$ = coefficient of through flow based on area $(2\pi r_o s)$
- ω , Angular velocity of rotor = $2\pi n/60$, rad/sec

Subscripts (see also definitions of main symbols having subscripts)

- a, Refers to values at $r = a$
- o, Refers to values when $Q = 0$
- r, Refers to values at any radius, r

USER SEDY
AUG 7 1979

Numerical Example

From the numerical example in Step 2 above:

$$(N_{Ta})_i = 6.58 \times 10^3$$

By inspection of Fig. 5-1 for this $(N_{Ta})_i$ and $(b/r_i) = 0.10$, Eq. (7) yields a value of c_f no lower than Eq. (8), so Eq. (7) is the proper choice. Equation (7) yields:

$$c_f = \frac{0.476(6.58 \times 10^3)^{0.8}}{20,800} = 0.00184$$

and this result can also be obtained from segment cd of Figure 5-1.

Step 4. "Windage" Torque and Power

Evaluate the "windage" torque, M , and power, P , from Eq. (1) and Eq. (2) above:

Numerical Example:

$$\begin{aligned} M &= c_f(\pi r_i^4 L \omega^2 / g) \\ &= 0.00184 [\pi \times (0.30)^4 \times 2 \times 0.075 \times (377)^2 / 32.2] \\ &= 0.031 \text{ lb ft.} \\ P &= M\omega = 0.031 \times 377 \\ \text{so } P &= 11.7 \text{ ft lb/sec} \\ \text{and } q_w &= 1.358P = 15.9 \text{ watts} \end{aligned}$$

JOSEF SEDY
AUG 7 1979

NASA CONTRACTOR
REPORT

NASA CR-1772

A REVIEW OF CONFINED VORTEX FLOWS

by W. S. Lewellen

Prepared by

MASSACHUSETTS INSTITUTE OF TECHNOLOGY
Cambridge, Mass. 02139

for

NATIONAL AERONAUTICS AND SPACE ADMINISTRATION - Washington, DC - July 1971

5.4 Flow in the End-Wall Boundary-Layer

Confined vortex flow is usually considerably more complicated than the flow between rotating cylinders. In particular, the flow is complicated by the end wall boundary layers which have characteristic instabilities of their own. Some ideas on the conditions leading to transition in these boundary layers may be obtained by looking at the results of investigations into the stability of Ekman layers. The boundary layer on the axial end walls of a vortex chamber may be viewed as a nonlinear Ekman layer with the Rossby number of order 1 or larger. Here the Rossby number is defined as

$$R_o \equiv \frac{V_1}{\Omega r} \quad (5.4-1)$$

with V_1 the difference between the tangential velocity outside the boundary layer and that of the wall. The principal results of Ekman-layer stability investigations, as summarized by Greenspan (1968) are given in Fig. 5.5. Two distinct types of instabilities have been detected. The waves of both families form a series of horizontal roll vortices whose spacing is related to the depth of the boundary layer. Transition to general turbulence occurs at a Reynolds number somewhat higher than that for the onset of instability.

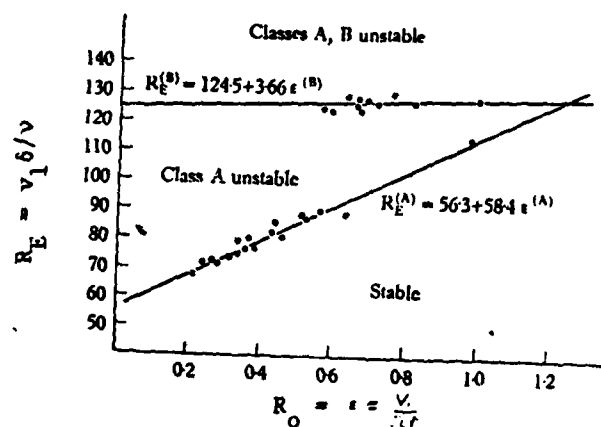


Fig. 5.5 The critical Reynolds number vs. Rossby number for Class A and Class B instabilities in an Ekman boundary layer. (Tatro and Mollo-Christensen, 1967).

The results of Fig. 5.5 can be used to estimate the transition Re_t for flow in the end wall boundary layer of a vortex chamber. For a stationary end wall

$$\begin{aligned} R_o &\geq 1 \\ V_1 &= \Gamma/r \\ \delta &= \left[\frac{\nu}{\Gamma}\right]^{1/2} r \end{aligned} \quad (5.4-2)$$

Therefore $\frac{V_1 \delta}{\nu} \geq 125$ whenever

$$Re_t \equiv \frac{\Gamma}{\nu} = \left(\frac{V_1 \delta}{\nu}\right)^2 \geq (125)^2 \quad (5.4-3)$$

i.e.

$$Re_{t(crit)} \geq 1.5 \times 10^4 \quad (5.4-4)$$

This suggests that the end wall boundary layer will transition from laminar to turbulent flow where Re_t is much above 10^4 .

It is not surprising to find that the oscillating profile distributions of the Ekman layer lead to instabilities at lower Reynolds numbers than do the monotonic profile distributions associated with a rotating disk. The flow field of a rotating disk becomes unstable when (Schlichting, 1968)

$$Re_t \equiv \frac{\Omega r^2}{\nu} \geq 1.9 \times 10^5$$

and transition occurs when

$$Re_t \geq 2.8 \times 10^5$$

In terms of the Reynolds number based on the boundary-layer thickness as in Fig. 5.5 this corresponds to $\delta V_1 / \nu = 550$ for the stability limit and 670 for transition. The instability in the rotating disk boundary layer is of the same type as the Class B in Fig. 5.5.

5.5 Stability in a Confined Vortex

The general flow pattern for a strong vortex as represented by Fig. 3.13 is too complicated for the prediction of general stability conditions, but some indication of the expected transition Reynolds numbers can be obtained from the

preceding sections. When the external boundary condition is a rotating, porous cylinder and there is radial inflow, turbulence probably first appears in the end wall boundary layers. According to the last section this should occur when

$$Re_t \geq 10^4 \quad (5.5-1)$$

Also, transition may be expected at a rather low Re_t in the region of $r > \hat{r}$ when the necessary condition on the Richardson Number is violated, i.e. transition should have occurred when

$$r^3 \left(\frac{dw}{dr} \right)^2 > 4 \frac{d\Gamma^2}{dr} \quad (5.5-2)$$

Since the approximate solution discussed in Section 3.5 calls for significant axial velocities in this region of $r > \hat{r}$ while at the same time calling for Γ to be essentially constant, flow in this region may be expected to be unstable.

These speculations are confirmed by Travers' (1965, 1967) experimental investigations. By taking microflash pictures of dye filaments in a water vortex, he was able to observe clear demarcations between regions of turbulence and apparently laminar regions and to identify the dividing line with the radial stagnation surface. An example of these photographs is reproduced in Fig. 5.6. For the conditions of the photograph ($Re_t \approx 1 \times 10^5$, $N \approx 30$, and $L/D \approx 3$) the end wall boundary layer should be turbulent and the \hat{r} based on turbulent boundary-layer calculation (see Chapter 6) falls close to the demarcation line between the laminar and turbulent region. This division of turbulent and laminar regions by the radial stagnation surface was observed for all tangential Reynolds numbers tested ($Re_t = .5$ to 2.5×10^5) whether the vortex was driven by rotating the peripheral wall, by injecting flow tangentially through slots, or by injecting through a large number of discrete jets.

Travers and Clark (1968) also demonstrated that a vortex with radial outflow is more unstable than that for radial inflow. A one inch diameter, porous tube was installed in the center of the vortex discussed in the last paragraph and also provisions made to rotate either the central tube or the end walls. For small amounts of outflow ($-N \leq 100$) the flow was turbulent for $r \geq 0.3 r_0$ and laminar for smaller radii when both the inner tube and the end walls were stationary (Re_t was varied from 1.2×10^4 to 3.2×10^5 for these

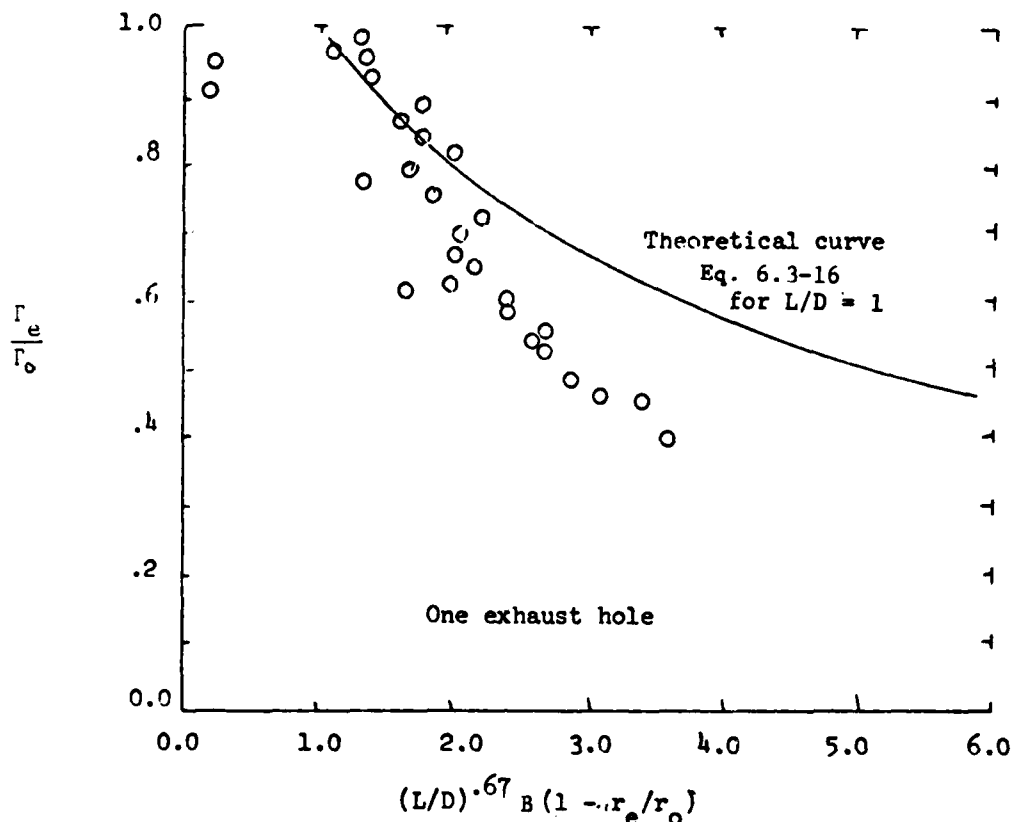


Fig. 6.9 The circulation ratio as a function of L/D , r_e/r_o , and the boundary layer interaction parameter for incompressible flows.

6.4 Cylindrical Wall Boundary Layer

Since the confined vortex is usually driven by tangential injection of fluid near the outer wall it is necessary to consider losses that occur due to shear on the cylindrical wall. This problem was considered for laminar flow in Section 3.8. Equation 3.8-1 may be applied to turbulent flow if τ_w is interpreted as the turbulent wall shear and μ in the last term is replaced by ϵ_T .

$$\dot{m} \Gamma_1 = \dot{m} \Gamma_o + 2\pi r_o^2 \ell \tau_w - 2\pi r_o \ell \epsilon_T \frac{2\Gamma_o}{r_o} \quad (6.4-1)$$

The difficulty in applying this equation, of course, is involved in the uncertainty in these two parameters τ_w and ϵ_T . Most attempts at semi-empirically determining the jet recovery factor, Γ_o/Γ_1 , have neglected the last term involving ϵ_T . Thus implying that the wall boundary layer can be decoupled from the vortex core.

Kendall (1962) estimated values of Γ_o from end wall pressure distributions and used Eq. 6.4-1 with the last term neglected to determine τ_w . On this basis he found τ_w to be only about 10% above that which would be predicted for turbulent flow over a flat plate at the same Reynolds number based on the peripheral path length, $2\pi r_o$, and the wall velocity, Γ_o/r_o .

With $\tau_w = \frac{C_f}{2} \rho_o v_o^2$ and the last term neglected, Eq. 6.4-1 may be written as

$$\frac{\Gamma_o}{\Gamma_i} = \frac{1}{1 + \frac{C_f}{2} \frac{v_o}{u_o}} \quad (6.4-2)$$

Alternatively when all of the flow is introduced tangentially, with no compressibility effects

$$\frac{v_o}{u_o} = \frac{2\pi r_o \ell}{A_i} \quad \frac{\Gamma_o}{\Gamma_i} = \frac{A_w}{A_i} \frac{\Gamma_o}{\Gamma_i} \quad (6.4-3)$$

and Eq. 6.4-2 may be written in the form given by Roschke (1966)

$$\frac{\Gamma_o}{\Gamma_i} = \frac{[(2 C_f A_w/A_i) + 1]^{1/2} - 1}{C_f A_w/A_i} \quad (6.4-4)$$

Equation 6.4-4 is plotted in Fig. 6.10 with a number of experimental points from various investigators reviewed by Rodoni (1969). The general trend of the curve is supported but a wide variation in C_f is required to explain the scatter in the curve. A correlation of C_f as a function of tangential Reynolds number based on a comparison between this figure and Eq. 6.4-4 shows that it is equivalent to setting

$$C_f = \frac{0.29}{Re_t^{0.275}} \quad (6.4-5)$$

This is substantially different than that which would be predicted by the Blasius expression for a flat plate of length $2\pi r_o$, i.e.

$$C_f = \frac{0.052}{Re_t^{0.2}} \quad (6.4-6)$$

The large values of C_f obtained cannot be explained in terms of the ϵ_T term which was neglected in reducing Eq. 6.4-1 to 6.4-4. Including this term would only serve to increase the empirical values of C_f since it represents angular momentum which is transmitted by shear in the fluid radially outward to the cylindrical wall layer. One reason for the higher values of C_f is that local jet velocities may be much higher than the v_o which is used in the

APPENDIX V

FACE SEALS BIBLIOGRAPHY

Whipple, R. T. P., "The Inclined Groove Bearing", AERE T/R 622 (revised), U. K. Atomic Energy Research Establishment, Harwell, Berkshire, England, 1958.

Wordsworth, D. V., "The Viscosity Plate Thrust Bearing", AERE E/R 2217, U. K. Atomic Energy Research Establishment, Harwell, Berkshire, England, 1958.

Summers-Smith, D., "Laboratory Investigation of the Performance of a Radial Face Seal," Proc. Intern. Conf. on Fluid Sealing, British Hydromechanics Research Assoc., 1961, paper D-1.

Denny, D. F., "Some Measurements of Fluid Pressures Between Plane Parallel Thrust Surfaces With Special Reference to Radial-Face Seals", Wear, Vol. 3, 1961, pp. 64-83.

Glasgow, L. E., "Experience with SRE," Nucleonics, Vol. 20, No. 4, April 1962, pp. 61-65.

Nau, B. S., "Hydrodynamics of Face Seal Films," Proc. Second Intern. Conf. on Fluid Sealing, B.S. Nau, H. S. Stephens, and D. E. Turnbull, eds., British Hydromechanics Research Assoc., 1964, pp. F5-61 to F5-80.

"Research and Development of a Friction Controlled Face Seal", AD-609 17, Sept. 1964.

"Summary of Shaft Face Seal Development Program", TIM-903, June 20, 1965.

Malanoski, S. G. and Pan, C. H. T., "The Static and Dynamic Characteristics of the Spiral-Grooved Thrust Bearing", J. Basic Engr., Trans. ASME, Sept. 1965, p. 547.

Muyderman, E. A., "New Possibilities for the Solution of Bearing Problems by Means of the Spiral-Groove Principle", Proc. Inst. Mech. Engrs. 1965-66, Vol. 180, Pt. 3K, p. 174.

Kelly, Robert E., Wood, Glenn M., and Manfredi, Daniel V., "Cermet Face Seals for Inert Gas Environments", Lubrication Engineering, Vol. 22, No. 2, Feb. 1966, pp. 41-49.

Hamilton, D. G., Walowit, J. A., and Allen, C. M., "A Theory of Lubrication by Microirregularities," J. Basic. Engr., Vol. 88, No. 1, March 1966, pp. 17-185.

Golubiev, A. I., "On the Existence of a Hydraulic Film in Mechanical Seals", Proc. Third Intern. Conf. on Fluid Sealing, A. L. King, B. S. Nau, and H. S. Stephens, eds., British Hydromechanics Research Assoc., 1967, pp. E1-1 to E1-8.

Cheng, H. S. and Snapp, R. B., "A Study of the Radial Film and Pressure Distribution of High Pressure Face Seals," Proc. Third Intern. Conf. on Fluid Sealing, A. L. King, B. S. Nau, and H. S. Stephens, eds., British Hydromechanics Research Assoc. 1967, pp. E3-21 to E3-40.

Lohou, J., Discussion on paper entitled, "A Study of Radial Film and Pressure Distribution of High Pressure Face Seals", by H. S. Cheng and R. B. Snapp, Proc. Third Intern. Conf. on Fluid Sealing, A. L. King, B. S. Nau, and H. S. Stephens, eds., British Hydromechanics Research Assoc., 1967, pp. E3-25 to E3-26.

Kojabashian, C. and Richardson, H. H., "A Micropad Model for the Hydrodynamic Performance of Carbon Face Seals," Proc. Third Intern. Conf. on Fluid Sealing, A. L. King, B. S. Nau, and H. S. Stephens, eds., British Hydromechanics Research Assoc., 1967, pp. E-41 to E4-71.

Parks, A. J., McKibbin, R. H., Ng, C. C. W. and Slayton, R. M., "Development of Main-Shaft seals for Advanced Air Breathing Propulsion Systems," Pratt & Whitney Aircraft Rep. PWA 3161, NASA CR-72338, 1967.

Heck, J. A., "The Circumferential Seal: Its Application, Its Place in the Seal Spectrum Relative to Gas Turbines", SAE Preprint 670062, Automotive Engineering Conference, Detroit, Michigan, January 9-13, 1967.

"Improving Performance of Face Contact Seal in Liquid Sodium (400 deg. to 1000 deg. F) by Incorporation of Spiral-Groove Geometry", N67-25842, May 1967.

Muijderman, E. A., "Analysis and Design of Spiral-Groove Bearing", J. Lub. Tech., Trans. ASME, July 1967, p. 291.

Elrod, H. G. and Ng, C. W., "A Theory for Turbulent Fluid Films, and Its Application to Bearings", ASME Transactions, J. Lub. Tech., Vol. 89, Series F, July 1967, p. 346.

"Mean Free Path Effect in Spiral Grooved Thrust Bearings", AD-671 830, Nov. 1967.

"Spiral Groove Face Seal Concepts, Comparison to Conventional Face Contact Seals in Sealing Liquid Sodium (400 deg to 1000 deg F)," ID No. N68-17610 presented at ASME Seal Symp., Pittsburg, Nov. 12-16, 1967.

"On Local Compressibility Effect in Spiral Groove Bearings and Sealing Systems", ID No. EI70X008221, Rev Roumaine Des Sciences Techniques-Serie de Mechanique Appliques, V. 13, N. 3, 1968, pp. 489-506.

Sneck, H. J., "The Effects of Geometry and Inertia on Face Seal Performance-Laminar Flow", J. Lub. Tech., Trans. ASME, April 1968, p. 333.

Sneck, H. J., "The Effects of Geometry and Intertia on Face Seal Performance-Turbulent Flow", J. Lub. Tech., Trans. ASME, April 1958, p. 342.

Burton, R. A., "An Experimental Study of Turbulent Flow in A Spiral-Groove Configuration", J. Lub. Tech., Trans. ASME, April 1968, p. 443.

Cheng, H. S., Chow, C. Y. and Wilcox, D. F., "Behavior of Hydrostatic and Hydrodynamic Noncontacting Face Seals", J. Lub. Tech., Trans. ASME, April 1968, p. 510.

Findlay, J. A., "Inward Pumping in Mechanical Face Seals", J. Lub. Tech., ASME Trans., Paper 68-Lub-2.

Sneck, H. J. A., "Reversed Flow in Face Seals", J. Lub. Tech., ASME Trans., Paper 68-Lub-9.

Sneck, H. J., "Thermal Effects in Face Seals", J. Lub. Tech., ASME Trans., Paper 68-Lub-14.

Pape, J. G., "Fundamental Research on a Radial Face Seal", Am. Soc. Lubri. Engrs. Trans., Vol. 11, No. 4, Oct. 1968, p. 302-309.

Johnson, R. L., and Ludwig, L. P., "Shaft Face Seal With Self-Acting Lift Augmentation for Advanced Gas Turbine Engines", NASA TN D-5170, 1969.

Bottasma, J., "The Effect of Viscosity Variations With Temperature on the Performance of Spiral Groove Bearings", ASLE Transactions, Vol. 12, 1969, pp. 287-296.

"Compressible Narrow Groove Theory - An Approximate Analysis of Gas Lubricated Spiral-Grooved Bearings at Large Compressibility Numbers", AD-686 027, Feb. 10, 1969, 71p.

"A Universally Valid Compressible Theory for Gas-Lubricated, Narrow, Spiral-Grooved Thrust Bearing", AD-686 028, April 1969, 39p.

"Shaft Face Seal With Self-Acting Lift Augmentation for Advanced Gas Turbine Engine", N69-23232, April 1969, 23p.

Orcutt, F. K., "An Investigation of the Operation and Failure of Mechanical Face Seals", Preprint 22, Am. Soc. Lubri. Engrs., May 1969.

"Optimum Design of a Spiral Groove Bearing", ID No. EI71X021396, Tribology Conv. 1969. Conv of Triology Group of Inst. Mech. Eng., May 28-30, 1969, Chalmers Tek Hogsk, Gothenburg, Sweden Inst. Mech. Eng. Proc. 1969-69 V. 183, pt 3P, London, 1969, Paper 18, pp. 147-51.

"Design and Test of an Unloading Gas Barrier Face Seal", ID No. EI71X035387, ASLE, 4th Int. Conf. Fluid Sealing, Philadelphia, PA, May 5-8, 1969, Spec. Publ. SP-2, p. 13-17.

"Friction and Wear Characteristics of Hot Pressed Composites in a Face Seal Configuration", ID No. EI71X034214, ASLE, 4th Int. Conf. Fluid Sealing, Philadelphia, PA, May 5-8, 1969, Spec. Publ. SP-26, 6-12.

"Shaft Face Seal With Self-Acting Lift Augmentation for Advanced Gas Turbine Engines", ID No. EI71X028113, Proc. of the 4th Int. Conf. on Fluid Sealings, May 6-9, 1969, Philadelphia, PA, by Brit. Hydromech. Res. Assoc. pp. 252-61.

"Film Cavitation Observations in Face Seals", ID No. EI71X027988, Proc. of the 4th Int. Conf. on Fluid Sealings, May 6-9, 1969, Philadelphia, PA by Brit. Hydromech. Res. Assoc., pp. 190-8.

Barber, J. R., "Thermoelastic Instabilities in the Sliding of Conforming Solids", Proceedings of the Royal Society, Vol. 312, No. 1510, Sept. 1969, pp. 381-394.

Sneck, H. J., "The Misaligned, Eccentric Face Seal", J. Lub. Tech., Trans. ASME, Oct. 1969, p. 695.

Zuk, J. and Smith, P.J., "Computer Program for Viscous, Isothermal, Compressible Flow Across a Sealing Dam With Small Tilt Angle", NASA TN D-5373, Aug. 1969.

Zuk, J. and Ludwig, L. P., "Investigation of Isothermal, Compressible Flow Across a Rotating Sealing Dam: I - Analysis", NASA TN D-5344, Sept. 1969.

Zuk, J. and Ludwig, L. P., "Investigation of Isothermal, Compressible Flow Across a Rotating Sealing Dam: II - Combustor Program", NASA TN D-5345.

Sneck, H. J., "The Eccentric Face Seal With a Tangentially Varying Film Thickness", J. Lub. Tech., Trans. ASME, Oct. 1969, p. 748.

Sneck, H. J., "Gas Turbine Face Seal Thermal Deformation and Computer Program for Calculation of Axisymmetric Temperature Field", NASA TN D-5605.

"Gas Turbine Face Seal Thermal Deformation and Computer Program for Calculation of Axisymmetric Temperature Field", N70-15390, Dec. 1969, 111p.

"Axial Response of a High-Speed, Gas-Lubricated, Rotor-Bearing Assembly to Shock and Vibration", ID No. EI71X019488, U.S. Naval Res. Lab., Shock Vib. Bull. 40 pt 3 Dec. 1969, pp. 275-92.

"Thermal Distortion of Spiral-Grooved Gas-Lubricated Thrust Bearings", AD-700 683, Dec. 29, 1969, 47p.

Mayer, E., "Thermodynamics in Mechanical Seals", Proc. Fourth Intern. Conf. on Fluid Sealing, A. L. King, B. S. Nau, and H. S. Stephens, eds., British Hydromechanics Research Assoc., 1970, pp. 124-128.

Zuk, J., Ludwig, L. P., and Johnson, R. L., "Design Study of Shaft Face Seal With Self-Acting Lift Augmentation. I - Self-Acting Pad Geometry", NASA TN D5744, 1970.

"Face Seal Wear of MoS₂-Ni Composite", ID No. EI71X053377, Tribology (London) V. 3, N. 2, May 1979, p. 95-96.

"Proceedings of the Fourth International Conference on Fluid Sealing," May 6-9, 1969, Philadelphia, PA, held in conjunction with the Annual Meeting of the Amer. Soc. of Lubric. Eng., and jointly sponsored by the Amer. Soc. of Lubric. Eng., the Brit. Hydromech. Res. Assoc., and the Amer. Soc. of Mech. Eng., ID No. EI71X027956, BHRA, Cranfield, Bedford, England, 1970.

"Spiral Groove Face Seal Development for Snap 8 Final Report, 31 May 1968, 7 Aug. 1970", N71-20333, Aug. 7, 1970.

"Development of 24% Hydrostatic Seal", ID No. EI71X003124, Lubrication Eng., V. 26, N. 8, Aug. 1979, p. 26-72.

"Analysis and Development of a Dry Face Mechanical Shaft Seal Concept", ID No. EI71X008961, Lubrication Eng., V. 26, N. 8, Aug. 1970, pp. 273-80.

"Theoretical Performance of Rarefied-Gas Viscoseals," ID No. EI71X015677, ASLE Trans., V. 13, N. 4, Oct. 1970, pp. 296-303.

"Design Study of Shaft Face Seal With Self-Acting Lift Augmentation", N71-11579, Nov. 1970 29p.

Povinelli, V.P. and McKibbin, A. H., "Development of Mainshaft Seals for Advanced Air Breathing Propulsion Systems: Phase III", NASA CR-72987, 1971.

Iny, E. H., "A Theory of Sealing With Radial Face Seals", Wear, Vol. 18, 1971, pp. 51-69.

Mayer, E., "High Duty Mechanical Seals for Nuclear Power Stations", Proc. Fifth Intern. Conf. on Fluid Sealing, A. L. King, B. S. Nau, and H. S. Stephens, eds., British Hydromechanics Research Assoc., 1971, pp. A5-37 to A5-47.

"Air Bearings for High-Speed Mirrors Rotating in a Vacuum", ID No. EI71X034202, J. Lub. Tech., Trans ASME, V. 93, Ser. F N. 1, Jan. 1971.

"Dismountable End Face Seal for Screw Compressors", ID No. EI72X032881, Khim I Neft Mashinoetr N 2, Feb. 1971, p. 40. See also English translation in Chem. Petrol. Eng. N. 1-2, Jan.-Feb. 1971, pp. 167-8.

"Design Study of Shaft Face Seals With Self-Acting Lift Augmentation", N71-20392, Mechanical Components, March 1971, 19p.

"Grease Lubricants for Spiral Groove Bearings", ID No. EI71X170254, Lubric. Eng., V. 27 N. 5, May 1971, pp. 164-73.

"Design and Experimental Evaluation of a Turbopump Liff-Off Seal", N71-25734, Final Report, May 12, 1971, 99p.

Stangham-Batch, B. A., "Face Lubrication in Mechanical Seals", Proceedings of the Tribology Convention, May 12-15, 1971, Institution of Mechanical Engineers, London, England.

Zirin, L. I., "Bearings and Seal Scalability Study", USAAMRDL Technical Report 71-27, June 1971.

Paladini, W., "Static and Rotating Air/Gas Seal Evaluation", USAAMRDL TR-71-28, June 1971.

"Selection, Analysis and Preliminary Design of a Steam-Lubricated, Steam-Turbine, Shaft Seal", ID No. EI72X014978, ASLE Trans., Vol. 14, No. 3, July 1971, pp. 226-36.

"An Improved Spiral Groove Seal", Patent Application, Filed 13 July 1970, N71-28679, 11p.

"Turbulence and Inertia Effects in the Aligned Face Seal", AD-730, August 1971, 143p.

"Rotary Shaft Seal Selection Handbook for Pressure-Equalized, Deep-Ocean Equipment", AD-889 330/7ST, October 1971, 73p.

Hady, W. F., and Ludwig, L. P., "Experimental Investigation of Self-Acting-Lift-Pad Characteristics for Main-Shaft Seal Applications", NASA TN D-6384, N71-85830, October 1971, 21p.

"Design Study of Shaft Face Seal With Self-Acting Lift Augmentation. Performance in Simulated Gas Turbine Engine Operation", N72-2419, Dec. 1971, 20 p.

"Spiral Groove Vacuum Seal", ID No. EI72X016623, ASME Paper 71-WA/PID-5 for meeting Nov. 28-Dec. 2, 1971, 4p.

"Mercury Rankine Program (SNAP 2). Development of Liquid-Mercury-Lubricated Bearings. Volume VI. Spiral-Groove Thrust Bearing Experimental Results", NAA-SP-6320 (Vol. 6), for Atomics International, Canoga Park, CA, 93p.

Dow, T. A. and Burton, R. A., "The Role of Wear in the Initiation of Thermo-elastic Instabilities of Rubbing Contact", ASME Paper 72-Lub-45, New York, NY, 1972.

Colsher, R. and Shapiro, W., "Predicting Performance of Gas-Lubricated Seals Using Advanced Numerical Techniques", Franklin Inst. FIRL-I-C2429-4, AD-745333, 1972.

Smally, A. J., "The Narrow Groove Theory of Spiral Grooved Gas Bearings: Development and Application of a Generalized Formulation for Numerical Solution", ASME Transactions, J. Lub. Technol., Jan. 1972, pp. 86-92.

"Formulation of a Generalized Narrow Groove Theory for Spiral Grooved Viscous Pumps", ID No. EI72X036446, J. Lub. Technol., Trans. ASME, Vol. 94, Ser F, N. 1, Jan. 1972, pp. 81-5.

"Narrow Groove Theory of Spiral Grooved Gas Bearings. Development and Application of a Generalized Formulation for Numerical Solution", ID No. EI72X035655, J. Lub. Technol., Trans. ASME, Vol. 94, Ser. F, No. 1, Jan. 1972, pp. 86-92.

"A Spiral Groove Seal", filed Jan. 24, 1972, N72-27522, 12 p.

Mahler, F. H., "Advanced Seal Technology", Technical Report AF-APL-TR-72-8, U.S. Air Force, Feb. 1972, Pratt & Whitney Aircraft, East Hartford, CN.

"Dynamic Stability of Gimballed Spiral-Grooved Thrust Bearings", AD-753 315, Revision of Report dated 5 May 71. Supersedes report dated May 71, AD-725 164, Feb. 25, 1972, 14p.

"Application of the Turbulent Eddy Diffusivity Transport Equation to the Analysis of Turbulent Flow in the Radial Face Seal", ID No. EI731153245, Southeast Conf. on Theory and Appl. Mech., 6th Prov., Univ. of South Florida, Tampa, March 23-24, 1972, pp. 389-409. Available from Univ. of South Florida, Tampa, 1972.

"Design Study of Shaft Face Seal With Self-Acting Lift Augmentation. IV - Force Balance", N72-22500, April 1972, 28p.

"New Circumferential Seal Design Concept Using Self Acting Lift Geometries", N72-23504, May 1972, 11p.

Zuk, J., Ludig, L. P. and Johnson, R. L., "Quasi-One-Dimensional Compressible Flow Across Face Seals and Narrow Slots: I - Analysis", NASA TN D-6668, June 1972.

"On the Computation of Edge Correction for the Locally-Incompressible Narrow-Groove Theory", AD-754 300, Nov. 1972, 42p.

"Mechanical Face Seal for Helium Gas SEM Dashes an Aerospace Application", ID No. EI730315047, Lubric. Eng., V. 28, N. 12, Dec. 1972, pp. 453-458.

"Preliminary Proposal for Dynamic and Face Seal Investigations for High Temperature Liquid Metal Applications", CNLM-5693, 14p.

"Quasi-One-Dimensional Compressible Flow Across Face Seals and Narrow Slots: II - Computer Program", NASA TN D-6787.

"Fretting of Secondary-Seal-Ring Candidate Materials in Air at Temperatures to 816°C", NASA TN D-7073, N73-12549 (MF).

"Analysis of Face Deformation Effects on Gas Film Seal Performance", NASA TM X-68022.

"Analytical Investigation of the Spiral Groove Face Seal", ID No. EI730732944, ASME Paper, N. 73-Lub-F, 1973, 12p.

Burton, R. A., Nerlikar, U. and Kilapaiti, S. R., "Thermoelastic Instabilities in a Seal-Like Configuration," Wear, Vol. 24, 1973, pp. 177-188.

Lynwander, P., "Development of Helicopter Engine Seals", NASA CR-134647, 1973.

Stanghan-Batch, B. and Iny, E. H., "A Hydrodynamic Theory of Radial-Face Mechanical Seals", J. Mech. Engr. Sci., Vol. 15, N. 1, Feb. 1973.

Ludwig, L. P., "Self-Acting and Hydrodynamic Shaft Seals", NASA TM X-68214, April 1973.

Sneck, H. J. and McGovern, J. F., "Analytical Investigation of the Spiral Groove Face Seal", Journal of Lubrication Technology, Trans. ASME, April 1973, p. 499.

"Analytical Study of Pressure Balancing in Gas Film Seals", NASA TM X-68227.

"Performance of Gas-Lubricated Nonconforming Pivoted-Pad Journal Bearings and a Flexibly Mounted Spiral-Groove Thrust Bearing", N73-24086, May 1973, 28p.

Povinelli, V. P. and McKibbin, A. H., "Development of Mainshaft Seals for Advanced Air Breathing Propulsion Systems: Phase II", NASA CR-72737, June 1973.

"High Speed, Self-Acting Shaft Seal", Filed 19 July 1973, 12p. N73-29457/1.

"Development of a Mechanical Seal for the Main Shafts of Pump-Turbines", ID No. EI731154767, Water Power, V. 25, N. 8, August 1973, pp. 309-314.

"Seals (1973-1974 Seals Reference Issue)," Machine Design, Vol. 45, No. 22, Sept. 13, 1973.

"Analysis of Grease and Oil Lubricated Spiral Grooved Bearings", ID No. EI740205432, ASME Paper, N. 73-LUB-20 for meeting October 16-18, 1973, 9p.

"Spiral Groove Seal", Patented 23 Oct. 1972, 4p. Misc-Filed 21 Dec. 1970. N74-10474/6.

"Asperity Lubrication and Cavitation in Face Seals", ID No. EI740851277, Natl. Bur. Stand., Spec. Publ. 394, 1974, for meeting Boulder, Colorado, October 31-Nov. 2, 1973, pp. 77-83.

Hayden, T. S. and Keller, C. H., "Design Guide for Helicopter Transmission Seals", SER-50791; United Aircraft Corp., 1974 (also NASA CR-120997).

"Analytical Solutions for Incompressible Spiral Groove Viscous Pumps", ID No. EI741172735, ASME Paper 74-LUB-K, 1974, 5p.

"Gas-to-Liquid Interface of Spiral Groove Journal Bearings and its Effect on Stability", ID No. EI741167906, ASME Paper 74-LUB-N, 1974, 9p.

"Spiral Groove Seal", U.S. Patent Appl. SN-54540, filed 13 July 1970, which is a continuation-in-part of abandoned U.S. Patent Appl. SN-723465, filed 23 April 1968, Patented 1 Jan. 1974, 6p. N74-15125/9.

Haardt, R., "Flow Considerations Around the Cavitation Area in Radial Face Seals", Cavitation and Related Phenomena in Lubrication, Proceedings of the First Leeds-Lyon Symposium on Tribology, Sept. 1974, Mechanical Engineering Publications Ltd., London, p. 221.

"Low Capacitance Electrical Feedthrough and Simple, Reuseable Closure Seal for Hydrostatic Pressures to 7 Kilobar and Temperatures to 200 degrees C: Application to NMR", ID No. EI740529973, Rev. Sci. Instrum., V. 45, N. 1, Jan. 1974, pp. 111-113.

Zuk, J. and Smith, P. J., "Computer Program or Quasi-One-Dimensional Compressible Flow With Area Change and Friction - Application to Gas Film Seals", TN D-7481, February 1974, NASA.

"Performance of Gas-Lubricated Cruciform-Mounted Tilting-Pad Journal Bearings and a Damped Flexibly Mounted Spiral-Groove Thrust Bearing", N74-18129/8, March 1974, 25p.

"Hydrostatic Stern Gear", ID No. EI740631548, Trans. North East Coast Inst. Eng. Shipbuild, V. 90, N. 4, March 1974, p. 97-110.

"Start-Stop Testing of Two Self-Acting Air-Lubricated Spiral Groove Thrust Bearing Coatings", N74-31945/OST, April 1974, 72p.

Haardt, R. and Godet, M., "Axial Vibration of a Misaligned Radial Face Seal Under a Constant Closure Force", Preprint 74AM-7D-1, Am. Soc. Lubri. Engrs., April-May 1974.

"Investigation of Sealing Surfaces in Radial Thrust Seals", Konstr Masch App Geraetebau, V. 25, N. 6, June 1974, pp. 207-214.

Meric, R. A. and Macken, N. A., "Convective Inertia Effects in the Viscoseal", J. Lubr. Tech., Trans. ASME, July 1974, pp. 443.

"Interface Wear Reactions in Nickel-Nickel Simulated Face Seals", ID No. EI740958307, Wear, V. 29, N. 2, August 1974, p. 195-207.

"Flow Consideration Around the Cavitation Area in Radial Face Seals", ID No. EI761069941, Leeds-Lyon Symp. on Tribol., 1st Proc. Pap and Discuss: Cavitation and Related Phenom. in Lubr., Univ. of Leeds, Yorks, England, Sept. 1974, pp. 221-225. Publ. by Mech Eng Fuel, Ltd, New York, NY, 1974. Fuel for Inst. of Tribol. Leeds Univ., Yorks, England, and Inst. Natl. Des. Sci. Appl. de Lyon, France.

Ludwig, L. P. and Johnson, R. L., "Sealing Technology for Aircraft Gas Turbine Engines", AIAA Paper 74-1188, October 1974.

"Characteristics of Non-Newtonian Power Law Lubricants in Step Bearings and Hydrostatic Step Seals", ID No. EI741167924, Wear, V. 30, N. 1, Oct. 1974, pp. 51-71.

"Dynamic Tracking of Noncontacting Face Seals", ID No. EI641280653, ASLE Paper, 1974, for meeting, Montreal, Que., Oct. 8-10, 1974, Paper 74LC-1C-3, 4p.

"Development of Materials Resistant to Wear and Corrosion for Mechanical-Face-Seal Applications", AD-787 642/8SL, Nov. 1974, 19p.

"Dynamic Response and Stability of a Gas-Lubricated Rayleigh-Step Pad", NASA CR-121156, N75-19697 (MF).

"Analysis and Optimization of Hydrostatic Seal for Primary Pump", ID No. EI7609855285, Conf. on Fluid Mach., 5th Proc. Budapest, Hungary, 1975, V. 1, pp. 53-65. Publ. by Akad Kiado, Budapest, Hungary, 1975.

"Liquid-Lubricated Spiral-Groove Bearings", ID No. EI7602097680, Philips Res. Ref. Suppl., N. 7, 1975, 185p.

"Push-Pull Spiral-Groove Bearings - A Thrust Bearing With Self-Adjusting Internal Preloading", ID No. EI750957270, Philips Tech. Rev., Vol. 35, N. 1, 1975, pp. 11-14.

"Noncontacting Face Seal Application for Sealing Gas at 105 psig, 7,000 rpm", ID No. EI750319618, Lubr. Eng., V. 31, N. 1, Jan. 1975, pp. 16-19.

"Axial Vibration of a Misaligned Radial Face Seal, Under a Constant Closure Force", ID No. EI750319623, ASLE Trans., V. 18, N. 1, Jan. 1975, pp. 55-61.

Povinelli, V. P., "Current Seal Designs and Future Requirements for Turbine Engine Seals and Bearings", Journal of Aircraft, Vol. 12, No. 4, April 1975, p. 274.

Smalley, A. J., Albrecht, P. R. and Elrod, C. W., "The J-Seal: Novel Concept for a Resilient Noncontacting Face Seal", Journal of Aircraft, Vol. 12, No. 4, April 1975.

Zuk, J., "Dynamic Sealing Principles", NASA TM-71851, 1976.

Metcalfe, R., "End Face Seals in High Pressure Water-Learning From Those Failures", Lubrication Engineering, Vol. 32, No. 12, Dec. 1976, p. 625.

Ludwig, L. P., "Technique Eliminates Gas Entrained Dirt From Shaft Seals", NASA Tech. Brief LEW-11855, 1977.

END

FILMED

2-85

DTIC